




Universitetet  
i Stavanger

DET TEKNISK-NATURVITENSKAPELIGE FAKULTET

## MASTEROPPGAVE

Studieprogram/spesialisering: Konstruksjoner og materialer – Master i teknologi/siv.ing.	Vårsemesteret, 2019  Åpen / Konfidensiell
Forfatter: Martin Iveland Henriksbø	 (signatur forfatter)
Fagansvarlig: Sudath Siriwardane  Veileder(e): Sudath Siriwardane, Ashish Aeran	
Tittel på masteroppgaven: Vipping av stålbjelker – En analytisk, eksperimentell og numerisk studie  Engelsk tittel: Lateral-Torsional Buckling of Steel Beams – An Analytical, Experimental and Numerical Study	
Studiepoeng: 30	
Emneord: Lateral-torsional buckling, steel beam, elastic critical moment, point load, lateral deflection, finite element method, ANSYS,	Sidetall: 55  + vedlegg/annet: 41  Stavanger, 15.06.2019 dato/år



# Lateral-Torsional Buckling of Steel Beams – An Analytical, Experimental and Numerical Study

By

Martin Iveland Henriksbø

In cooperation with supervisors

Sudath Siriwardane and Ashish Aeran

Institute of Materials and Constructions at the Faculty of Technology and Science,  
University of Stavanger (UiS)

Norway

15<sup>th</sup> of June 2019

# Table of Contents

- Abstract ..... iii
- Preface ..... iv
- 1 Introduction ..... 1
  - 1.1 Background and Motivation ..... 1
  - 1.2 Objectives ..... 2
- 2 Theory of Lateral-Torsional Buckling ..... 3
  - 2.1 General ..... 3
  - 2.2 Definitions ..... 5
    - 2.2.1 Nomenclature ..... 5
    - 2.2.2 Reference System and Principle Axes ..... 6
  - 2.3 Derivation of the Elastic Critical Moment ..... 7
  - 2.4 Modifications to the Elastic Critical Moment ..... 11
- 3 Experimental Analysis ..... 13
  - 3.1 Experimental Setup ..... 13
    - 3.1.1 Support and Loading Configuration ..... 13
    - 3.1.2 Measuring Equipment ..... 14
    - 3.1.3 Beam Dimensions and Material ..... 14
    - 3.1.4 Testing Procedure ..... 16
  - 3.2 Experimental Results ..... 16
  - 3.3 Previously Conducted Experimental Tests ..... 21
- 4 Numerical Analysis ..... 24
  - 4.1 Software ..... 24
  - 4.2 Model ..... 25
    - 4.2.1 Linear and Nonlinear Buckling Analyses ..... 26
    - 4.2.2 Force Convergence Theory ..... 27
  - 4.3 Initial Testing ..... 29
    - 4.3.1 Preliminary Eigenvalue Buckling Analysis ..... 29
    - 4.3.2 Testing Procedure ..... 33

4.4 Numerical Results .....	33
4.5 Previously Conducted Numerical Analyses .....	39
5 Comparisons and Discussion .....	40
5.1 Comparison Between Experimental and Numerical Results .....	40
5.1.1 Lateral Deflections .....	40
5.1.2 Specifics Regarding the Numerical Analysis.....	45
5.2 Possible Reasons for Differences in Results .....	45
6 Conclusion .....	47
6.1 Conclusion Based on Comparisons and Discussion .....	47
6.2 Further Work .....	47
References .....	48
Appendix .....	49

# Abstract

This thesis compares results from experimental and numerical analyses of structural steel I-beams subjected to lateral-torsional buckling due to a vertical point load located at the mid-span. The aim is to find a suitable finite element model for estimating buckling load and lateral deflection of the beam under increasing load, and to provide information on how beam dimensions affect the results of the numerical simulation relative to the experimental analysis. Fundamental theory of the lateral-torsional buckling of beams is provided, along with previously conducted research on the field.

# Preface

I would like to thank Sudath Siriwardane and Ashish Aeran of the Institute of Materials and Constructions at the Faculty of Technology and Science, University of Stavanger (UiS) for great cooperation and guidance with regards to this thesis.





# 1 Introduction

## 1.1 Background and Motivation

Steel as a structural material is of great importance in the modern world's society. It is widely used in structural elements in construction projects, such as high-rise buildings, bridges and offshore structures, and it is also used in ship hulls, pipes, pressure vessels, containers and wind turbines. Due to its material properties, cost and availability, structural steel is preferred in situations that require high tensile strength or high ductility. Additionally, it has a high flexibility in terms of shape and area of use.

Because of its importance, steel structures have been and are still being widely researched. From material properties related to the crystallographic structure to macro-scale behavioral studies, structural steel and its uses comprise many aspects that require attention regarding the design of structures and its constituent elements.

One of these aspects are the failure modes of steel beams and columns subjected to externally applied load. Failures include global failures, such as overall buckling, and local failures, including cross-sectional yielding, local buckling, web crushing.

This thesis focuses on lateral-torsional buckling. Many of the behaviors of steel members are well understood, both in terms of material properties and geometric properties. However, this field is still subject to a lot of research, as it is important to fully grasp these concepts to further improve engineering standards and guidelines, especially from a safety point of view. Limit state design is the design philosophy used to provide the best possible material and geometry choice for a given engineering problem, and these design principles have been derived from extensive knowledge of structural steel.

## 1.2 Objectives and Overview

The main objectives of this thesis are related to the analysis of beams undergoing lateral-torsional buckling. They are:

- To find a suitable model for estimating buckling loads and lateral deflection
- To compare results of applied load vs. lateral deflection from experimental and numerical analyses.
- To check whether the formulas for elastic critical moment are compatible with the experimental and numerical results
- To look for patterns and trends in the results that will aid in the prediction of critical values applicable for design
- To check whether the numerical models are conservative with regards to design loads

To engage in these problems the thesis has been structured in a way that separates the analyses of lateral-torsional buckling of beams into three categories. These are:

1. Theoretical background and analytical derivation
2. Experimental analysis through laboratory testing
3. Numerical analysis through FEM software simulation

Chapter 2 involves the theory behind lateral-torsional buckling. Renowned researchers on the field such as Trahair et al. are referenced to provide a fundamental understanding of the behavior of steel beams under loading conditions that inhibit lateral-torsional buckling. The derivation of the elastic critical moment along with modifications and applications of this are presented.

Chapter 3 gives an overview of experimental testing conducted at the University of Stavanger by M. Ruud in association with a bachelor thesis. A total of nine steel I-beam specimens were tested with a range of different profiles and beam lengths. Results from these tests are presented, referencing Ruud's work, along with information on previously done work in the field of testing for lateral-torsional buckling.

Chapter 4 focuses on numerical analysis, and presents models, theory and results for the numerical simulations that were done using ANSYS Workbench 17. Finite element models of the nine different specimens used in the lab testing were developed using a combination of Autodesk Inventor and ANSYS. Additionally, some fundamental theory of FEA, linear and nonlinear buckling and convergence is provided.

Chapters 5 and 6 include comparisons and discussion of the findings in the previous chapters, along with a conclusion. Suggestions to further work are also proposed. Finally, an appendix consisting of ANSYS generated reports for the numerical simulations is given.

# 2 Theory of Lateral-Torsional Buckling

## 2.1 General

Lateral-torsional buckling, abbreviated LTB, is a phenomenon occurring with structural members subjected to certain loading conditions. The name comes from the types of deformation the member undergoes, namely lateral displacement and torsional twisting. Lateral displacements involve the lateral shifting of a local cross section relative to its initial position, and twisting involves the rotation of the cross-sectional axes relative to their original position.

Fig. 1 presents the principle of LTB. The beam is supported or otherwise restrained in the right end, hence the local cross section at this position is fixed in place. The left end may represent the free end section of a cantilever beam or the mid-section of a beam supported in both ends.

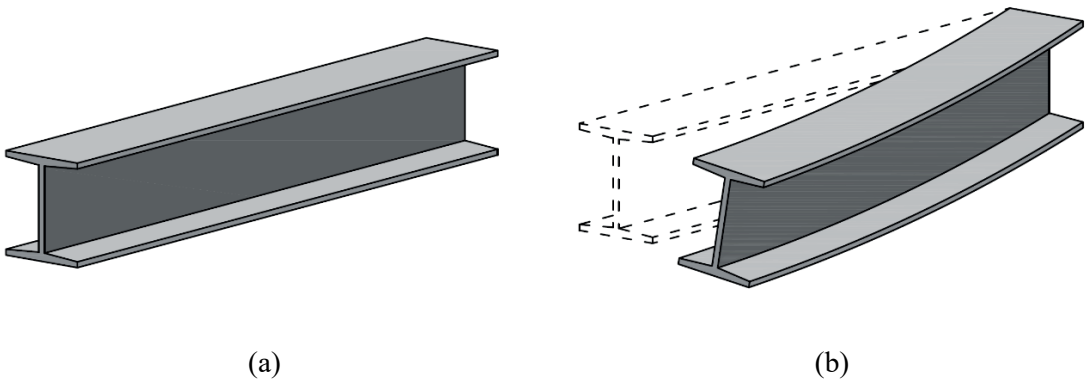


**Fig. 1.** Schematic representation of lateral-torsional buckling showing (a) an undeformed beam segment and (b) the beam segment undergoing displacement and twisting.

Lateral torsional buckling is one of the known failure modes of beams and columns. It is a global failure, in which the entire beam assumes a buckled shape due to longitudinal compressive or transverse loads.

The mechanics of LTB are related to the behavior of the two flanges of the beam. While undergoing bending, the top flange of the beam is subjected to compression and the bottom flange is subjected to tension. Because of the materials resistance against deformation, the compression flange will try to retain its original length. The “path of least resistance” for doing this is bending out of the vertical plane. The top flange therefore undergoes vertical and lateral deflection.

In order to retain its original length, the tensile flange will stay straight relative to the longitudinal axis of the beam. It undergoes vertical and lateral deflection just like the top flange. However, the lateral deflection of the bottom flange is insignificant relative to that of the top flange.

The larger lateral deflection of the compressive flange and the smaller lateral deflection of the tensile flange result in a twisting motion of the beam cross section. The centroid of the deformed section is located at a different position than that of the undeformed section, and the deformed section is rotated, i.e. oriented at an angle, relative to the undeformed section.

LTB in I-beams can be reduced or prevented by lateral restraints. These will work in a way that stiffen the web and thereby increasing the bending resistance, making the member less susceptible to LTB. Lateral restraints are spaced out evenly throughout the beam length (or column height), with a spacing length dependent on the section dimensions and the nature and magnitudes of the external loading on the structure. Closed sections like rectangular hollow sections RHS have sufficient resistance in the lateral direction and are not susceptible to LTB. These sections tend to fail due to other modes like local buckling and material failure.

A schematic view of a beam cross section subjected to LTB is shown in Fig. 2. The dotted line represents the position and orientation of an undeformed section, while the shaded area represents those of a deformed section. When operating in a 2D plane, three parameters can be used to describe the change in position and orientation between the two sections. These are the vertical deflection  $w$ , the horizontal deflection  $v$  and the rotation angle  $\phi$ . The horizontal deflection is often referred to as the lateral deflection. For a beam with a central vertical point load the largest value of all these parameters occur at the center span of the beam. Refer to section 2.2 for further definitions of the principal axes, displacement and angles.

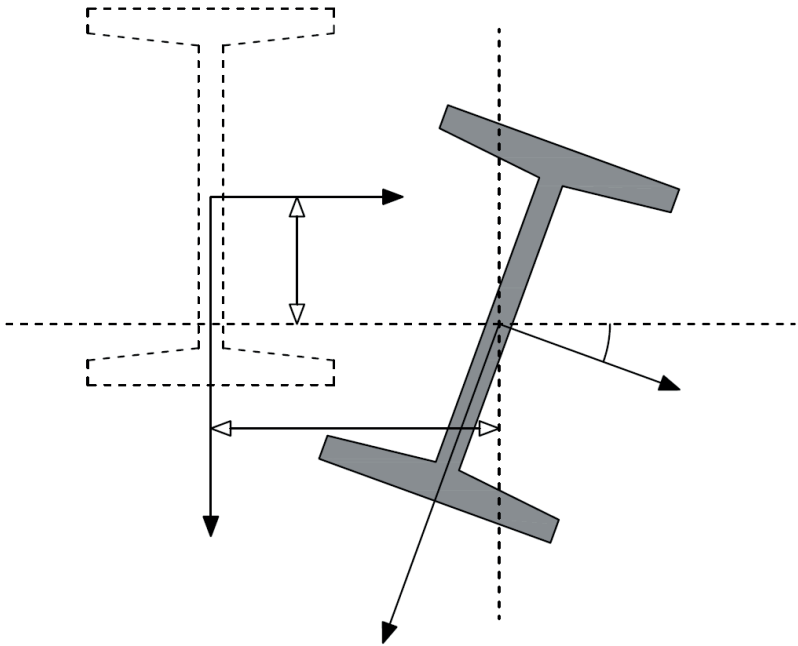


**Fig. 2.** Schematic view of a beam cross section subjected to LTB. Note: The translations and rotations of the deformed cross section relative to the initial cross section are highly exaggerated; A structural steel beam would fail due to local buckling and collapse before reaching such a large deformation relative to the cross-sectional dimensions.

## 2.2 Definitions

### 2.2.1 Nomenclature

Table 1 provides an overview of the different symbols used in the figures and equations presented in this thesis. All the units are given in terms of standard SI units.

**Table 1.** Symbols, definitions and units used in this thesis.

<b>Symbol</b>	<b>Definition</b>	<b>Unit</b>
$I_y$	Moment of inertia about the $y$ -axis	$m^4$
$I_z$	Moment of inertia about the $z$ -axis	$m^4$
$I_w$	Warping constant	$m^6$
$I_t$	St. Venant's torsional constant	$m^4$
$E$	Young's modulus	$N/m^2$
$G$	Shear modulus	$N/m^2$
$M_y$	Moment about the $y$ -axis	$Nm$
$v$	Lateral displacement along the $y$ -axis	$m$
$w$	Lateral displacement along the $z$ -axis	$m$
$\varphi$	Twisting angle	$rad$
$M_{cr}$	Elastic critical moment for lateral-torsional buckling	$Nm$
$L$	Beam length	$m$
$P$	Point load	$N$
$A$	Cross-sectional area	$m^2$
$h$	Height of cross section	$m$
$b$	Width of cross section	$m$
$t_f$	Thickness of flange	$m$
$t_w$	Thickness of web	$m$
$P$	Applied concentrated load	$N$
$z_Q$	Distance (height) from neutral axis to the point of loading	$m$
$f_y$	Yield strength of steel/material	$N/m^2$

## 2.2.2 Reference System and Principal Axes

The global coordinate system used in this thesis for definitions, references and analysis is defined as shown in Fig. 3.

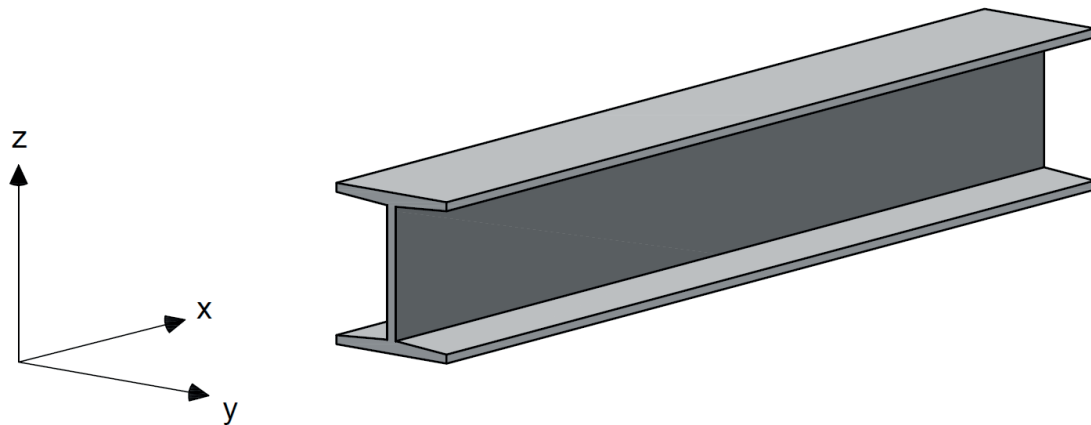


**Fig. 3.** Figure showing the coordinate system corresponding to the beam axes.

The principal axes of a beam are defined in accordance with Fig. 3. The  $x$ -axis is the longitudinal axis of the beam. The  $y$ -axis is the horizontal, or lateral, axis and the  $z$ -axis is the vertical axis. The following sign convention is adopted:

- Positive direction along the  $z$ -axis is the same as the direction of loading, i.e. downwards for all theoretical, numerical and experimental considerations in this thesis.
- Positive direction along the  $x$ -axis is chosen arbitrarily for each separate consideration.
- Positive direction along the  $y$ -axis is towards the right when viewing along the positive direction along the  $x$ -axis.
- Positive rotation is clockwise when viewing along the positive direction along the  $x$ -axis.

This coordinate system of principal axes and the sign convention is used throughout the entire thesis unless stated otherwise. Note: In ANSYS Workbench 17 used in the numerical analysis, the naming of the axes in the reference coordinate system is different from the ones stated above.

## 2.3 Derivation of the Elastic Critical Moment

The elastic critical moment  $M_{cr}$  is the value of the buckling moment about the y-axis,  $M_y$ , at which out-of-plane deformations start to occur [1]. These deformations are said to be out-of-plane because they do not occur in the stiffer principal plane of the beam, i.e. the plane consisting of the longitudinal and vertical axes of the beam. In-plane bending is the case of deformations aligning with the direction of loading, and this happens when  $M_y < M_{cr}$ .

In this section the derivation of the elastic critical moment is written out according to da Silva et al. [2]. The following assumptions are made:

- The beam is perfect, i.e. there are no imperfections with respect to geometry or material. Geometrical imperfections in general can be described as initial deviations from a straight beam and from the intended cross section.
- The cross section is doubly symmetric, i.e. there is symmetry about both the y- and the z-axis.
- The material behaves in a linear elastic manner, i.e. the distribution of strain is linear within any given cross section throughout the beam length, and hence, initially plane sections remain plane after deformation.
- The lateral displacements of the beam are small. When the displacement of a point close to the middle of the beam is small relative to the beam length, the angle of rotation, or the slope, of the beam is small. Mathematically, this translates to  $\sin \varphi \approx \varphi$  and  $\cos \varphi \approx 1$ .

It is necessary to establish expressions that describe the mathematical relations of bending and torsion with corresponding deformations. These are given in Eq. 1-3.

Bending about  $y'$ -axis:

$$EI_y \frac{d^2 w(x)}{dx^2} + M_y = 0 \quad \text{Eq. 1}$$

Bending about  $z'$ -axis:

$$EI_z \frac{d^2 v(x)}{dx^2} + \varphi(x) M_y = 0 \quad \text{Eq. 2}$$

Torsion about  $x'$ -axis:

$$EI_w \frac{d^3 \varphi(x)}{dx^3} - GI_t \frac{d\varphi(x)}{dx} + M_y \frac{dv(x)}{dx} = 0 \quad \text{Eq. 3}$$

At any given point along the beam, the lateral displacements are given as the distances between the centroids of the initially undeformed cross section and the deformed cross section. The rotation is defined as the angle between the principal axes of the undeformed cross section and those of the deformed cross section.

Differentiating Eq. 3 with respect to  $x$  results in the following:

$$EI_w \frac{d^4 \varphi(x)}{dx^4} - GI_t \frac{d^2 \varphi(x)}{dx^2} + M_y \frac{d^2 v(x)}{dx^2} = 0 \quad \text{Eq. 4}$$

Rearranging Eq. 2 yields:

$$\frac{d^2 v(x)}{dx^2} = -\frac{M_y}{EI_z} \varphi(x) \quad \text{Eq. 5}$$

Inserting Eq. 5 into Eq. 4 results in a 4<sup>th</sup> order differential equation with only one variable,  $\varphi(x)$ :

$$EI_w \frac{d^4 \varphi(x)}{dx^4} - GI_t \frac{d^2 \varphi(x)}{dx^2} - \frac{M_y^2}{EI_z} \varphi(x) = 0 \quad \text{Eq. 6}$$

The solution to this differential equation is given in the following form:

$$\varphi(x) = D_1 \sin mx + D_2 \cos mx + D_3 e^{nx} + D_4 e^{-nx} \quad \text{Eq. 7}$$

Where the constants  $m$  and  $n$  are given by the below equations:

$$m = \sqrt{-a + \sqrt{a^2 + b}} \quad n = \sqrt{a + \sqrt{a^2 + b}} \quad \text{Eq. 8a-d}$$

$$a = \frac{GI_t}{2EI_w} \quad b = \frac{M_y^2}{EI_z EI_w}$$

The supports prevent both lateral displacement and twisting:

$$\text{At } x = 0 \text{ and } x = L: \quad v = w = \varphi = 0 \quad \text{Eq. 9}$$



When warping torsion is induced on a cantilever beam, the fixed end disables warping and results in warping moments  $M_{sup}$  and  $M_{inf}$  being developed. These moments act perpendicular to the cross-sectional plane, and are related to what is known as the bimoment,  $B = M_{sup}h_m = M_{inf}h_m$ , where  $h_m$  is the distance between the moments. The bimoment is responsible for the normal stress related to warping,  $\sigma_w$ .

The equation for the relation between the lateral displacement of the upper flange,  $v_{sup}$ , and the corresponding warping moment,  $M_{sup}$ , is as follows:

$$\frac{d^2 v_{sup}(x)}{dx^2} = -\frac{M_{sup}}{EI_{fz}} \quad \text{Eq. 10}$$

The expression for the lateral deflection of the upper flange is given in terms of the twisting angle and half the bimoment lever arm distance:

$$v_{sup}(x) = \varphi(x) \frac{h_m}{2} \quad \text{Eq. 11}$$

Since warping is allowed,  $M_{sup}$  does not develop:

$$M_{sup} = 0 \Rightarrow \frac{d^2 v_{sup}(x)}{dx^2} = 0 \quad \text{Eq. 12}$$

Differentiation of Eq. 11 twice yields:

$$\frac{d^2 v_{sup}(x)}{dx^2} = \frac{d^2 \varphi(x)}{dx^2} \frac{h_m}{2} \quad \text{Eq. 13}$$

Equating the two expressions in Eq. 11 and Eq. 12 leads to the following observation:

$$\text{At } x = 0 \text{ and } x = L: \quad \frac{d^2 \varphi}{dx^2} = 0 \quad \text{Eq. 14}$$

Inserting the above results in Eq. 7 leads to the following constant values:

$$D_2 = 0 \quad , \quad D_3 = -D_4 \quad \text{Eq. 15}$$

Inserting the constant values from Eq. 15 into Eq. 7 and applying the hyperbolic trigonometric identity  $\sinh ax = (e^{ax} - e^{-ax})/2$  results in the following equation for  $x = L$ :

$$D_1 \sin mL - 2D_4 \sinh nL = 0 \quad \text{Eq. 16}$$

Differentiating Eq. 16 twice and using the result in Eq. 13 yields:

$$D_1 m^2 \sin mL + 2D_4 n^2 \sinh nL = 0 \quad \text{Eq. 17}$$

For a non-trivial solution of Eq. 16 and Eq. 17 to be obtained, the determinant of this system of equations must equal zero:

$$(\sin mL)(\sinh nL)(2m^2 + 2n^2) = 0 \quad \text{Eq. 18}$$

The non-trivial solution is only obtained if  $\sin mL = 0$  as  $m$  and  $n$  are positive real quantities and  $\sin nL = 0$  only if  $nL = n = 0$ . The first solution to  $\sin mL = 0$  is given by  $m = \pi/L$ , which results in the following:

$$-a + \sqrt{a^2 + b} = \left(\frac{\pi}{L}\right)^2 \quad \text{Eq. 19}$$

The formula for  $M_{cr}$  is obtained by combining Eq. 19 and the expressions for  $a$  and  $b$  in Eq. 8c-d, denoting  $M_y$  as  $M_{cr}$ :

$$M_{cr} = \frac{\pi}{L} \sqrt{GI_t EI_z \left(1 + \frac{\pi^2 EI_w}{L^2 GI_t}\right)} \quad \text{Eq. 20}$$

This formula for  $M_{cr}$  is only valid for a beam with equal end moments and gives the reference value for the elastic critical moment. Trahair et al. denotes this value  $M_{zx}$  so that  $M_{cr} = M_{zx}$  for a beam with equal end moments. The same notation is adopted in this thesis.

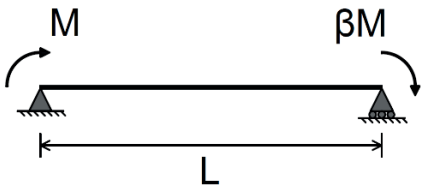
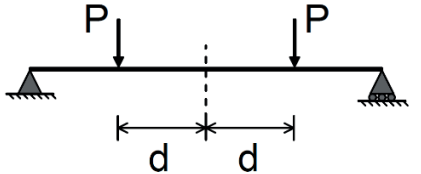
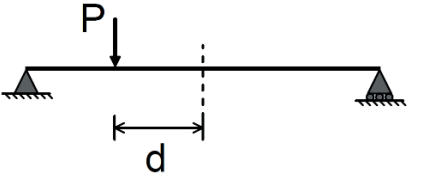
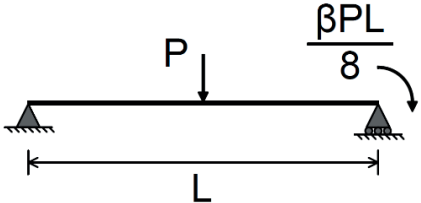
## 2.4 Modifications to the Elastic Critical Moment

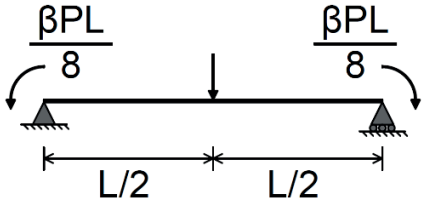
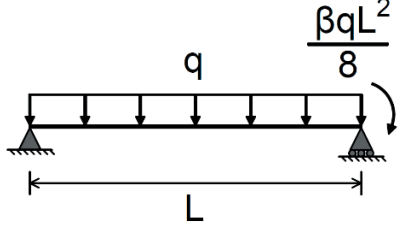
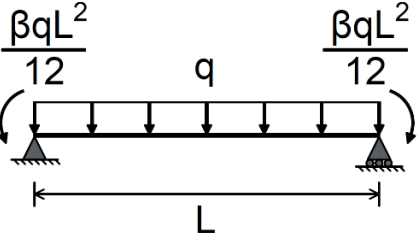
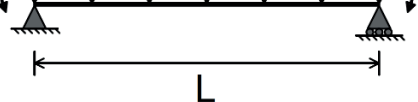
For other load situations a correction factor  $\alpha_m$  is introduced. The value of this factor is estimated so that the critical load for any given load situation is equal to:

$$M_{cr} = \alpha_m M_{zx} \tag{Eq. 21}$$

Values of the correction factor  $\alpha_m$  for different load configurations is given in Table 2.

**Table 2.** Loading conditions and corresponding modification factors, modified from Da Silva et al. [2].

Member and loading	Factor $\alpha_m$	Validity limits
	$1.75 + 1.05\beta + 0.3\beta^2 \leq 2.5$	
	$1.0 + 0.35 \left(1 - \frac{2d}{L}\right)$	
	$1.35 + 0.4 \left(\frac{2d}{L}\right)$	
	$1.35 + 0.15\beta$	
	$-1.2 + 3\beta$	

	$1.35 + 0.36\beta$	
	$1.13 + 0.10\beta$	
	$1.13 + 0.12\beta$	
	$-2.38 + 4.8\beta$	

# 3 Experimental Analysis

The experimental analysis was conducted in the lab for constructions and materials testing at the University of Stavanger by Mikael Ruud in relation to a bachelor thesis. This chapter is referencing the mentioned thesis [3] for details on the experimental setup and results from the testing.

## 3.1 Experimental Setup

### 3.1.1 Support and Loading Configuration

The entire experimental setup consisted of a supporting rig, a loading rig, the test specimens and measuring equipment. The beams were supported by two cut out steel plates that would prevent the beam ends from moving too far out of place. These plates act as simple supports for the beam, allowing rotation about the horizontal lateral axis and translation to a certain extent in the longitudinal direction, similar to that of a simply supported beam with a roller support at one end.

The vertical point load was applied by a high strength steel plate connected to a hydraulic extender, which in turn was connected to a control board. A connected computer allows for monitoring and extracting data on load magnitude vs. time.

The total test set consisted of nine specimens, each of a separate profile and length combination. Three different profiles – IPE200, IPE240 and IPE270 – and three beam lengths – 2.00, 2.25 and 2.50 meters – of each profile were used. The profiles are shown in Fig. 5. This choice was made for the testing to include different sections and beam lengths to see what effects these parameters has on the results.

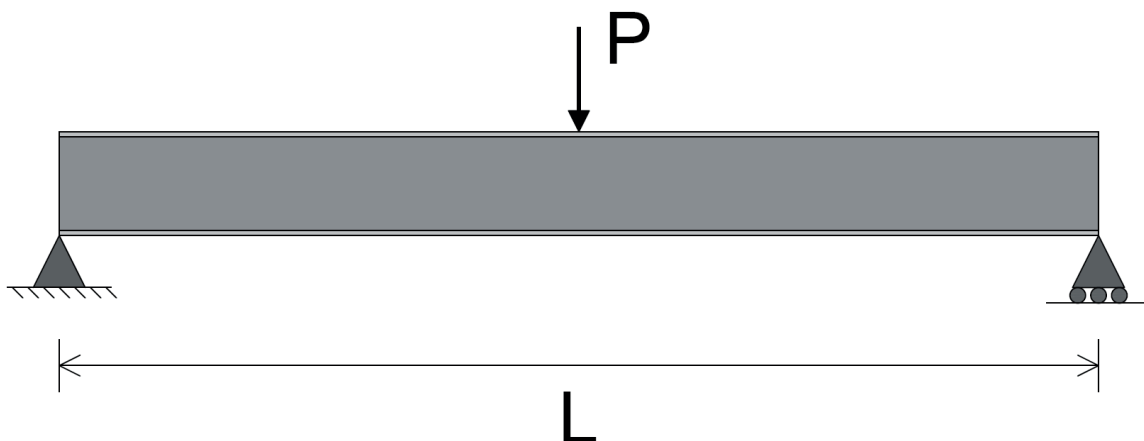


**Fig. 4.** Schematic view of the beam with supports and loading. The vertical point load acts at the mid-span of the beam directly on top of the upper flange.

### 3.1.2 Measuring Equipment

A total of three different measuring systems were used in the testing of the beams – Two response measuring devices and one force measuring device. The responses, namely deflections and strains, were measured using relative displacement rulers and a DIC system.

The rulers were placed in order to measure vertical deflection of the beam and the horizontal deflections of the top and bottom flanges, all measured at the mid-span where the deflections are largest. The measurements were recorded and used for plots of vertical load vs. deflection of the separate beams.

The DIC is short for Digital Image Correlation and is a system used to measure strain and displacement on surfaces by high precision imaging technology. The system utilizes a special camera that takes pictures with set time intervals during the deformation of the test specimen. The steel beams were spray painted with a white layer followed by black dots for the camera to be able to respond to shape changes.

### 3.1.3 Beam Dimensions and Material

**Table 3:** Material properties of the beams.

Material properties	
Material	Steel grade S355
Modulus of elasticity	210 GPa
Shear modulus	81 GPa
Poisson's ratio	0.3

**Table 4:** Cross section dimensions and geometrical properties of the three different beam cross sections.

Cross section dimensions and geometrical properties			
Cross section	IPE 200	IPE 240	IPE 270
Height	200 mm	240 mm	270 mm
Width	100 mm	120 mm	135 mm
Web thickness	5.6 mm	6.2 mm	6.6 mm
Flange thickness	8.5 mm	9.8 mm	10.2 mm
Roller radius	12 mm	15 mm	15 mm
Moment of inertia about y-axis	$19.4 \cdot 10^6 \text{ mm}^4$	$38.9 \cdot 10^6 \text{ mm}^4$	$57.9 \cdot 10^6 \text{ mm}^4$
Moment of inertia about z-axis	$1.42 \cdot 10^6 \text{ mm}^4$	$2.84 \cdot 10^6 \text{ mm}^4$	$4.20 \cdot 10^6 \text{ mm}^4$
St Venant's constant	$70.2 \cdot 10^3 \text{ mm}^4$	$129 \cdot 10^3 \text{ mm}^4$	$160 \cdot 10^3 \text{ mm}^4$
Warping constant	$12.99 \cdot 10^9 \text{ mm}^6$	$37.39 \cdot 10^9 \text{ mm}^6$	$70.58 \cdot 10^9 \text{ mm}^6$

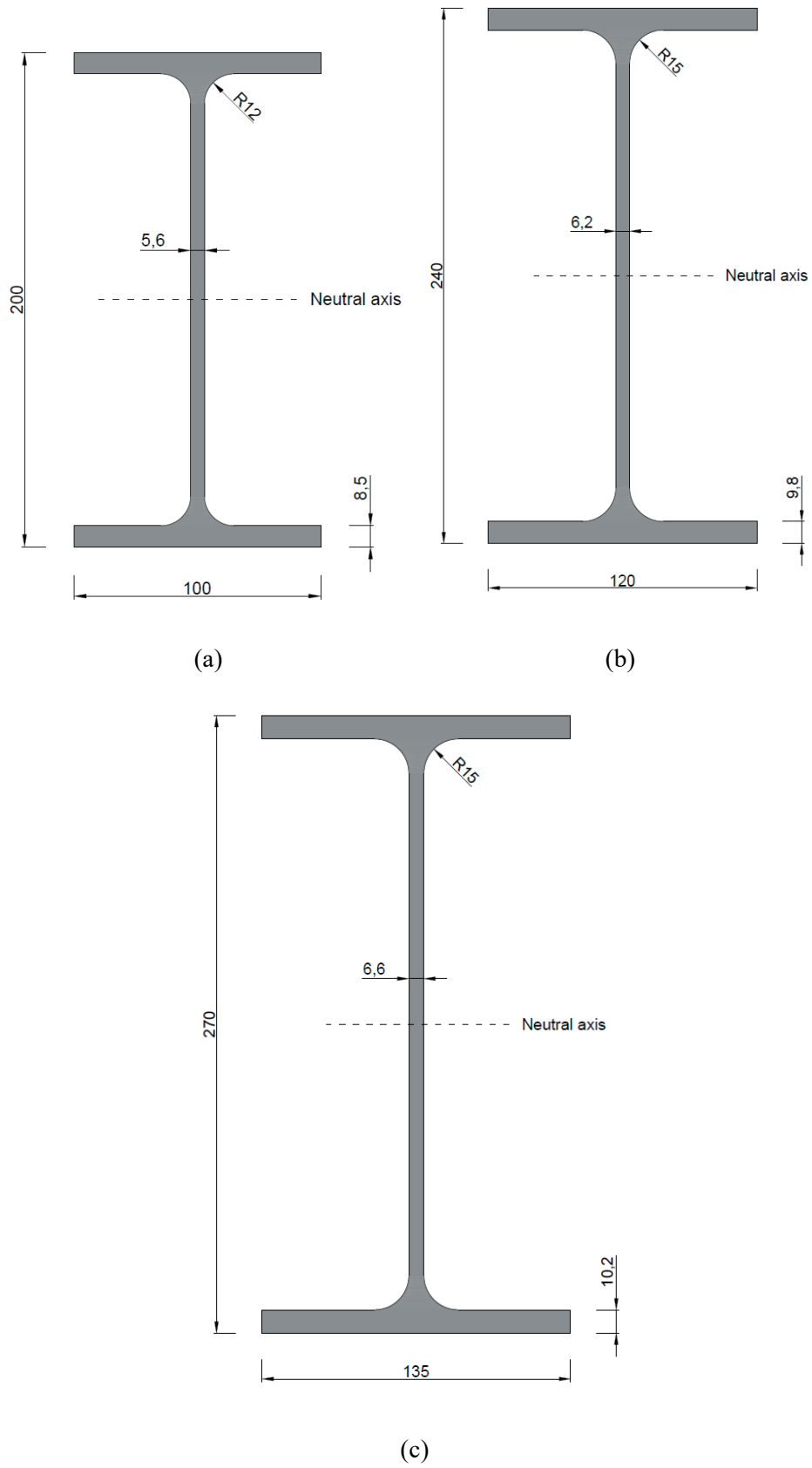


**Fig. 5:** Cross sectional views of the three different profiles used in the experimental testing and in the numerical simulations. (a) IPE200, (b) IPE240 and (c) IPE270.

### 3.1.4 Testing Procedure

During the experimental testing, the beams were loaded to the point of local buckling failure. The overall beams were still in the elastic region, as they returned to their original position after removing the load. This can also be verified by checking the maximum applied load vs. the theoretical elastic limit/strength of the beam. However, local failure occurred at the loading point of action. Technically speaking this is the mid span section of the beam, but it is referred to as a point.

## 3.2 Experimental Results

In this section, results from the experimental analysis are presented. These are plots of the vertical load vs. lateral deflection of the top flange at the mid-span of the beam, where the deflection is the largest. The results were compiled from the load data and the lateral displacement data, and each plot corresponds to one test specimen.

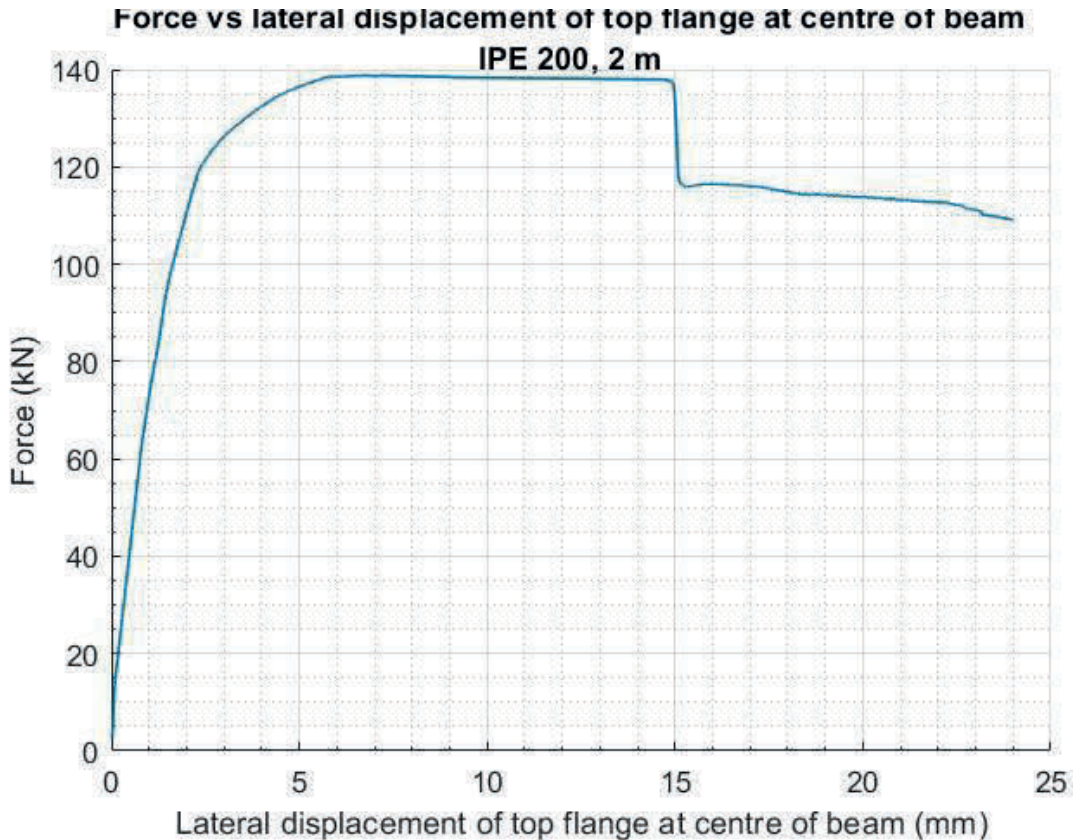
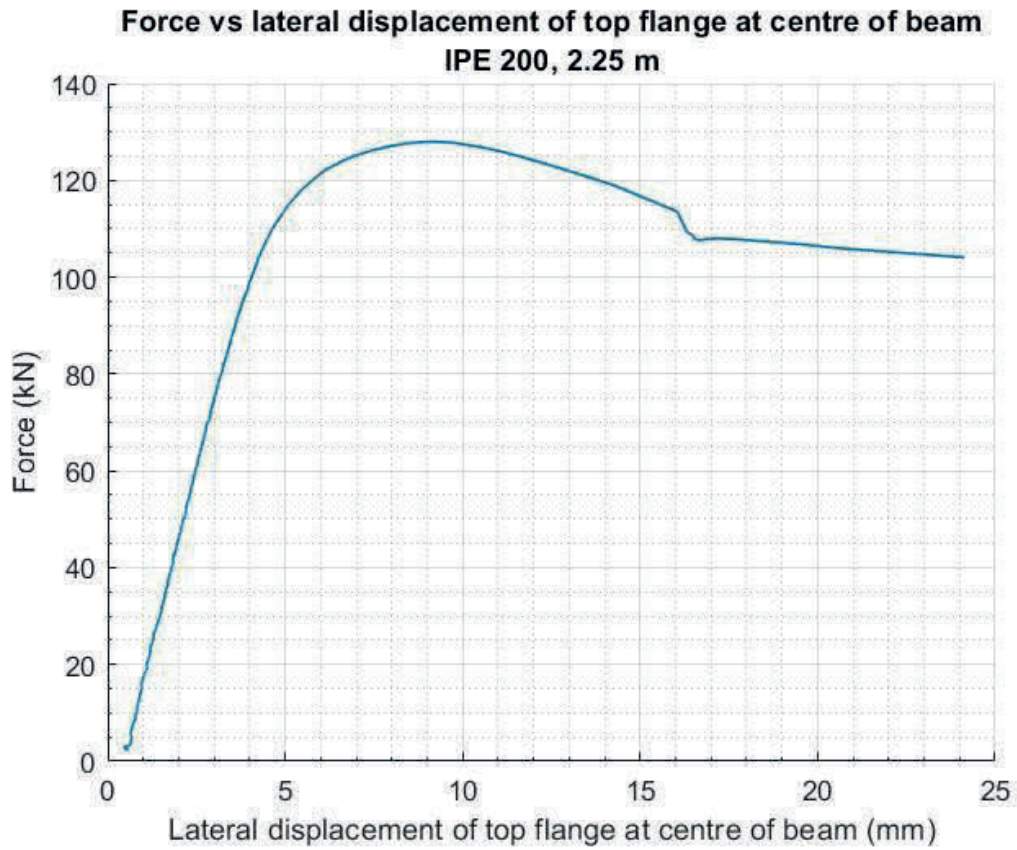
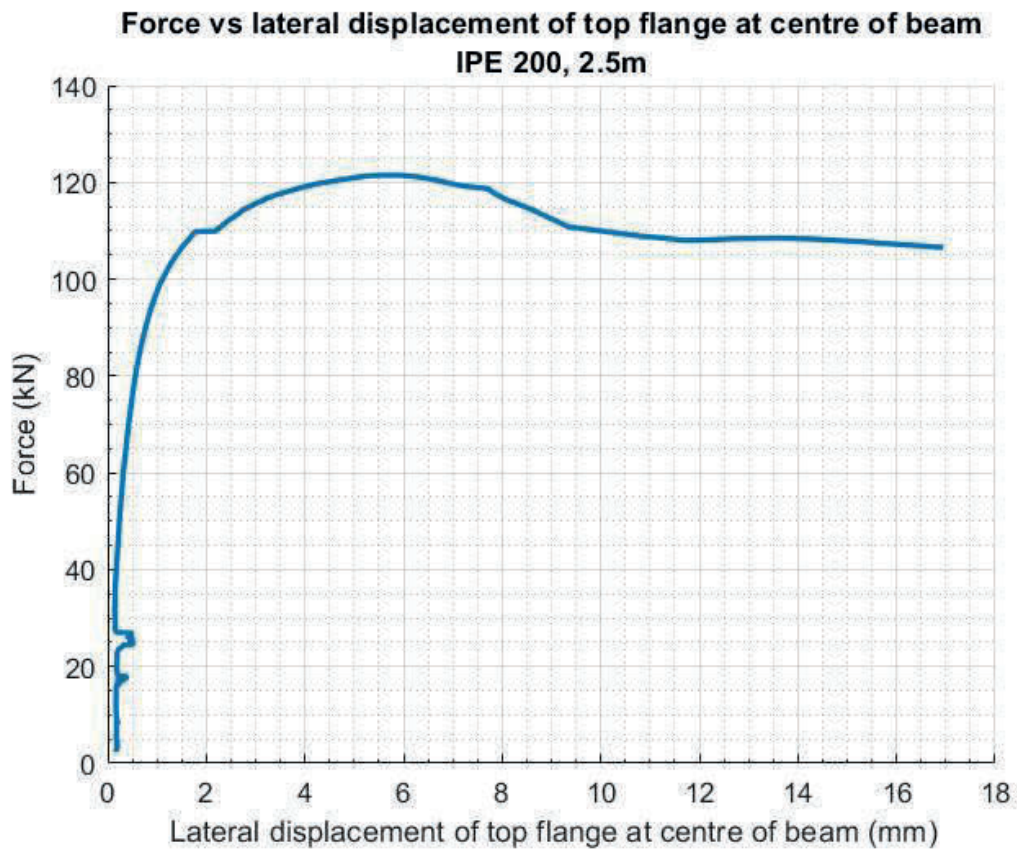


Fig. 6. Force vs. lateral displacement for IPE200, 2.00 m length.





**Fig. 7.** Force vs. lateral displacement for IPE200, 2.25 m length.



**Fig. 8.** Force vs. lateral displacement for IPE200, 2.50 m length.

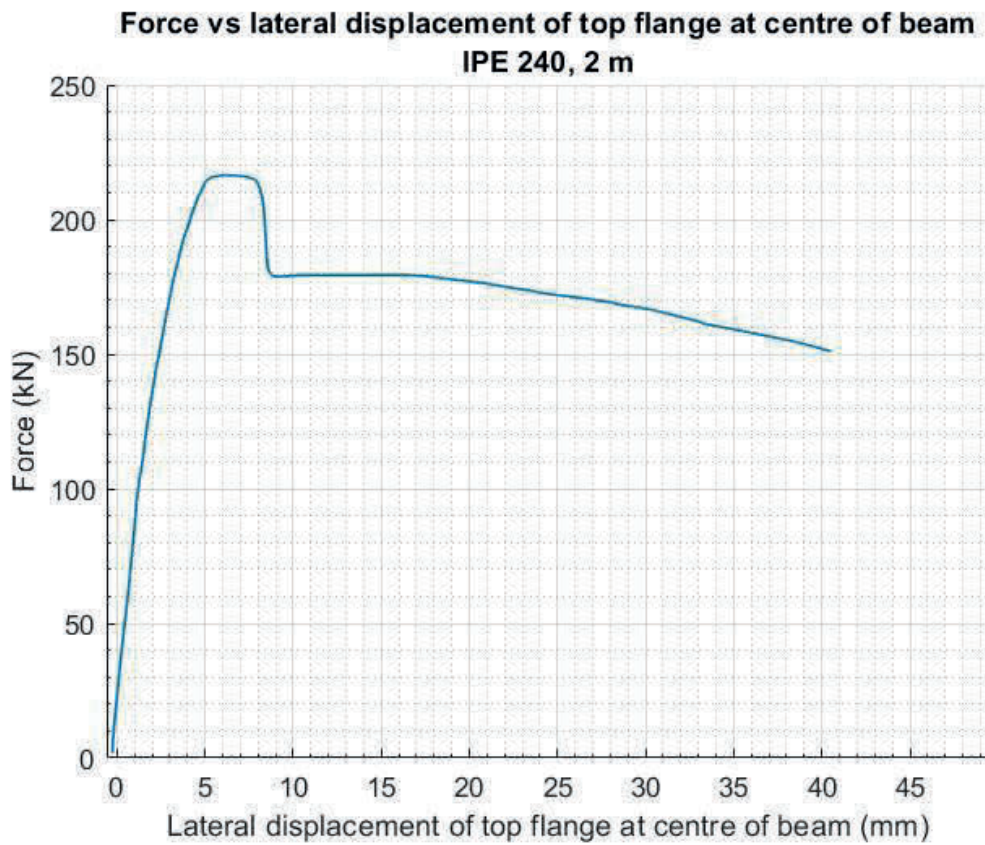


**Fig. 9.** Force vs. lateral displacement for IPE240, 2.00 m length.

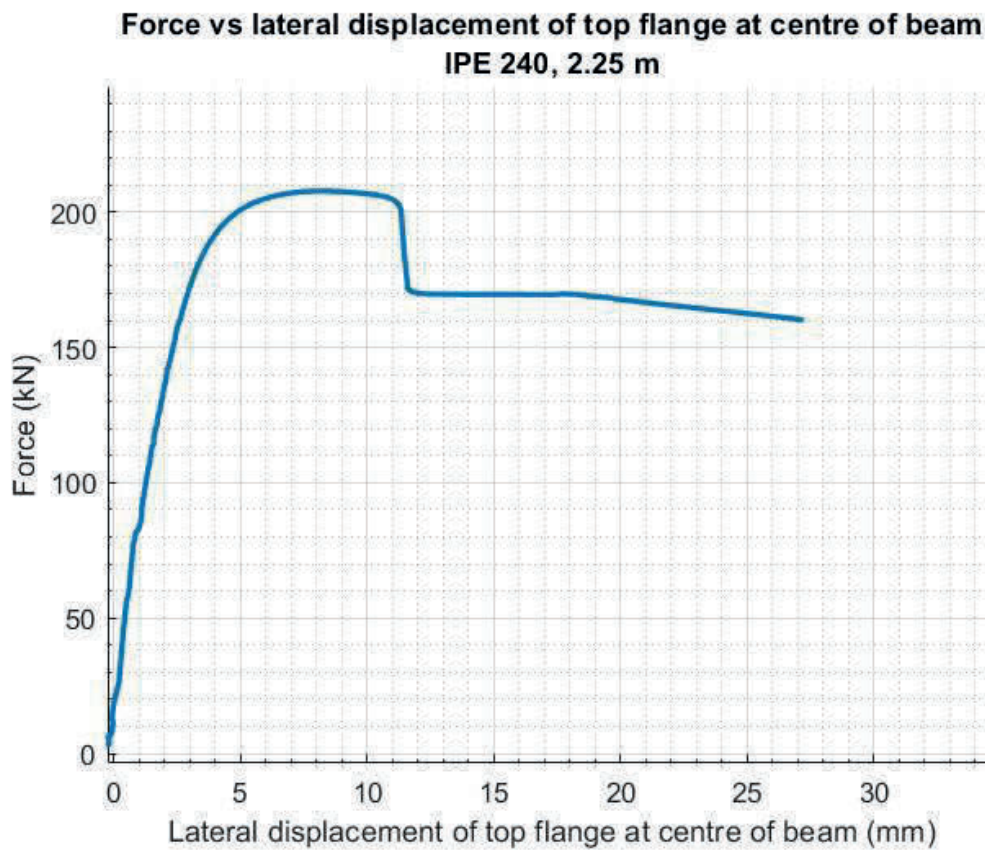


**Fig. 10.** Force vs. lateral displacement for IPE240, 2.25 m length.

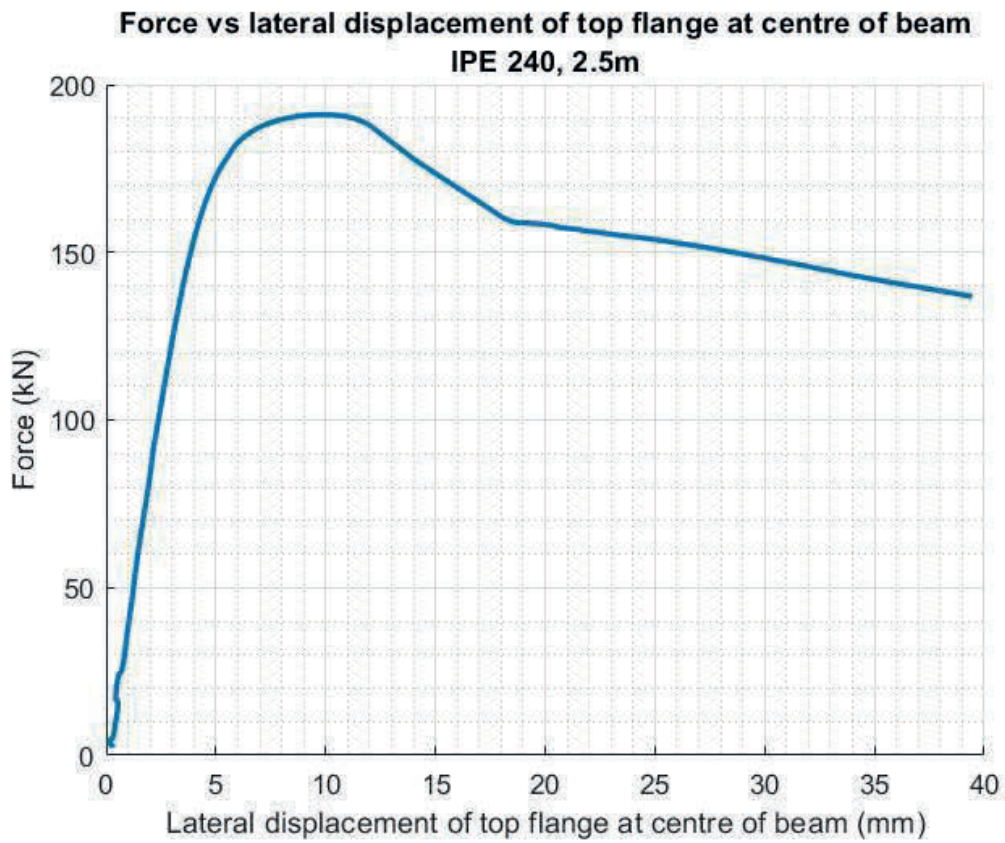


**Fig. 11.** Force vs. lateral displacement for IPE240, 2.50 m length.

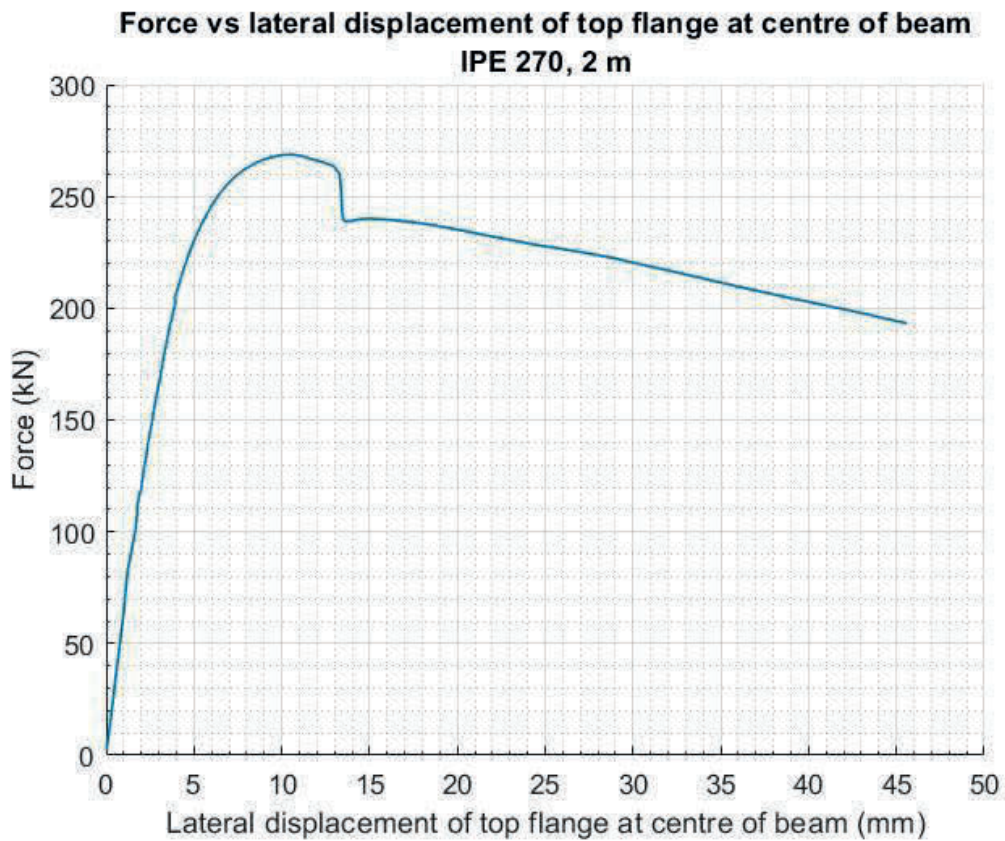


**Fig. 12.** Force vs. lateral displacement for IPE270, 2.00 m length.

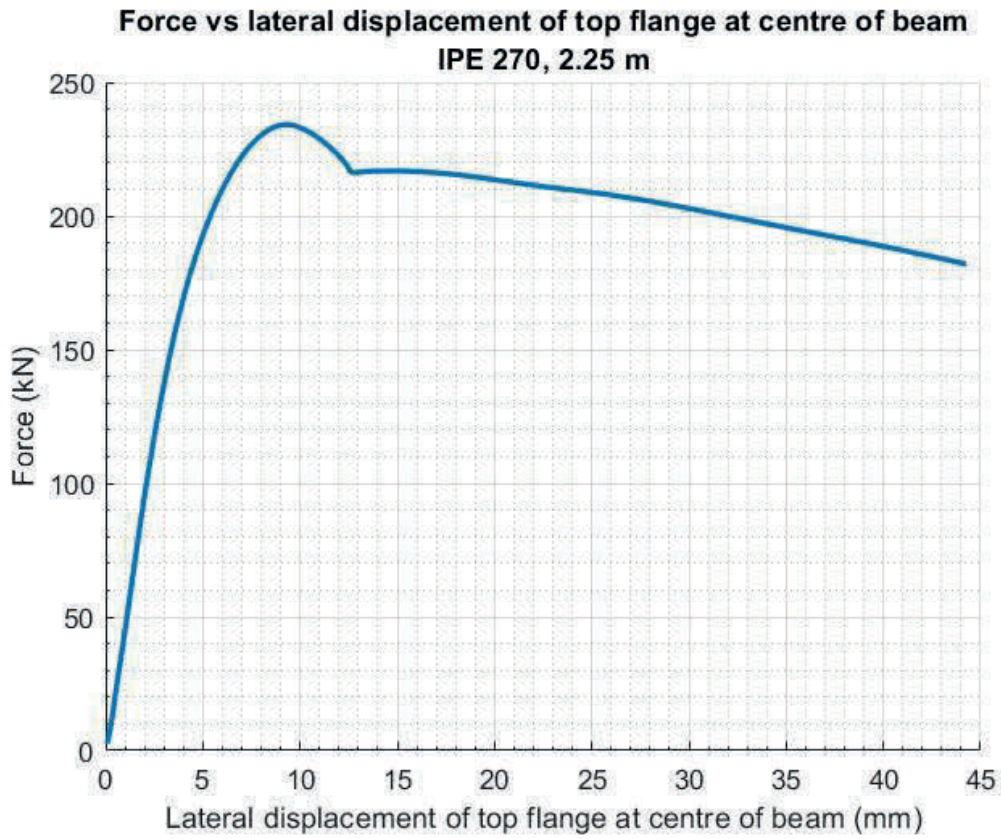


**Fig. 13.** Force vs. lateral displacement for IPE270, 2.25 m length.

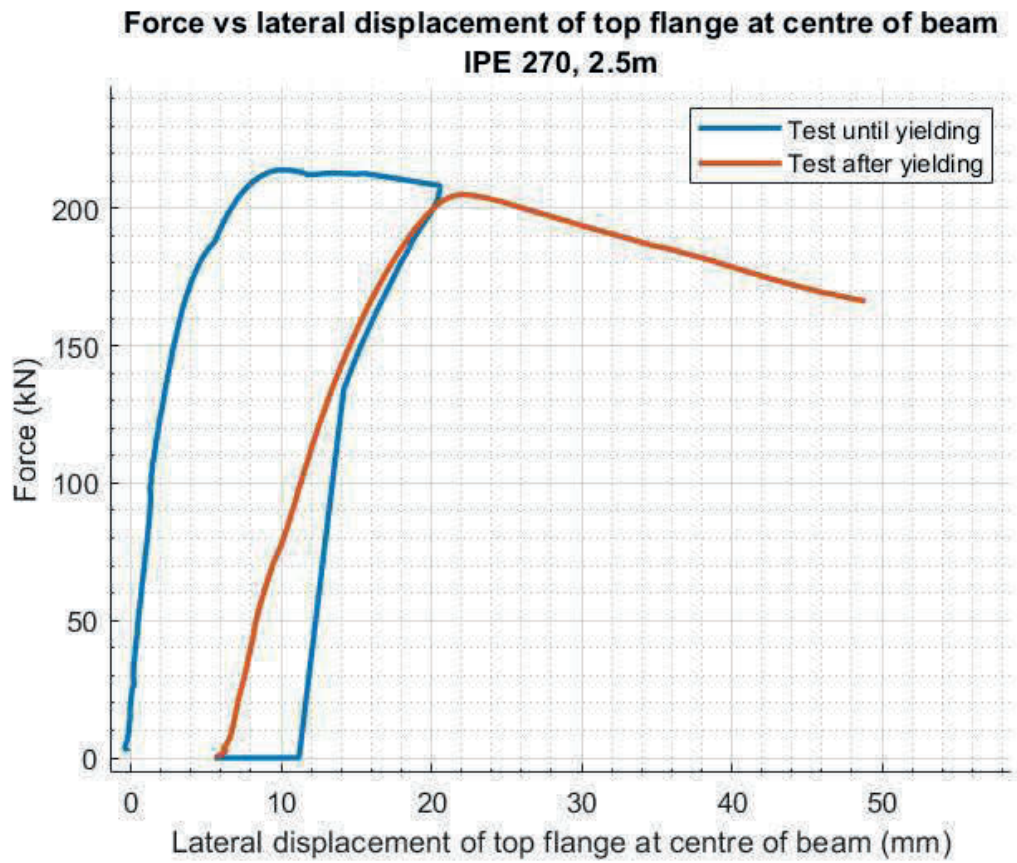


**Fig. 14.** Force vs. lateral displacement for IPE270, 2.50 m length.

### 3.3 Previously Conducted Tests

A substantial amount of work has been done regarding LTB and buckling capacity of steel members. This section will focus on previously conducted studies with the intent to provide a general overview of the type of work done, the different geometrical, material and loading configurations studied, the models used and the results of these tests.

Analytical, numerical and experimental analyses have been carried out, some of which have been used to compare with given code recommendations. Numerical analyses are presented in section 4.5. The current section will comprise some of the comparisons to give a perspective on which parameters are being calculated and discussed. The standards used in these studies include Eurocode 3, GB50017 and ANSI/AISC360-10.

Yang et al. [4] conducted an extensive experimental and numerical analysis on beams with I-section profiles. The members were made of Q460GJ steel plates welded together, where the specimens had the dimensions of 270x180x8x16 and 450x180x8x16 ( $h \times w \times t_w \times t_f$ ). Steel of this quality has a nominal yield strength of 460 MPa. The spans of the beams varied from 6 through 7 to 8 m. The beams were setup using simple supports.

Deflections were measured using linear variable displacement transducers, abbreviated LVDT's. These were placed at four different points along the beam's length. Strain gauges were used to measure strains at two of these points as well.

The results of this test were presented in the form of vertical load-displacement curves and lateral displacements versus normalized applied load. The greatest change in lateral direction was found to occur at a value of  $PL/(4M_{yc}) = 0.3$  in the pre-failure region. Failure occurred at  $PL/(4M_{yc}) = 0.8$ , represented by the load at which the LTB of the beam results in plastic deformation. In this post-failure region, a small change in applied load results in a large change in lateral displacement.

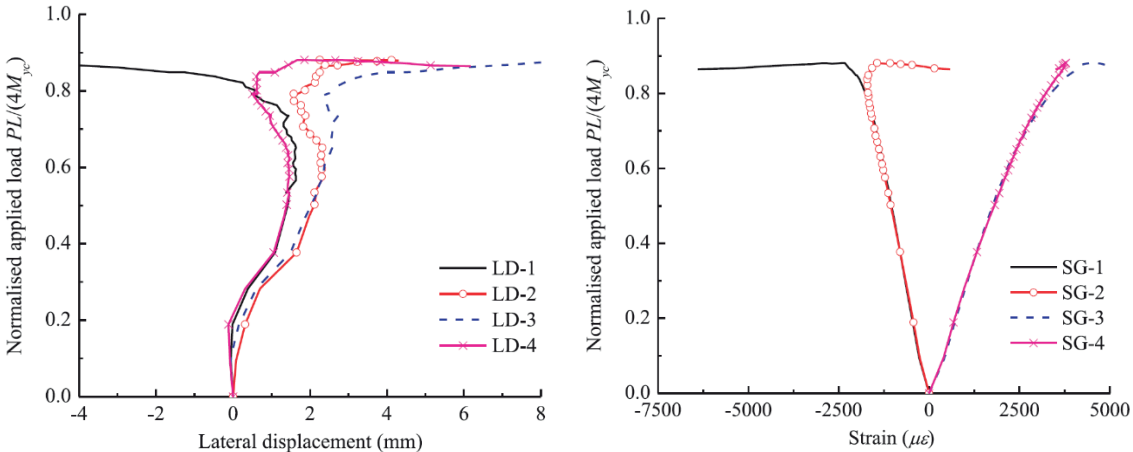


Fig. 15. Lateral displacements vs. normalized applied load. From Yang et al.

The plot of lateral displacement suggests that the beam undergoes LTB to one side in the beginning, but then assumes an antisymmetric buckling shape when close to failure. This means that one half of the beam buckles to one side while the other half buckles to the other.

The results were compared with different codes, namely GB50017-2003, GB50017-201X, Eurocode 3 and ANSI/AISC360-10. GB50017, which is the Chinese code of structural steel, provides a formula for buckling moment similar to that of EC3, which is the European code:

$$M_y = \chi_{LT} W_y f_y \quad \text{Eq. 22}$$

$$\chi_{LT} = \frac{1}{\Phi_{LT} + \sqrt{\Phi_{LT}^2 - \bar{\lambda}_{LT}^2}} \quad \text{Eq. 23}$$

$$\Phi_{LT} = 0.5[1 + \alpha_{LT}(\bar{\lambda}_{LT}^2 - 0.2) + \bar{\lambda}_{LT}^2] \quad \text{Eq. 24}$$

$$\bar{\lambda}_{LT}^2 = \sqrt{\frac{W_y f_y}{M_{cr}}} \quad \text{Eq. 25}$$

The ANSI/AISC360-10 is the code of the American Institute of Steel Construction, abbreviated AISC. This code provides a different formula for calculating the buckling moment:

$$M_n = C_b \left[ R_{pc} M_{yc} - (R_{pc} M_{yc} - F_L S_{xc}) \frac{L_b - L_p}{L_r - L_p} \right] \leq R_{pc} M_{yc} \quad \text{Eq. 26}$$

if  $L_p < L_b < L_r$   $M_n = F_{cr} S_{xc} \leq R_{pc} M_{yc}$

if  $L_r < L_b$

When comparing the experimental result with the different codes, the buckling moment of each test specimen was compared with the calculated value from each code. These were tabulated along with normalized values given by the ratio of the calculated value to the experimental value, so that the normalized values are given in the form of  $M_{calc}/M_{exp}$ . These are presented in Table below.

**Table 5:** Normalized values of analytical to experimental bending moments.

	<b>GB50017-2003</b>	<b>GB50017-201X</b>	<b>Eurocode 3</b>	<b>ANSI/AISC360-10</b>
Mean value for specimen with $h/b = 1.5$	1.00	0.95	0.91	0.84
Coefficient of variation for specimen with $h/b = 1.5$	0.030	0.010	0.045	0.063
Mean value for specimen with $h/b = 2.5$	0.93	0.80	0.80	0.92
Coefficient of variation for specimen with $h/b = 2.5$	0.022	0.025	0.014	0.077

As seen in the table above the experimental values compare well with the calculated values given in the Chinese code, especially for the profiles with an aspect ratio of 1.5. The values calculated in accordance to EC3 and the AISC standard deviate a bit more. Notably, the values obtained from AISC360-10 calculations have a relatively high variation with respect to the test results.

# 4 Numerical Analysis

This chapter focuses on the numerical analysis carried out for the purpose of handling this thesis' objectives.

## 4.1 Software

The software used to generate the model and obtain the results of the problem is ANSYS Workbench 17. This is a finite element analysis software, and the simulation process consists of separate systems comprising a flow chart model. The flow chart indicates the order in which the systems are processed.

There are different types of analysis systems. For the case of lateral-torsional buckling analysis it is necessary to use a combination of two separate systems, namely *Static structural* and *Eigenvalue buckling*. The static structural analysis system consists of the following cells:

1. Engineering data
2. Geometry
3. Model
4. Setup
5. Solution
6. Results

The *engineering data* is synonymous with the material model. All the material properties are listed in Appendix A section A.1. The *geometry* can be filled with a geometric model made within the program or imported from a file made in an external 3D CAD software. In this case the geometry is modelled in Autodesk Inventor. The *model* and *setup* cells provide the load model and finite element meshing of the geometry. Features like loads – i.e. forces, moments and pressures – and displacements can be added here in order to model the boundary conditions and external loads on the element or structure. The mesh is also generated and altered here. The *solution* shows the deformed model after every pre-processing and processing feature has been applied. The *results* can be shown in terms of different parameters calculated by the solution process. Examples are displacements, stresses, strains etc.

The eigenvalue buckling analysis system is identical to the static structural system in structure and consists of the same cells. The differences between the two systems are the analysis procedure, as the static structural solves the static equilibrium while the eigenvalue buckling estimates the eigenvalues and corresponding eigenvectors or modes similar to a modal analysis.

The two systems are connected within the flow chart so that the information from the cells *Engineering data* and *Model* is shared between the two blocks. The *solution* from the Static structural system is sent to the *setup* cell in the Eigenvalue buckling system. In this way the static structural analysis acts as a preliminary process to the buckling. Finally, another static structural system is used for the nonlinear buckling analysis. The information from the *Engineering data*, *Geometry* and *Model* cells in the Eigenvalue buckling system is shared with the second Static structural system. Refer to section 4.2.1 for theory on eigenvalue and nonlinear buckling.



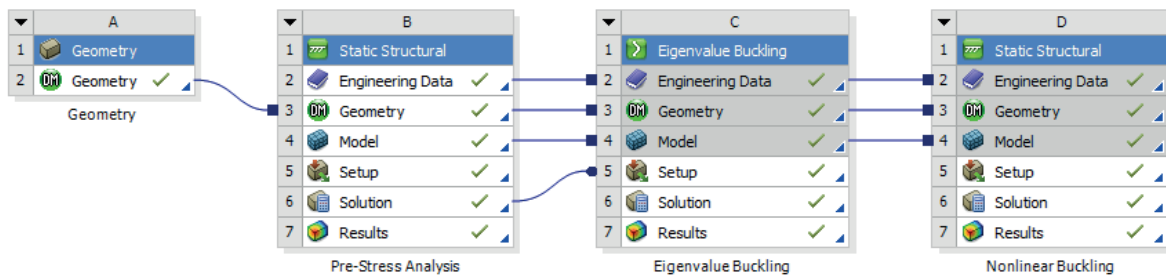


**Fig. 16.** Screenshot from ANSYS showing the flowchart model. System A is a component containing the geometry, system B and D are static structural systems and system C is an eigenvalue buckling system.

## 4.2 Model

The complete model can be described in terms of a geometric model, a material model and a load model. Combined, they provide the foundation for a numerical solution of the problem. Finite element modelling is summarized in the equation:

$$[\mathbf{K}][\mathbf{D}] = [\mathbf{R}] \quad \text{Eq. 27}$$

The material model is represented by the stiffness matrix  $[\mathbf{K}]$ , the load model is represented by the load matrix  $[\mathbf{R}]$  and the geometric model is represented by the size and shape of the matrices. The displacement matrix represents the solution of the problem, i.e. the results in terms of lateral displacement in this case. The ... equation can be altered in order to yield a different type of results, i.e. stress or strain instead of displacement.

The equation is of course a general representation of the load-displacement relationship of a structure or an element. The same relation can be found in special cases of axial deformation, bending and Hooke's law, known as the stress-strain relationship. In each of the cases related to structural mechanics, the stiffness matrix is derived from some sort of stiffness parameter. In axial deformation this parameter is  $AE$ , in bending cases it is  $EI$ , and in the stress-strain relationship it is simply  $E$ . In terms of shear stiffness, the parameter is given in terms of the shear modulus  $G$ , which is related to Young's modulus in the following way:

$$G = \frac{E}{2(1 - \nu)} \quad \text{Eq. 28}$$

## 4.2.1 Linear and Nonlinear Buckling Analyses

The buckling analysis consists of two separate concepts: Linear and nonlinear buckling.

The linear buckling analysis aims to provide a theoretical buckling load and theoretical buckling shape mode, much like in modal analysis. The theoretical buckling load, often given in terms of a unit load and a buckling load factor, is referred to as the eigenvalue of the analysis. Eigenvalue problems are solved by finding the eigenvectors and the corresponding eigenvalues of a mathematical problem.

The nonlinear buckling analysis is referred to as post-buckling analysis and aims to provide a definite solution of the buckling problem in terms of buckling loads and the corresponding quasi-static responses, i.e. final stresses or displacements. An increasing external load is applied to the element or structure in question. Every load increment is equal in magnitude, and the displacement corresponding to a given load is estimated for each step. For a single node in a FEA:

$$d_i = \frac{1}{k} \sum_{j=1}^i r_j \quad \text{Eq. 29}$$

For the entire system:

$$[\mathbf{D}]_i = \left( \sum_{j=1}^i [\mathbf{R}]_j \right) [\mathbf{K}]^{-1} \quad \text{Eq. 30}$$

With a given finite element model, consisting of a geometric model, material model and load model, the solution to this problem is found through a convergence series of data. If the intended result is lateral displacements of a beam, the buckling load can be found by running a convergence analysis in the form of tolerance and diminishing returns. The difference in lateral displacement between the last step and the second last step is calculated and compared to the total displacement throughout the entire iteration process. If the difference is less than a given tolerance level, often set to a percentage of the total lateral displacement at that step, the solution is given by the buckling load required for that displacement:

If  $d_i - d_{i-1} > e$  then continue iteration.

$$\text{If } d_i - d_{i-1} < e \text{ then stop iteration. Buckling load} = \sum_{j=1}^i r_j \quad \text{Eq. 31}$$

Generally, for the nonlinear buckling analysis to take place, an initial imperfection is necessary. This can be a small asymmetry in the finite element mesh or a small load, either nodal or body, in a given direction resulting in a slightly asymmetric loading situation.

With a solution for the buckling load, it is possible to obtain a solution for the resulting parameters like displacements and stresses, given geometric and material models. Using simulation software the solution for lateral displacement can be found, and ANSYS Workbench 17 offers/enables the opportunity to show the deformed shape of the structure under loading along with color coded contour plot showing the different values of the displacement.

In this thesis, the simulated buckling load is compared to the measured buckling load in the experimental analysis. The same comparison is done with the corresponding lateral displacements.

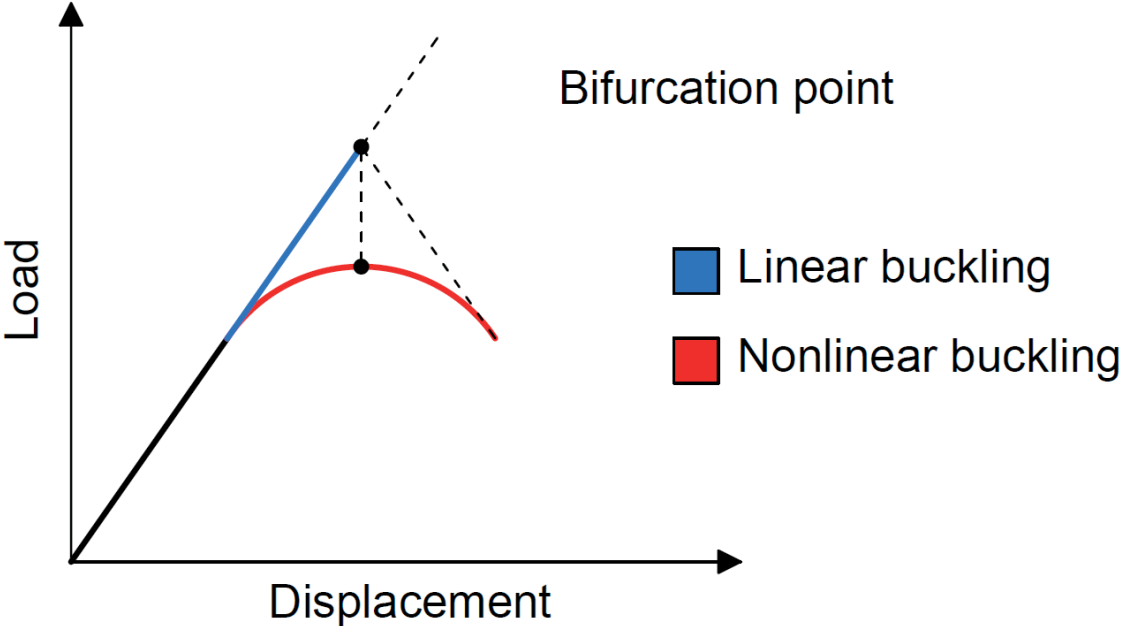


**Fig. 17.** Schematic figure of the load displacement relationship and the regions of linear and nonlinear buckling.

### 4.2.2 Force Convergence Theory

A convergence analysis is based on the principle that a parameter error or residual value must be smaller than a given tolerance level in order for the problem analysis to result in a balanced solution. In terms of a force convergence analysis the goal is to minimize the difference between external and internal forces so that the problem can be solved for a structure in equilibrium.

The difference between the externally applied loads and the internally reactive forces, termed the residual value, needs to be smaller than the given tolerance level, known as the convergence criterion, or more specifically the force criterion.

In the ANSYS force criterion solver output, the force convergence is the unbalanced force, or residual value, that is computed for each iteration of the finite element analysis of the model. The force criterion is the tolerance level below which the force convergence has to be at the end of the analysis.

The vertical lines corresponding to *Substep Converged* in the legend shows the step or substep number locations in the iteration process for which the value at that point converged, i.e. satisfies the convergence criterion.

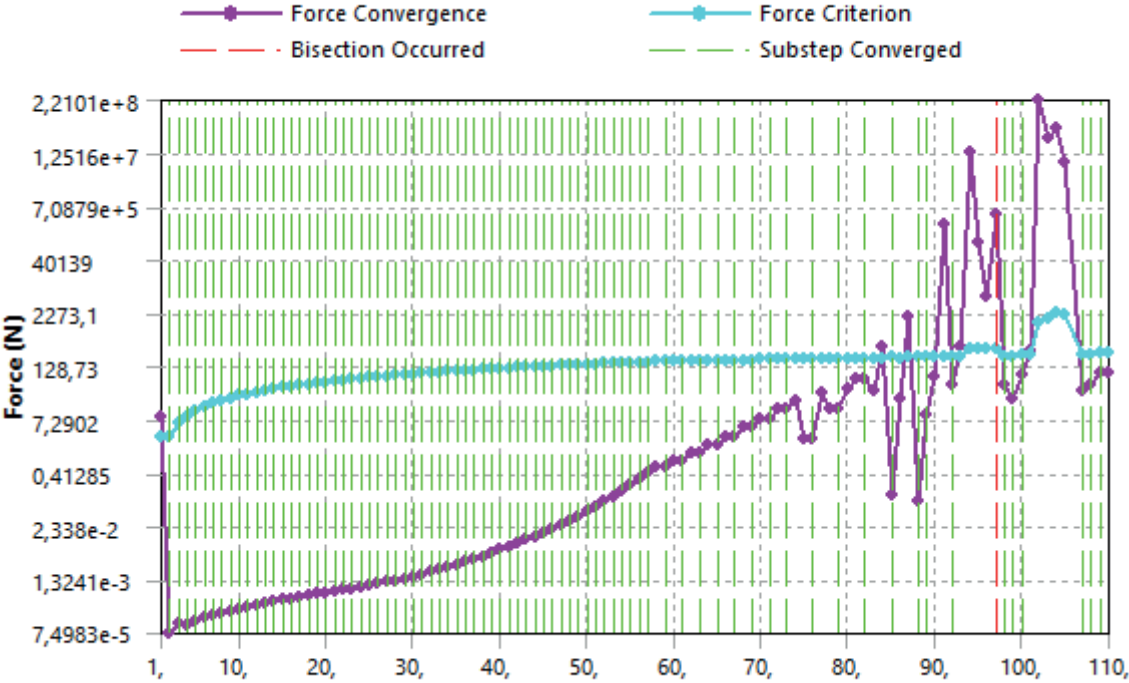


**Fig. 18.** Example of a force convergence plot. Taken from the ANSYS report on the simulation results for the IPE200 2-meter length beam model. Refer to Appendix.

As seen in the force convergence plots, the convergence value in the beginning of the analysis is around the order of  $10^{-5}$  while the criterion is in the order of  $10^1$ . This relation is characteristic of a balanced FE model. The convergence value steadily increases exponentially up until the time when the externally applied load is approximately 70-80 % of the total theoretical buckling load, or rather the applied vertical load in the program. This is the onset of the nonlinear behavior of the model (the equivalent of the elastoplastic region of materials), and the convergence value starts to increase drastically before returning to a value below the convergence criterion. This process repeats until the end of loading, resulting in the seemingly chaotic region of the convergence plot. This behavior of the algorithm is characteristic of the program’s attempt to model nonlinearity in the structural model, incorporating the given material properties and the mesh.

## 4.3 Initial testing

The initial testing phase involved trying out and finding the best boundary conditions, mesh configuration and iteration procedure details in the software in order to obtain the best results relative to the analytical and experimental data. The test was carried out/conducted using the beam model for the IPE200 cross section with a 2 m span length.

### 4.3.1 Preliminary Eigenvalue Buckling Analysis

The buckling analysis consists of two parts: Linear buckling, or eigenvalue buckling, and nonlinear buckling analyses. The first part involves finding the theoretical buckling load of the given model, and the second part incorporates a nonlinear analysis in the form of a force convergence solution.

A preliminary eigenvalue buckling analysis was carried out to find the best suited boundary conditions model when comparing the results to the experimental analysis. This was done by testing different support constraints at the end sections of the geometric beam model, conducting pre-stress and eigenvalue buckling analysis and comparing the results with the experimental results.

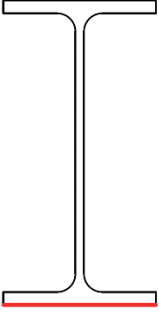
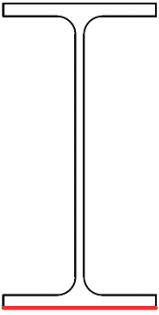
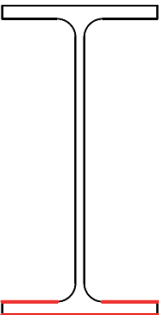
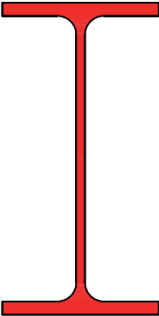
The pre-buckling analysis was done using the static structural analysis system in ANSYS. Common for all the tests were an externally applied unit load of 1 kN at the center span of the beam, placed centrally on the mid-section (just like in the ..., see FIG. X). Generally a unit load is placed where the real load in the model is to be placed. In this case it is a unit load of 1 kN. This way the buckling load factor/multiplier will provide the theoretical buckling load in kN when multiplied with the unit load of 1 kN.

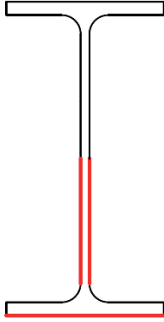
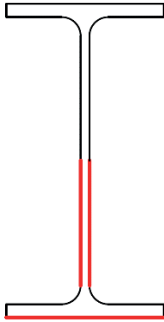
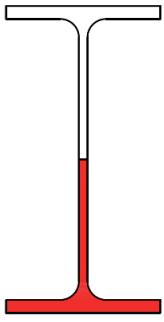
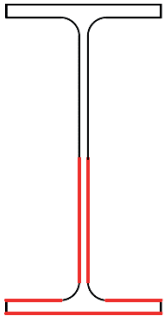
The linear buckling analysis was done using the eigenvalue buckling analysis system in ANSYS. This uses the pre-stress analysis solution and recognizes the resulting buckling modes, which essentially consists of eigenvectors – buckling mode shape – and eigenvalues – buckling mode values. The eigenvalue corresponds to a load factor or a load multiplier. By default the program solves the problem for two buckling modes. The convention when analyzing eigenvalue problems related to physical models is to neglect negative eigenvalues. Additionally, when considering structural engineering problems involving limit state design and failure, it is the lowest eigenvalue that should be assumed as solution for the most conservative design, as this corresponds to the first value that will be reached when applying external load to the structure.

The different boundary conditions are listed in the table below. The types of constraints for each end sections support are listed along with schematic figures of the constraints where the red colored line segments or areas represent the edges or faces that are constrained. Additionally the load factor for each case is listed.

The ultimate buckling load in the experimental analysis is 139 kN. Case 5 yields the best result compared to this value, as it is the value closest to and larger than the experimental value.

**Table 6:** Different support configurations and their corresponding load factors.

Case	Support A	Support B	Load factor	Schematic of constraints/BC
1	Fixed support, bottom flange edge	Displacement, bottom flange edge	103,32	
2	Fixed support, bottom flange edge	Fixed support, bottom flange edge	104,79	
3	Fixed support, bottom flange lower and upper edges	Fixed support, bottom flange lower and upper edges	110,97	
4	Fixed support, end section	Displacement, end section	-1671,3 635,18	

5*	Fixed support, bottom flange edge. Displacement, lower web edges	Displacement, bottom flange edge. Displacement, lower web edges	159,54	
6*	Fixed support, bottom flange edge. Fixed support, lower web edges	Displacement, bottom flange edge. Fixed support, lower web edges	193,21	
7*	Fixed support, lower half of end section	Displacement, lower half of end section	191,04	
8*	Fixed support, bottom flange lower and upper edges. Displacement, lower web edges	Displacement, bottom flange lower edge. Fixed support, bottom flange upper edges. Displacement, lower web edges	163,21	

The mesh model consists of an automatically generated shell element model and several refinements. An automatic mesh refinement was done for all faces of the geometry. In addition, manual face sizing was done for both the split end section faces and for the roller radii and flange sides. In this face sizing the element size was set to 20 mm on all faces. Fig. 19 are showing how the overall mesh looks like in one of the beam models.

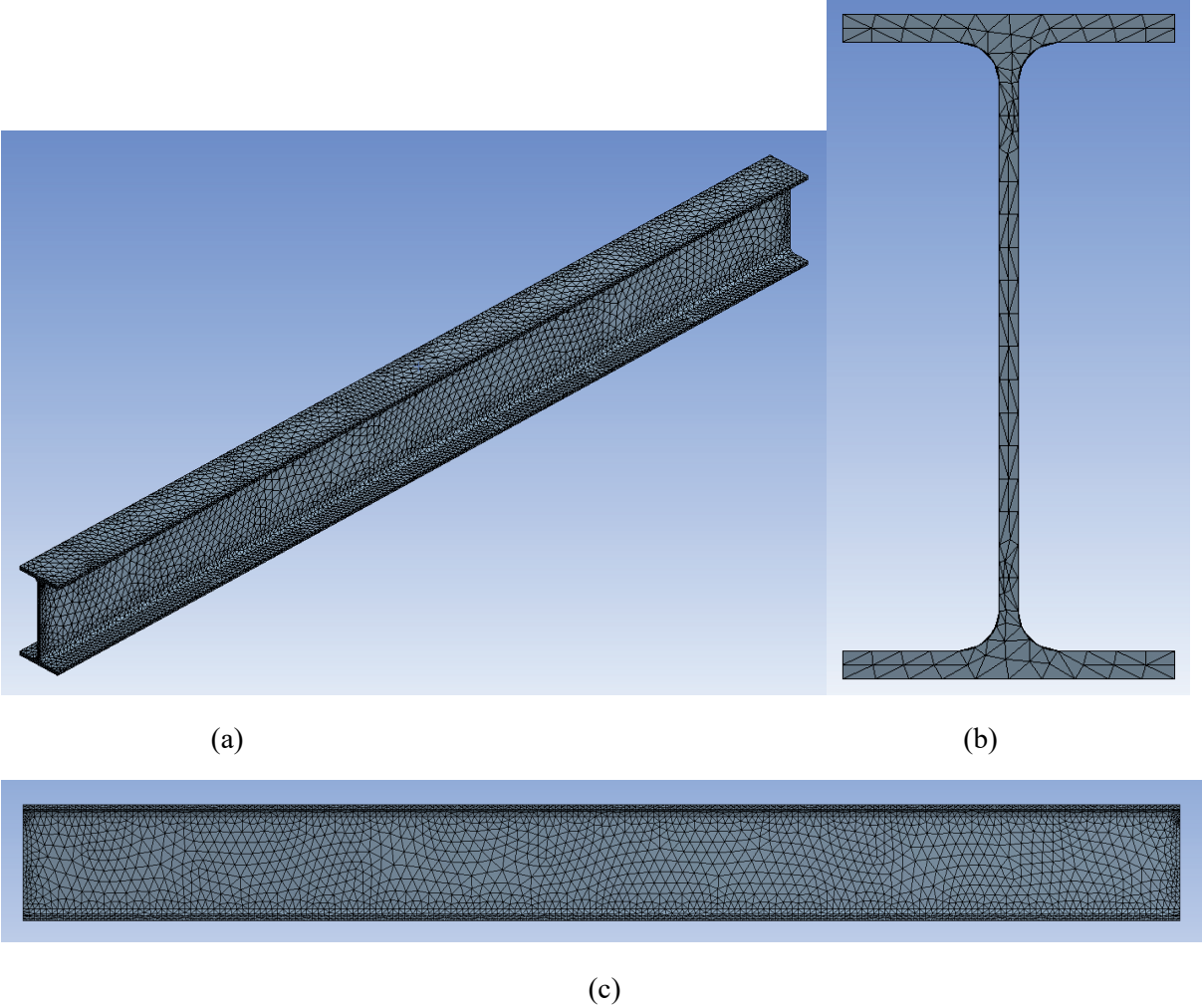


**Fig. 19.** Screenshots from ANSYS showing the visualized mesh model. (a) Overall isometric view, (b) end section view and (c) side view of an IPE200 2 m length beam.



### 4.3.2 Testing Procedure

Step 1: Initial loading, i.e. pre-stress analysis

The support reactions were chosen according to the best fit boundary conditions found in the preliminary Eigenvalue buckling analysis. Otherwise the settings and model parameters were identical to the pre-buckling analysis described in section 4.3.1.

Step 2: Eigenvalue buckling analysis

The procedure for the eigenvalue buckling analysis is described in section 4.3.1.

Step 3: Nonlinear buckling analysis

The nonlinear buckling analysis was conducted using a static structural analysis system. This was connected to the eigenvalue buckling analysis system, sharing Engineering data, Geometry and Model cell data.

In the Analysis settings the step controls for the FEA iteration process were changed from standard, so that the Step End Time were set to 100 s. The Auto Time Stepping feature was set to *On* so that it is possible to override the program controlled settings. This way the program runs an iteration process in which the load rate/increment is constant. Additionally the Large Deformation setting was turned on. This allows for the Solver Output to run a nonlinear analysis.

The initial testing resulted in a good estimation of the buckling load and corresponding lateral deflection when compared to the experimental results.

## 4.4 Numerical Results

This section presents the results of the numerical analyses carried out as described in the sections 4.1 through 4.3.

**Table 7:** Theoretical buckling loads based on eigenvalue buckling analysis.

Cross section	Beam length (mm)	Theoretical buckling load (kN)
IPE200	2000	142.12
	2250	126.20
	2500	111.56
IPE240	2000	196.48
	2250	183.82
	2500	169.23
IPE270	2000	215.66
	2250	206.58
	2500	195.87

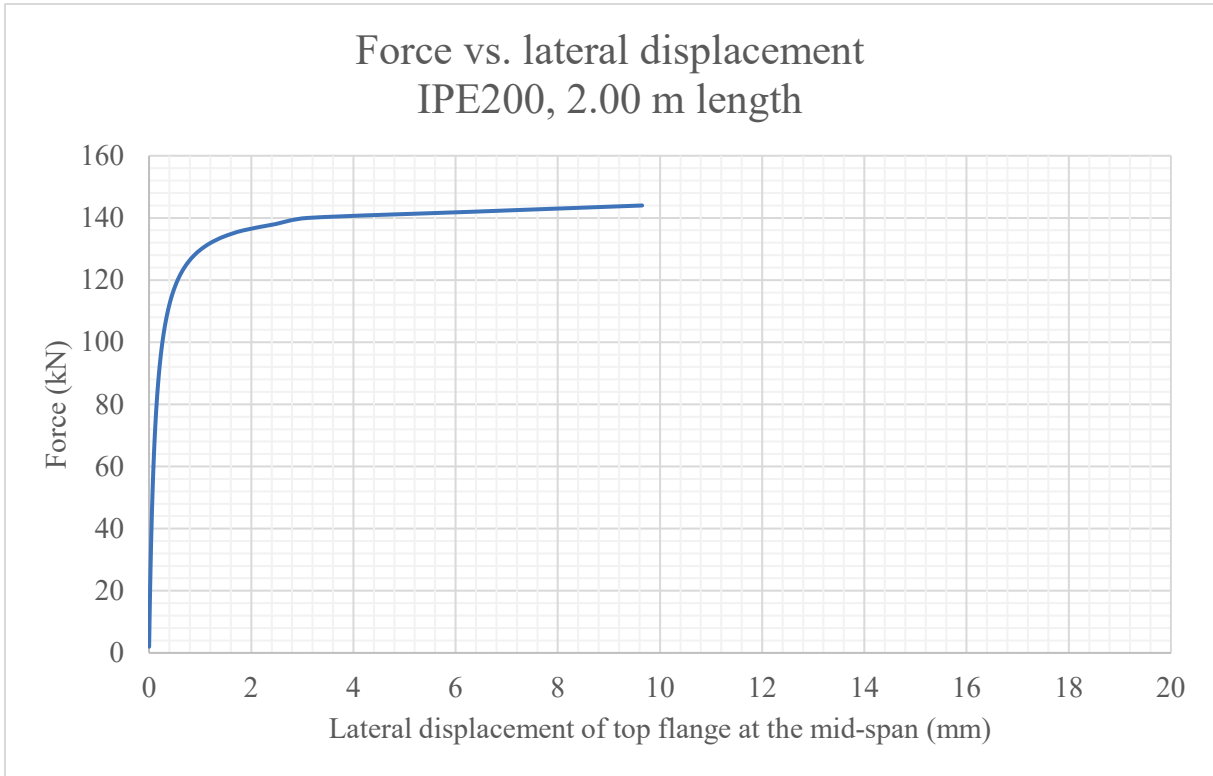


**Fig. 20.** Force vs. lateral displacement for IPE200, 2.00 m length.

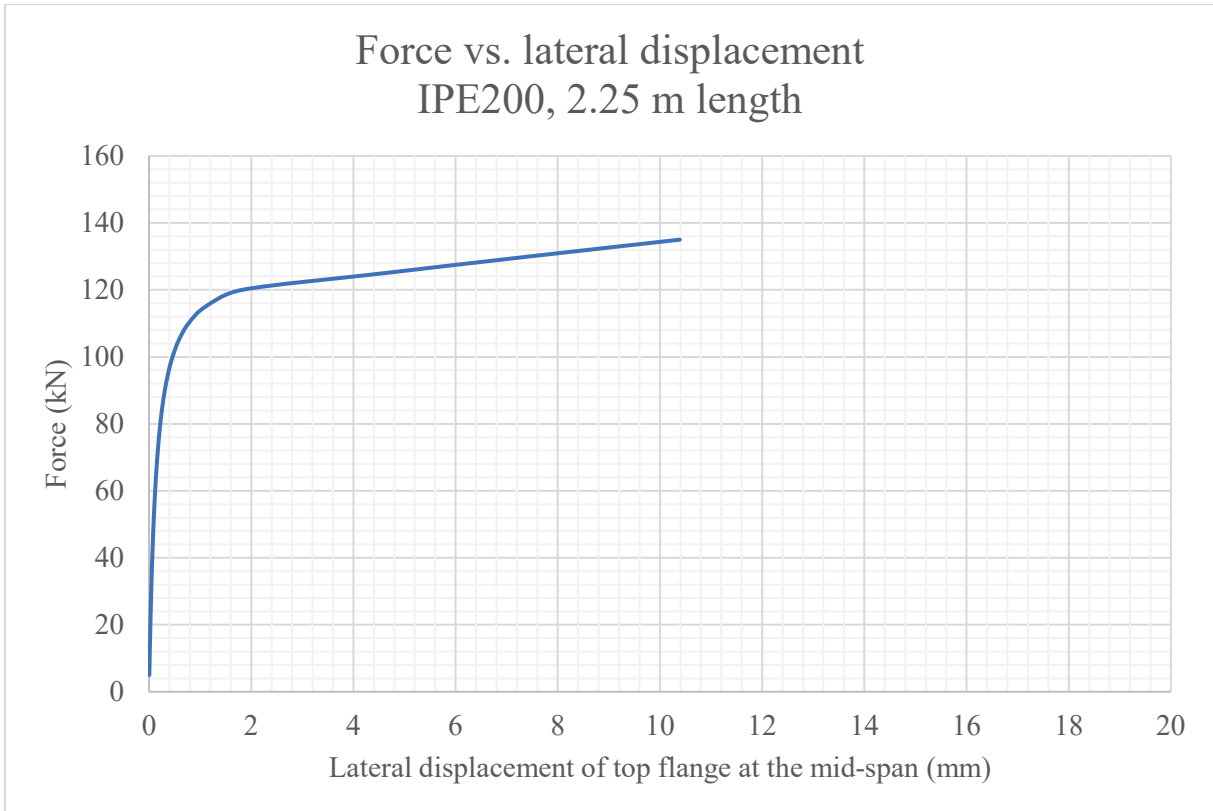


**Fig. 21.** Force vs. lateral displacement for IPE200, 2.25 m length.

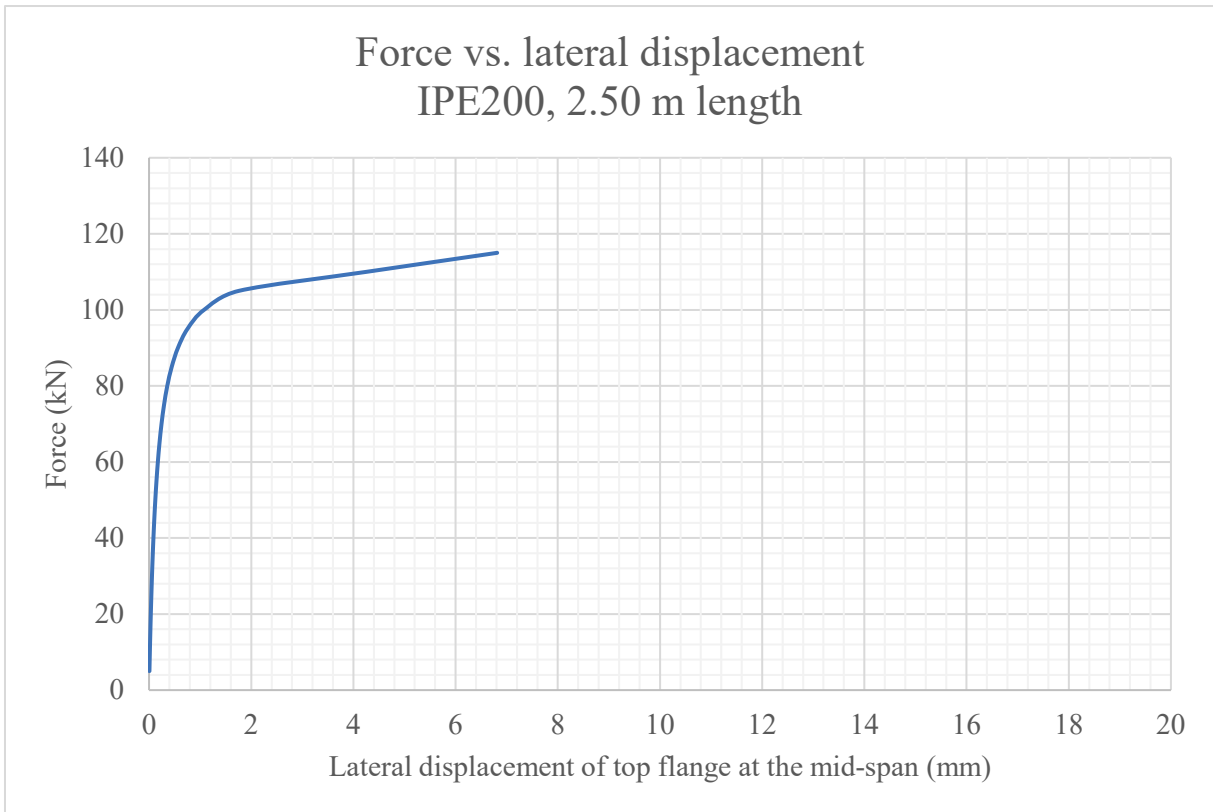


**Fig. 22.** Force vs. lateral displacement for IPE200, 2.50 m length.

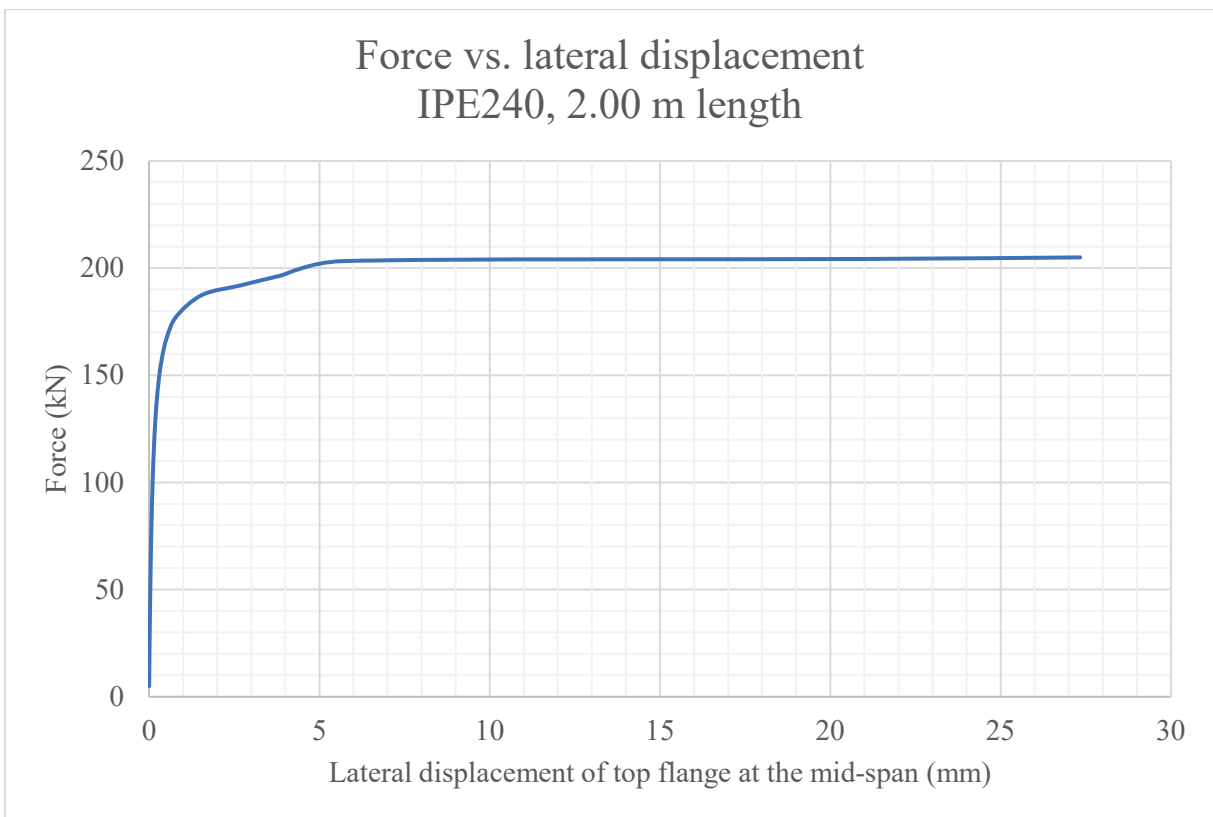


**Fig. 23.** Force vs. lateral displacement for IPE240, 2.00 m length.

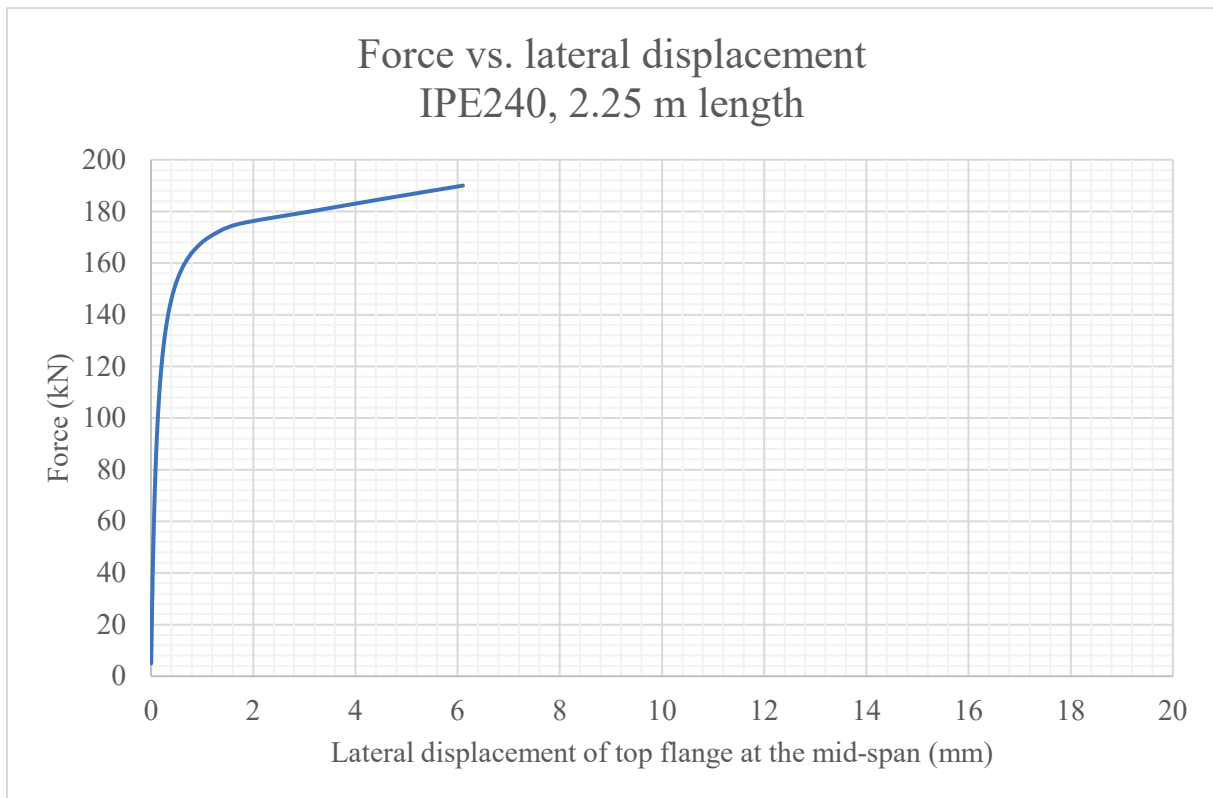


**Fig. 24.** Force vs. lateral displacement for IPE240, 2.25 m length.

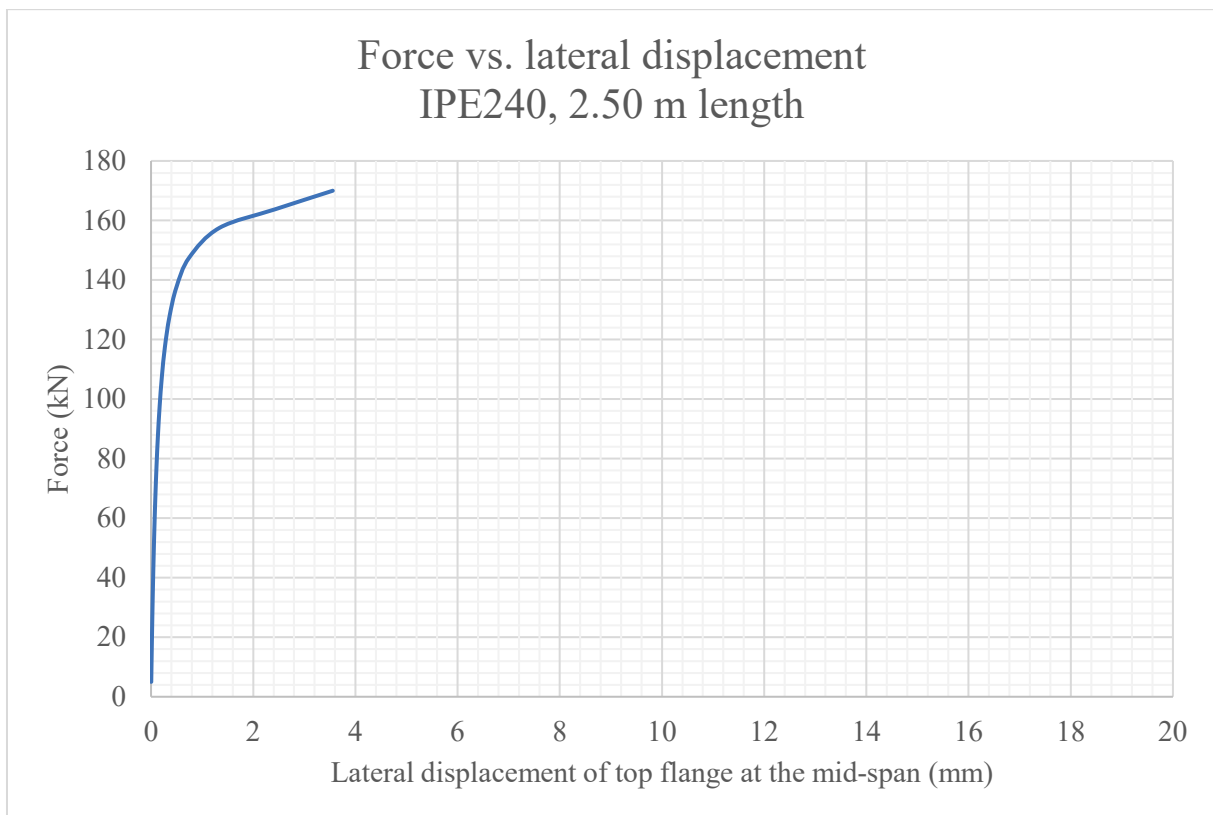


**Fig. 25.** Force vs. lateral displacement for IPE240, 2.50 m length.

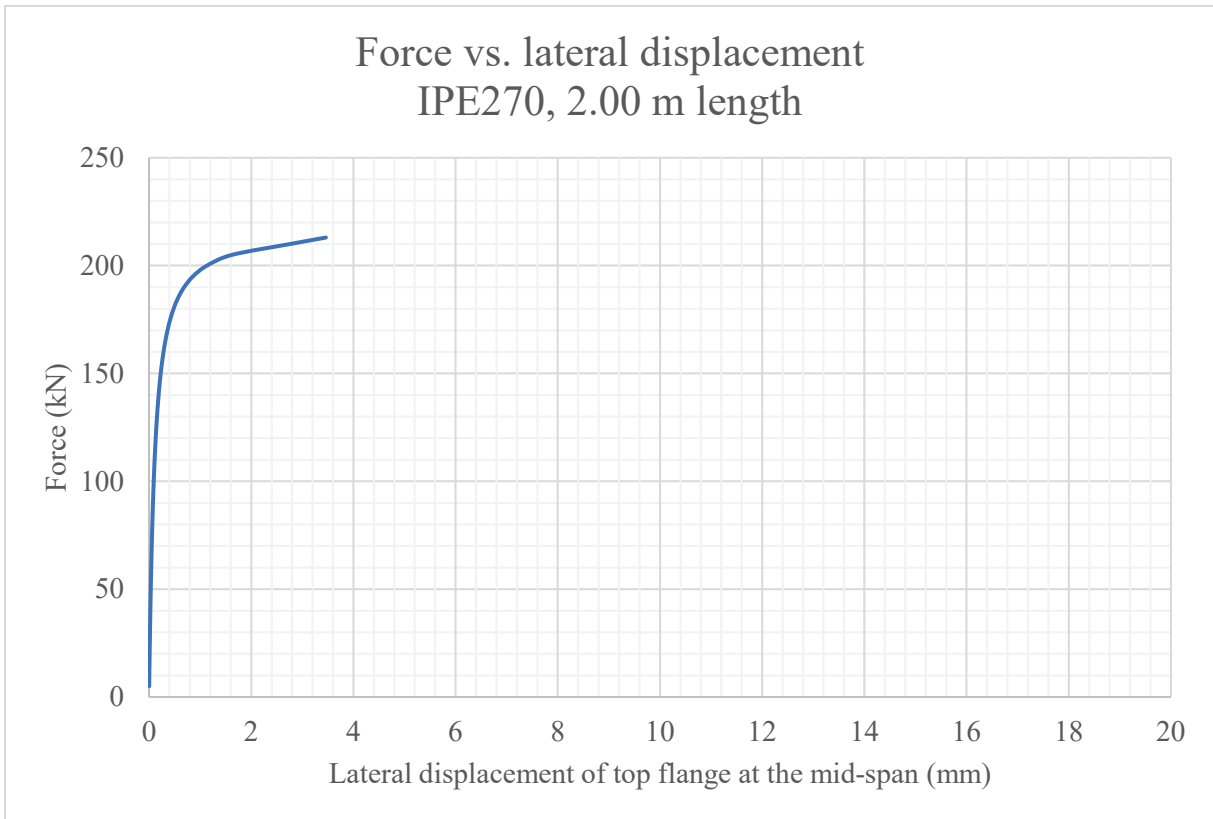


**Fig. 26.** Force vs. lateral displacement for IPE270, 2.00 m length.

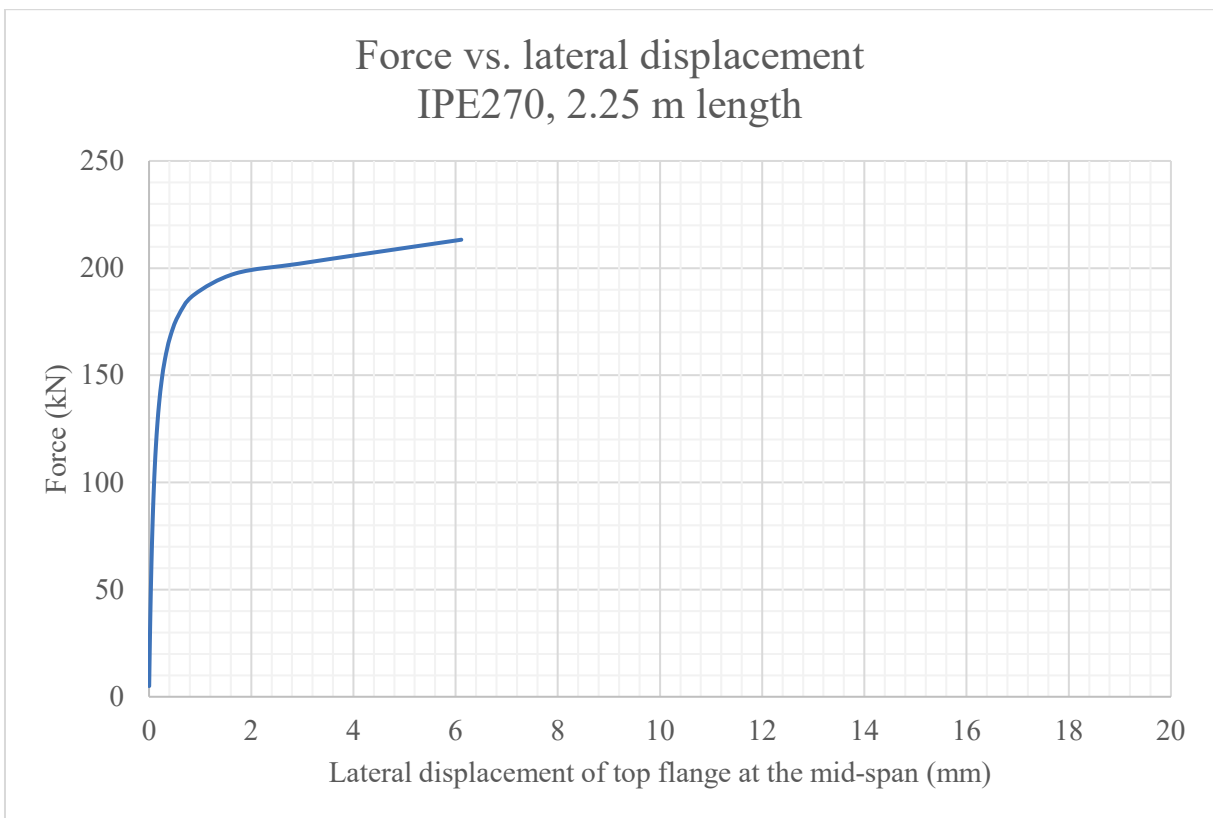


**Fig. 26.** Force vs. lateral displacement for IPE270, 2.25 m length.

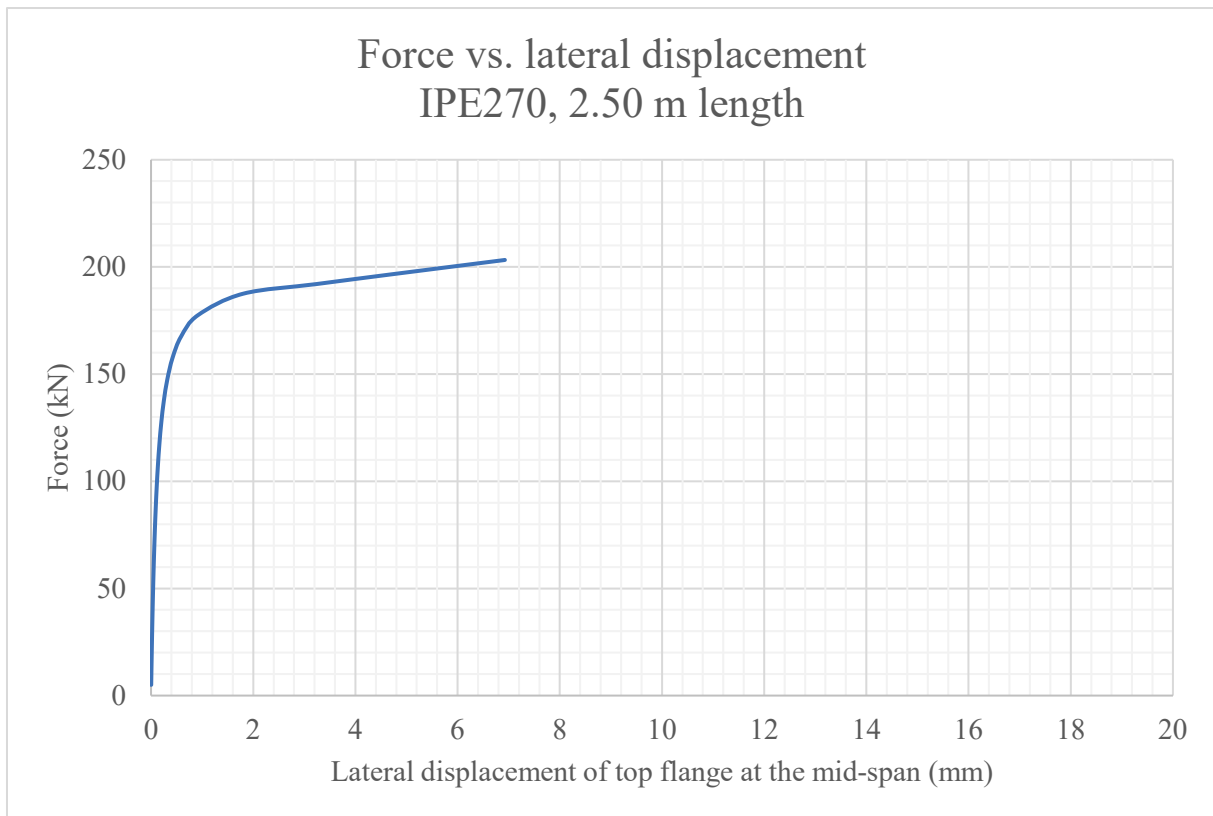


**Fig. 27.** Force vs. lateral displacement for IPE270, 2.50 m length.

## 4.5 Previously Conducted Numerical Analyses

Vales and Stan [5] compared different finite element models of I-sections. The FEA software programs ABAQUS and ANSYS were used to develop models and conduct numerical analyses.

ABAQUS model:

The geometrical model consisted of S4 shell elements. This element has four corner nodes with six degrees of freedom each. The beam was modelled having 16 elements along the flange width, 16 elements along the web height and 200 elements along the beam length.

ANSYS model:

The geometrical model consisted of SOLID185 elements. This element is prism-shaped with eight corner nodes. The beam was modelled having ten elements along the flange width, 20 elements along the web height, and two elements along the flange thickness. The number of elements along the beam length varied.

The moment was modelled as a linearly varying pressure along the vertical axis. The boundary conditions were modelled so that certain nodal displacements were linked to the displacement of a master node; The end nodes of the flanges were coupled with a master node located at the intersection between the flange and the web, and these end nodes of the web were coupled to a master node located in the centroid of the section. This way the boundary conditions needed only be applied at one node.

The vertical and lateral displacements in addition to the rotation about the longitudinal axis were set to equal zero at the end sections of the beam model. Additionally, the longitudinal displacement was set to zero at the mid-span of the beam in order to constrain the position of the model. These boundary conditions allowed for warping of the member at the supports, represented by local longitudinal displacements. Anywhere else along the beam length, sections could deflect vertically and laterally, and twist rotate.

As described in the paper, the fillet welds of the built-up I-section have almost no effect on the lateral-torsional buckling capacity of the profile. The beam was hence modelled having right angle inner edges in the transition between the web and the flanges with no excessive volume.

# 5 Comparisons and Discussion

## 5.1 Comparison between Experimental and Numerical Results

The comparisons between the experimental and numerical results is done based on observations made in regards to sections 3.2 and 4.4. The main focus is to analyze and characterize the results from the load vs. lateral deflection plots and the elastic critical moment calculations, and extract information that will help answer the question of whether numerical analysis can suffice in modelling lateral-torsional buckling and to what extent this tool is useful in further research.

### 5.1.1 Lateral Deflections

The load vs. lateral deflection curves from the numerical analysis do not differ a lot from the experimental ones.

It is possible to define three regions within the load vs. lateral displacement plots:

- The 1<sup>st</sup> linear region. This is the region from the origin of the diagram to the point where the moment reaches the elastic critical moment, i.e. first lateral deflection.
- The nonlinear region. This is the region in which lateral deflection and twisting of the cross section starts to govern the type of deformation.
- The 2<sup>nd</sup> linear region. This is the region beyond the nonlinear region in which the governing stiffness parameter of the beam is the moment of inertia about the weak axis. Lateral deflections and twisting increases with almost no additional load.

The program runs a nonlinear analysis, and the entire load vs. deflection plot is nonlinear as the rate of change is not constant. However, it is reasonable to assume a linear region of the curves as the rate changes are small compared to those of the nonlinear region.

It is hard to define the load magnitude for which the elastic critical moment has been reached. The values in Table 8 are extracted from the plots of load vs. lateral deflection based on where the curves changes are most abrupt.



**Table 8:** Estimated buckling loads and corresponding lateral deflections

<b>Cross section</b>	<b>Beam length (mm)</b>	<b>Estimated elastic critical buckling load (kN)</b>	<b>Corresponding lateral deflection (mm)</b>	<b>Estimated maximum buckling load (kN)</b>	<b>Corresponding lateral deflection (mm)</b>
IPE200	2000	110	0.4	135	2
	2250	95	0.4	120	2
	2500	80	0.4	115	2
IPE240	2000	140	0.3	190	2
	2250	130	0.3	175	2
	2500	120	0.3	160	2
IPE270	2000	160	0.3	205	2
	2250	145	0.2	200	2
	2500	135	0.2	190	2

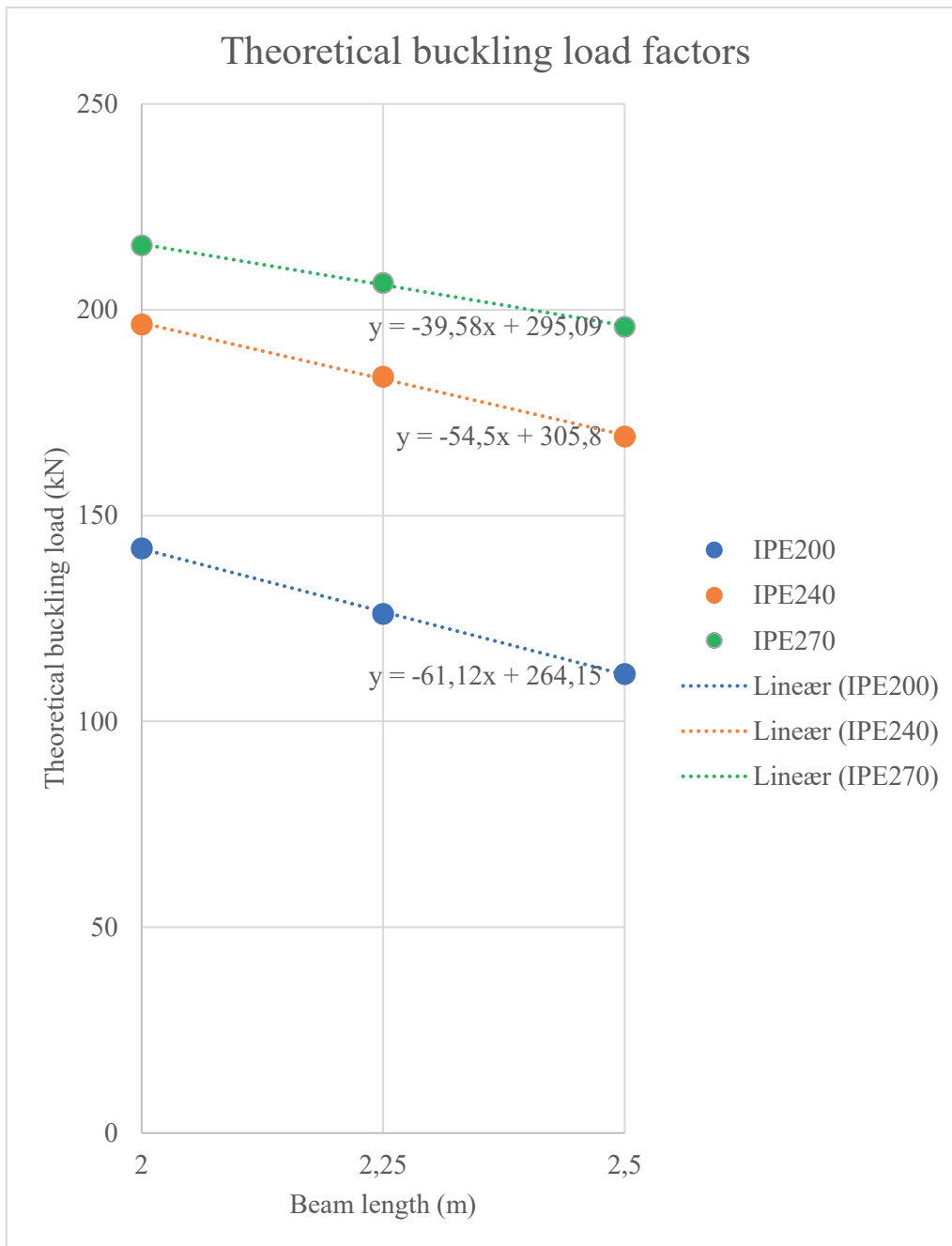


**Fig. 28.** Diagram of theoretical buckling load factors vs. beam lengths for the different profiles.

Within the data set containing the values for beam lengths the theoretical buckling load seems to decrease linearly with increasing beam length. This observation goes for all three profiles.

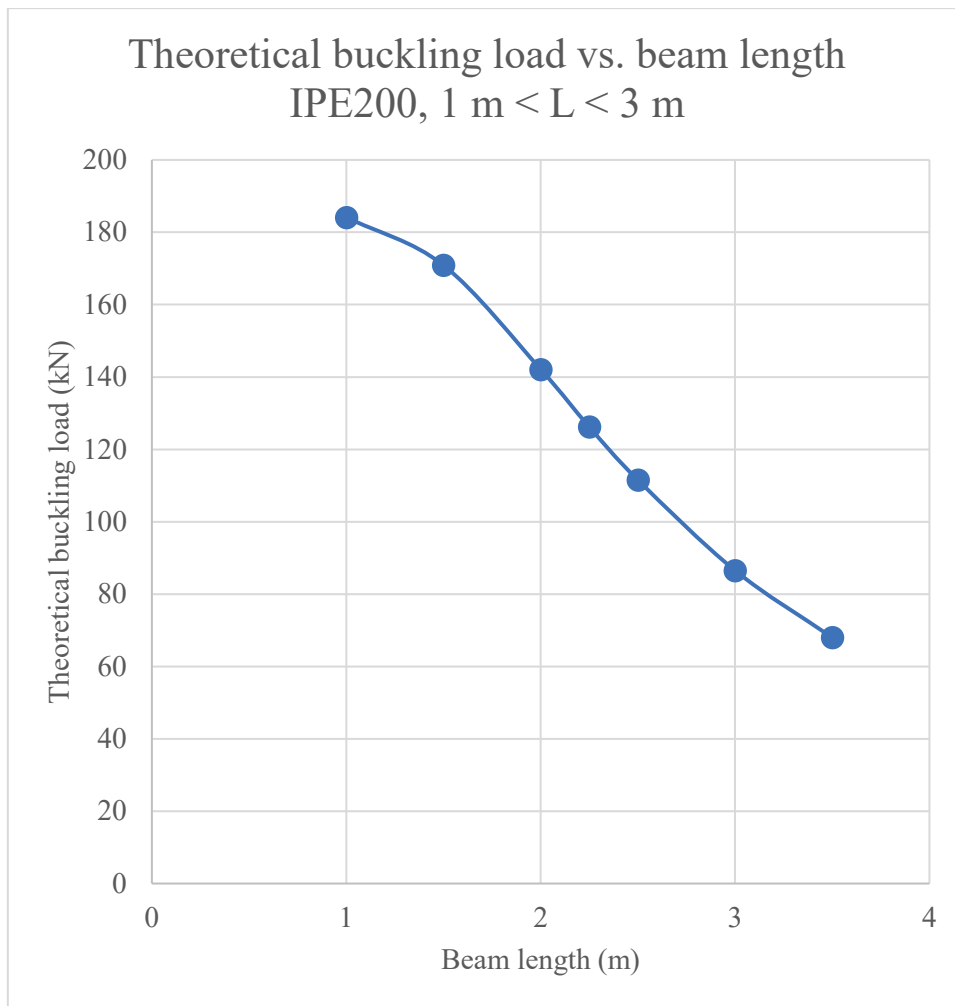


**Fig. 29.** Theoretical buckling load factors vs. beam lengths for the IPE200 profile.

Four additional beam models were tested, all of the same profile – IPE200. The beam lengths for these models were 1 m, 1.5 m, 3 m and 3.5 m. The entire FEM process was applied to these additional models to provide results outside of the original data set.

What seemed to be a linear trend for  $2\text{ m} < L < 2.5\text{ m}$  has been proven incorrect. The theoretical buckling load has a relatively low negative rate of change for beam lengths between 1 m and 1.5 m. It has a higher negative rate of change in the region of lengths between 2 m and 2.5 m, and then a decreasing negative rate of change as the length approaches 3 m.

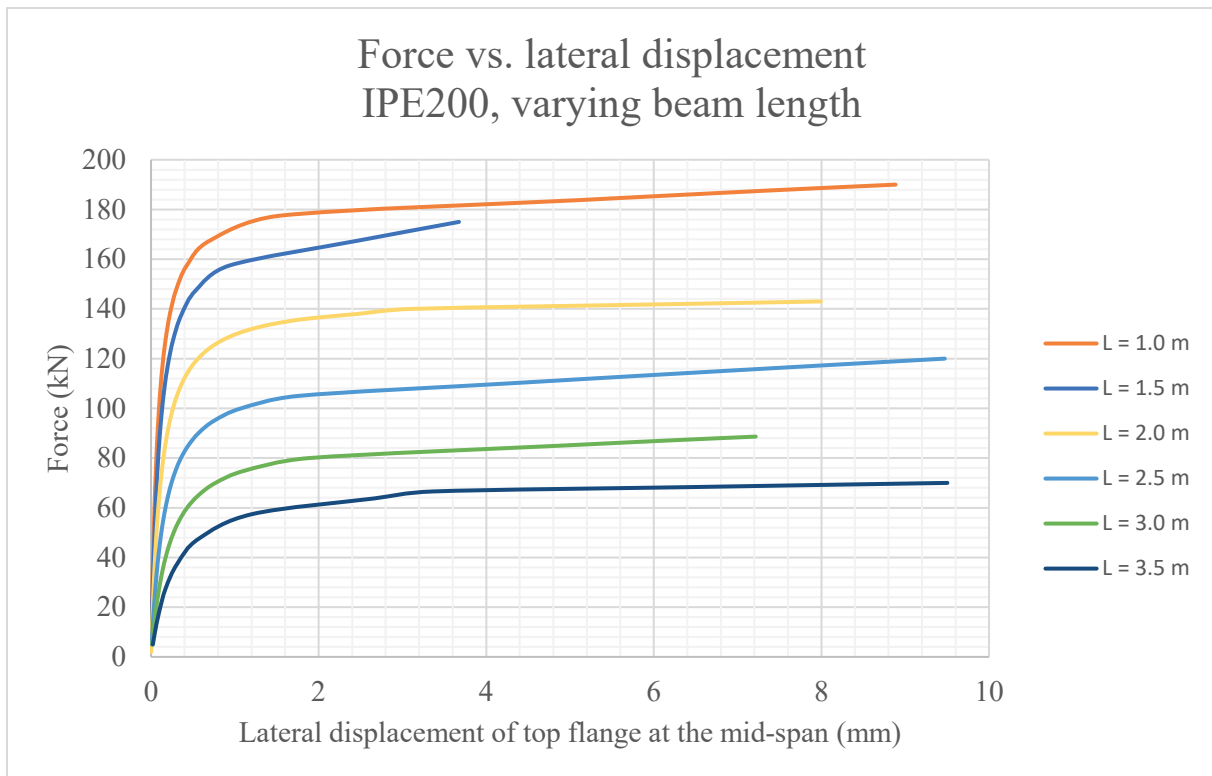


**Fig. 30.** Force vs. lateral displacement for different beam lengths of IPE200.

Fig. 30 shows another perspective on the varying numerically estimated buckling load. The larger the spacing between the different curves, the higher the rate of change of the theoretical buckling load. Additionally, it is worth noticing that theoretical buckling loads correspond to displacement values around 5 – 6 mm – the exception being for  $L = 1.5$  m, as it diverges relative to the other plots. A deflection of 5 – 6 mm is in the second linear region in every case.

General observations:

- The theoretical buckling loads seem to decrease linearly with increasing beam length.
- The theoretical buckling loads calculated from the eigenvalue buckling analyses decreases relative to the buckling loads when the cross sections increase in size.
- The load vs. lateral deflection curves from the numerical analysis overestimate the load required to ... a given lateral displacement in the nonlinear region relative to the curves from the experimental analysis.
- The numerical curves also underestimate the loads required to ... a given lateral displacement beyond the nonlinear region, i.e. the region of displacement divergence.

## 5.1.2 Specifics Regarding the Numerical Analysis

The nonlinear buckling analysis was unable to calculate lateral deflections for high maximum loads. This was due to a convergence error – The program was not able to obtain a converged solution of the force equilibrium when reaching certain load magnitudes above the theoretical buckling load. Another effect of this obstacle/difficulty is the slightly inaccurate calculation of deflections beyond the nonlinear region. When considering the numerically derived load vs. lateral deflection plots, the load continues to increase after having reached the third region, which in practice is linear and, in some cases, starts to dip. This prevents the use of the software to estimate deflections beyond the region of nonlinear behavior of the lateral-torsional buckling.

## 5.2 Possible Reasons for Differences in Results

Listed below are potential sources and reasons for the observed differences between experimental and numerical results.

- Geometric imperfections

Geometric imperfections are all types of geometric features that cause the symmetry about any of the principal axes of the beam to break, resulting in weaknesses in certain directions or planes. When external loading is applied, the geometric asymmetry leads to certain preferred deformation directions and modes, and ultimately reduces the capacity of the beam.

- Material defects

Material defects include impurities, dislocations and otherwise material features that ... anisotropic/orthotropic material behavior. A perfectly homogeneous and isotropic material is impossible to achieve in reality, however the material is assumed to have isotropic and linear-elastic properties given it is processed and manufactured using industry standard manufacturing equipment and procedures. Crystallographic theory teaches that material defects may act as strengthening mechanisms if the preferable type of impurities or dislocations are induced upon the material.

- Asymmetry in loading

If the vertical mid-span point load is asymmetric with respect to any of the principal axes of the beam, i.e. the real loading configuration is deviating from the ideal one presented in Fig. X, the resulting deformations may vary from what is to be expected in the case of an analytical or numerical analysis.

- Asymmetry in support rig

The setup for the experimental analysis, which also includes the loading configuration, is most likely not 100 % symmetric in geometry. The asymmetry is generally very small for manufactured rigs and parts, but after a long time of use it may experience some asymmetries.

- Mesh model in FEM

The mesh model in the finite element modelling software might not be generated in a way that, when incorporated into the final model with loading and boundary conditions and material properties, yields results that compares well with the results from experimental or analytical analysis. In most cases, a sufficiently accurate mesh model consists of an automatically generated global mesh with manually refined local sections around geometric features prone to relatively high stress concentrations.

- Initial lateral load in FEM

The lateral load of 100 N in this case was induced upon the top flange of the beam model for all the nine specimens in order to generate an initial imperfection for the nonlinear analysis to take place.

- Lack of material data input in FEM

The engineering data section was unedited, i.e. the standard settings and material properties for structural steel was used. There are however possibilities for adding additional material properties and behavioral models, like models related to elasticity, plasticity, creep and fatigue etc.

# 6 Conclusion

## 6.1 Conclusion Based on Comparisons and Discussion

Based on the comparisons between experimental and numerical results for load vs. deflection there are several points to be made.

- The numerical models predict lateral deflection to a certain degree, but struggle to extend the 2<sup>nd</sup> linear region of the load vs. deflection curves due to non-converging solutions with high loads.
- The numerical models seem to estimate a lower value for buckling load in the 2<sup>nd</sup> linear region where the maximum loads occur, something which is positive from a conservative design perspective.
- The data set is too small to make a certain conclusion on how the different beam dimensions affect the results, both in the experimental and numerical analyses.
- The points stated in section 5.2 must be taken into consideration when reflection on the analyses and results. Models need further refinement and testing before they can be verified. Refer to section 6.2 for suggestions on further work.

## 6.2 Further Work

Due to time limitations, simulations on other than the nine test specimens and the four additional beams could not be made. It is of interest to check whether the trends related to the values of lateral deflection and elastic critical moment can be extended to incorporate other beam profiles and beam lengths. If this is the case, a model can be developed to predict buckling loads and corresponding deformations by the means of numerical linear and nonlinear buckling analyses. Numerical simulation is of course a cheaper and less time-consuming way of testing beams given that the models are reliable. It is also preferable that the model and analysis procedure is ... conservative design.

It is also possible to check different mesh models with different levels of refinement and sizing. Different element types can also be checked to see what implications this will have on the load-displacement relationship. Different element types enable different modes of deformation and nodal forces.

The models should be extensively tested and compared with experimental and practical results before being used in real life design situations. Returning to the points made in the introduction chapter, all improvements made to design guidelines, procedures and models that helps increase safety and reduce costs in the design, construction and maintenance of structures are of great importance to society.

# References

1. Trahair et al. *The Behavior and Design of Steel Structures to EC3*. 4<sup>th</sup> Edition, 2008. Pp 227 – 234.
2. Da Silva et al. *Design of Steel Structures. Eurocode 3: Design of steel structures, Part 1-1: General rules and rules for buildings*. 1<sup>st</sup> Edition, 2010. Pp 198 – 203.
3. M. Ruud. Vippekapasitet til IPE-bjelker.
4. B. Yang et al. *Experimental and numerical study on lateral-torsional buckling of singly symmetric Q460GJ steel I-shaped beams*.
5. J. Vales, T.-C. Stan. *FEM Modelling of Lateral-Torsional Buckling using Shell and Solid Elements*.



# Appendix – ANSYS generated project reports

This appendix is a compilation of extracts of automatically generated project reports for all analyses in ANSYS Workbench 17 carried out for this thesis. Each extract consists of project data relevant for the results and discussion of the problem, including buckling eigenvalues, force convergence plots, and directional deformation plots. The directional deformations correspond to maximum lateral deflections of each beam under the linearly increasing loading conditions that the beams are subjected to in the analyses.

The settings used in the analyses are the default setting for the default structural steel preset, except from the strength parameters, which were changed from 250 MPa to 355 MPa. Theoretically, the material strength should not change the results in LTB analysis, however. The material data settings are the same for each project.

# 1. IPE200, 2.00 m

## Eigenvalue Buckling (C5)

### Solution (C6)

**FIGURE 10**  
Model (B4, C4, D4) > Eigenvalue Buckling (C5) > Solution (C6)

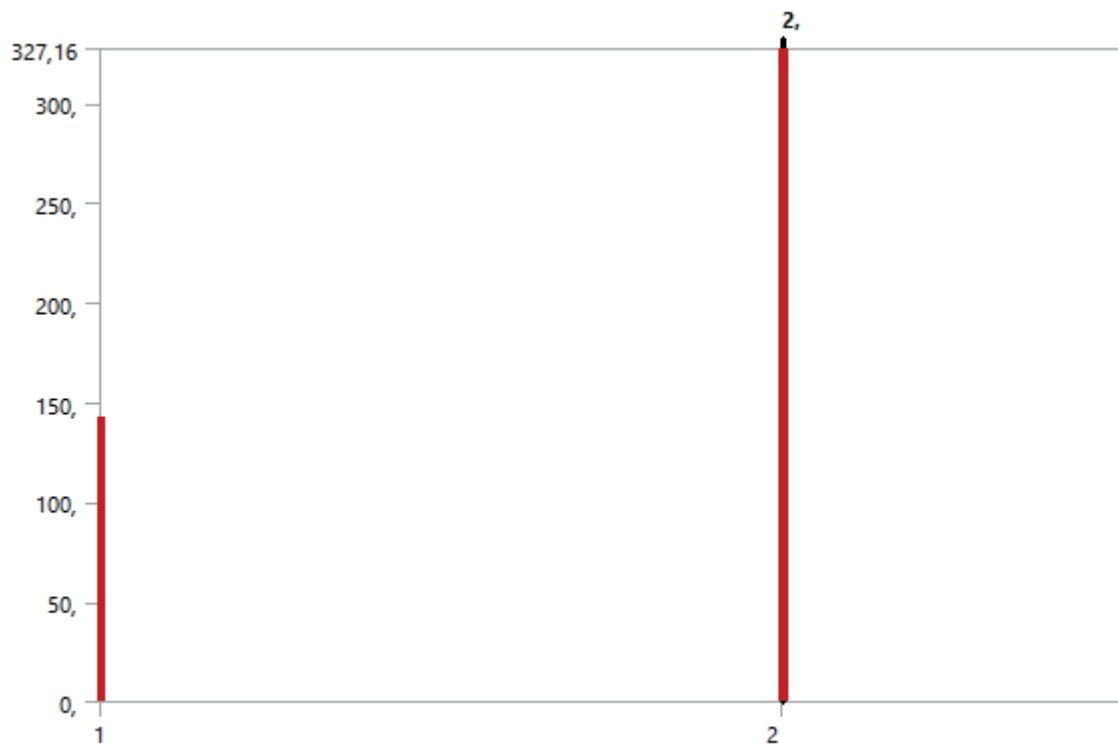


**TABLE 20**  
Model (B4, C4, D4) > Eigenvalue Buckling (C5) > Solution (C6)

Mode	Load Multiplier
1,	142,12
2,	327,16

# Static Structural 2 (D5)

## Solution (D6)

FIGURE 18  
Model (B4, C4, D4) > Static Structural 2 (D5) > Solution (D6) > Solution Information

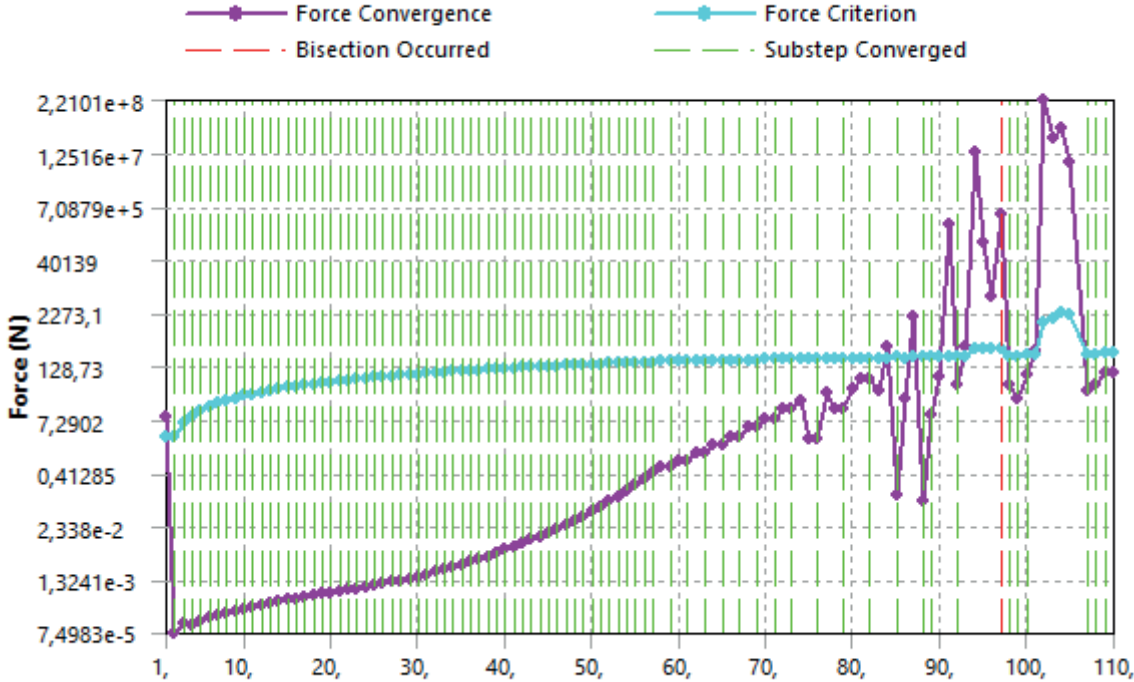


**FIGURE 19**  
**Model (B4, C4, D4) > Static Structural 2 (D5) > Solution (D6) > Solution Information**

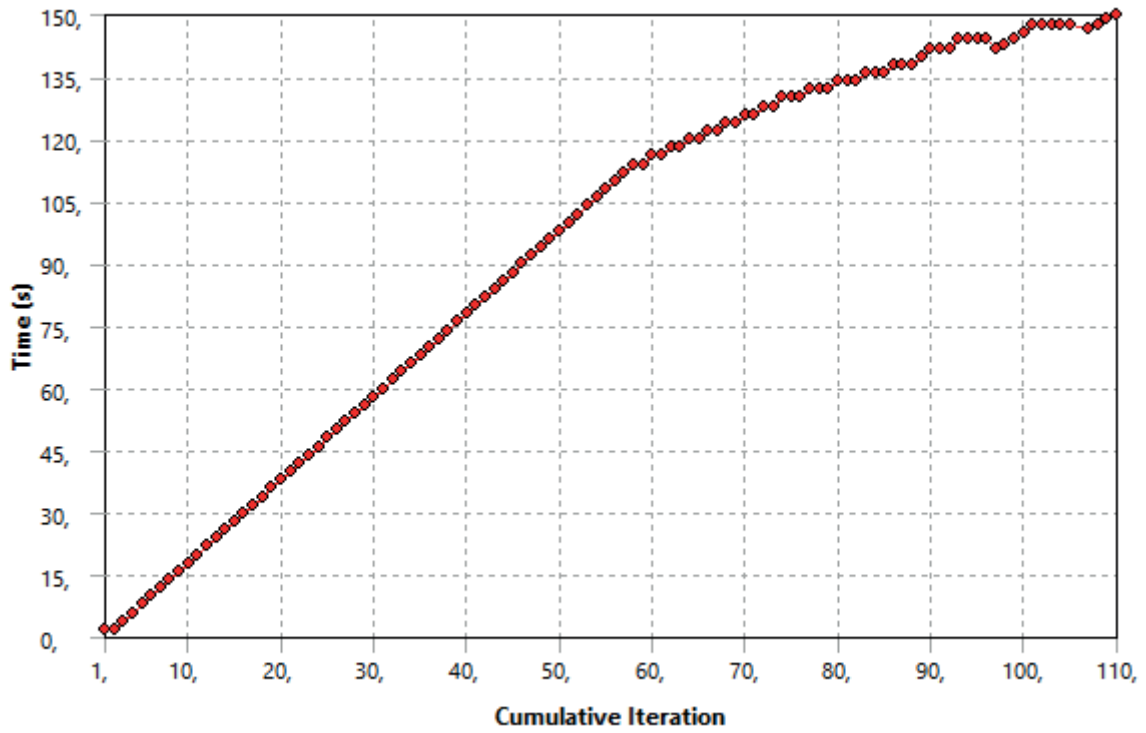


**FIGURE 20**  
**Model (B4, C4, D4) > Static Structural 2 (D5) > Solution (D6) > Directional Deformation**

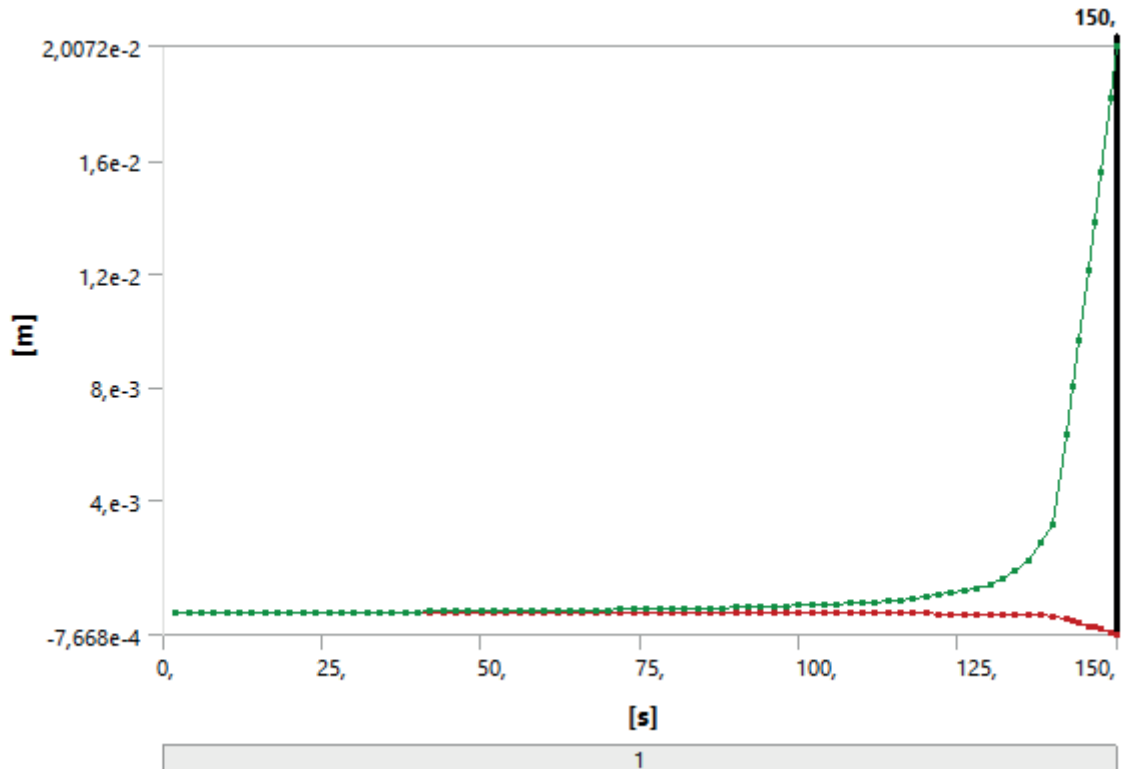


**TABLE 31**  
**Model (B4, C4, D4) > Static Structural 2 (D5) > Solution (D6) > Directional Deformation**

Time [s]	Minimum [m]	Maximum [m]
2,	-1,2295e-007	1,8292e-006
4,	-2,4746e-007	3,7021e-006
6,	-3,7359e-007	5,6206e-006
8,	-5,0138e-007	7,5867e-006
10,	-6,3092e-007	9,6026e-006
12,	-7,6228e-007	1,1671e-005
14,	-8,9553e-007	1,3793e-005
16,	-1,0307e-006	1,5972e-005
18,	-1,168e-006	1,8211e-005
20,	-1,3074e-006	2,0513e-005
22,	-1,4491e-006	2,288e-005
24,	-1,5931e-006	2,5316e-005
26,	-1,7395e-006	2,7825e-005
28,	-1,8885e-006	3,041e-005
30,	-2,0403e-006	3,3075e-005
32,	-2,1948e-006	3,5825e-005
34,	-2,3524e-006	3,8664e-005
36,	-2,513e-006	4,1597e-005
38,	-2,677e-006	4,4629e-005
40,	-2,8445e-006	4,7767e-005
42,	-3,0157e-006	5,1016e-005
44,	-3,1907e-006	5,4383e-005
46,	-3,3699e-006	5,7875e-005
48,	-3,5535e-006	6,1501e-005
50,	-3,7417e-006	6,5268e-005
52,	-3,9348e-006	6,9185e-005
54,	-4,1332e-006	7,3264e-005
56,	-4,3372e-006	7,7515e-005
58,	-4,5473e-006	8,1949e-005

60,	-4,7637e-006	8,658e-005
62,	-4,987e-006	9,1423e-005
64,	-5,2177e-006	9,6493e-005
66,	-5,4563e-006	1,0181e-004
68,	-5,7035e-006	1,0739e-004
70,	-5,96e-006	1,1325e-004
72,	-6,2264e-006	1,1942e-004
74,	-6,5037e-006	1,2593e-004
76,	-6,7928e-006	1,3281e-004
78,	-7,0948e-006	1,4008e-004
80,	-7,4108e-006	1,4779e-004
82,	-7,7423e-006	1,5597e-004
84,	-8,0907e-006	1,6469e-004
86,	-8,4579e-006	1,7398e-004
88,	-8,8457e-006	1,8391e-004
90,	-9,2566e-006	1,9456e-004
92,	-9,6931e-006	2,06e-004
94,	-1,0158e-005	2,1833e-004
96,	-1,0656e-005	2,3167e-004
98,	-1,119e-005	2,4614e-004
100,	-1,1766e-005	2,6189e-004
102,	-1,2389e-005	2,7911e-004
104,	-1,3067e-005	2,9802e-004
106,	-1,3808e-005	3,1889e-004
108,	-1,4623e-005	3,4204e-004
110,	-1,5525e-005	3,6787e-004
112,	-1,653e-005	3,9688e-004
114,	-1,7662e-005	4,2975e-004
116,	-1,8942e-005	4,6722e-004
118,	-2,0409e-005	5,104e-004
120,	-2,2109e-005	5,607e-004

122,	-2,4106e-005	6,2005e-004
124,	-2,6488e-005	6,9116e-004
126,	-2,9387e-005	7,7791e-004
128,	-3,2997e-005	8,8612e-004
130,	-3,7627e-005	1,0249e-003
132,	-4,3789e-005	1,2094e-003
134,	-5,2407e-005	1,4663e-003
136,	-6,5315e-005	1,8482e-003
138,	-8,6704e-005	2,4721e-003
140,	-1,0681e-004	3,113e-003
142,	-2,2847e-004	6,3525e-003
143,	-2,9048e-004	7,9942e-003
144,	-3,5269e-004	9,6508e-003
145,5	-4,4849e-004	1,2155e-002
146,5	-5,1392e-004	1,3855e-002
147,5	-5,826e-004	1,5597e-002
149,	-6,9056e-004	1,8246e-002
150,	-7,668e-004	2,0072e-002

## 2. IPE200, 2.25 m

### Eigenvalue Buckling (C5)

#### Solution (C6)

**FIGURE 8**  
Model (B4, C4, D4) > Eigenvalue Buckling (C5) > Solution (C6)

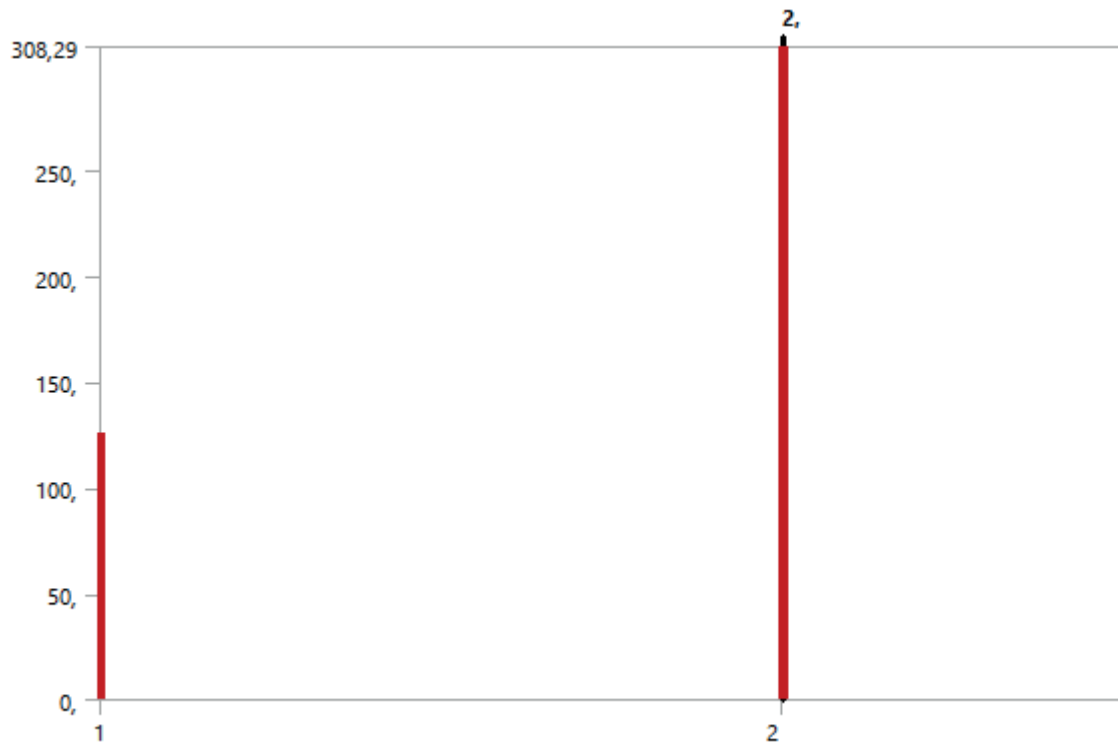


**TABLE 18**  
Model (B4, C4, D4) > Eigenvalue Buckling (C5) > Solution (C6)

Mode	Load Multiplier
1,	126,2
2,	308,29



# Static Structural 2 (D5)

## Solution (D6)

FIGURE 16  
Model (B4, C4, D4) > Static Structural 2 (D5) > Solution (D6) > Solution Information

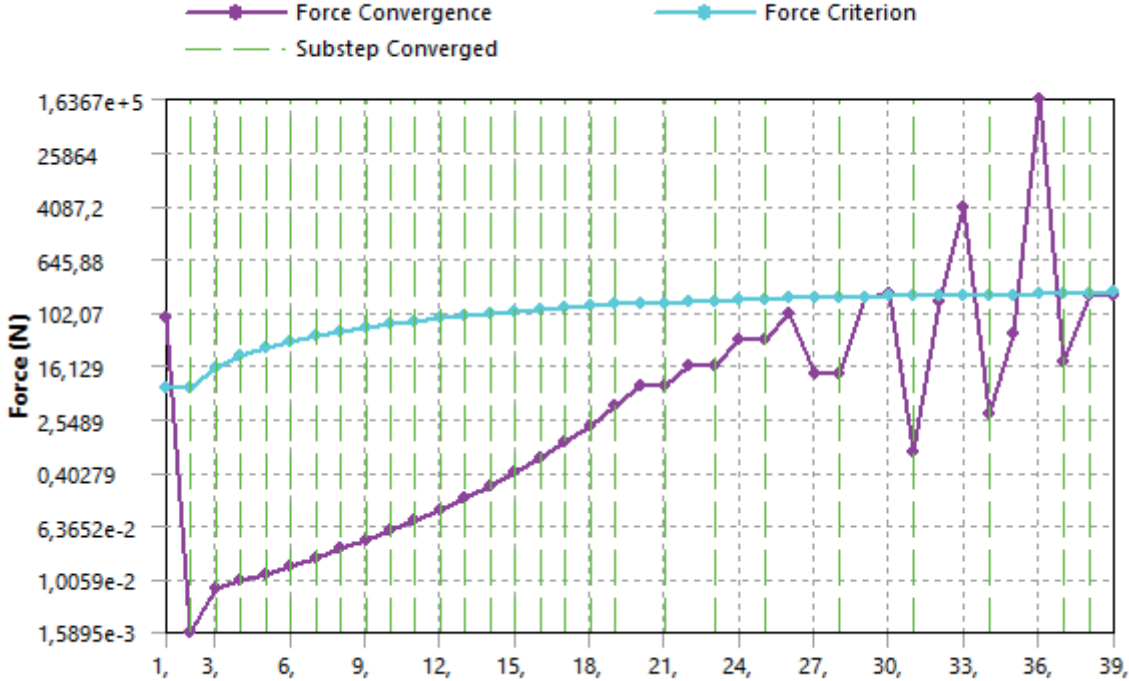


**FIGURE 17**  
**Model (B4, C4, D4) > Static Structural 2 (D5) > Solution (D6) > Solution Information**

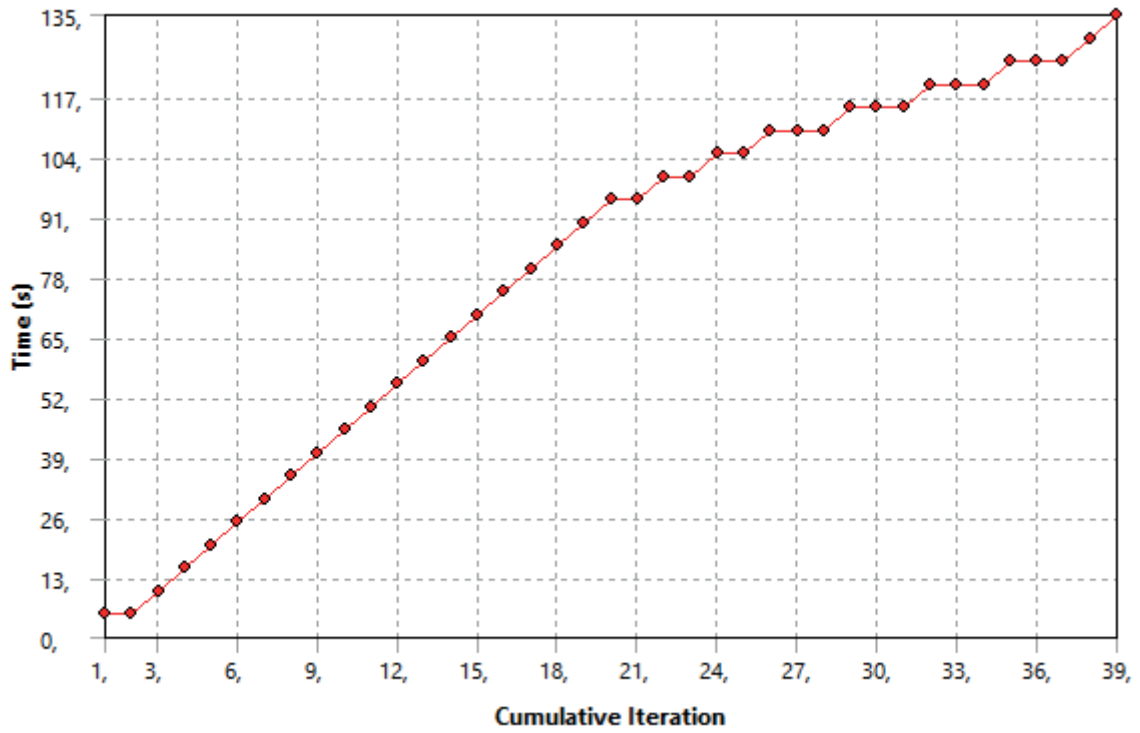


**FIGURE 18**  
**Model (B4, C4, D4) > Static Structural 2 (D5) > Solution (D6) > Directional Deformation**

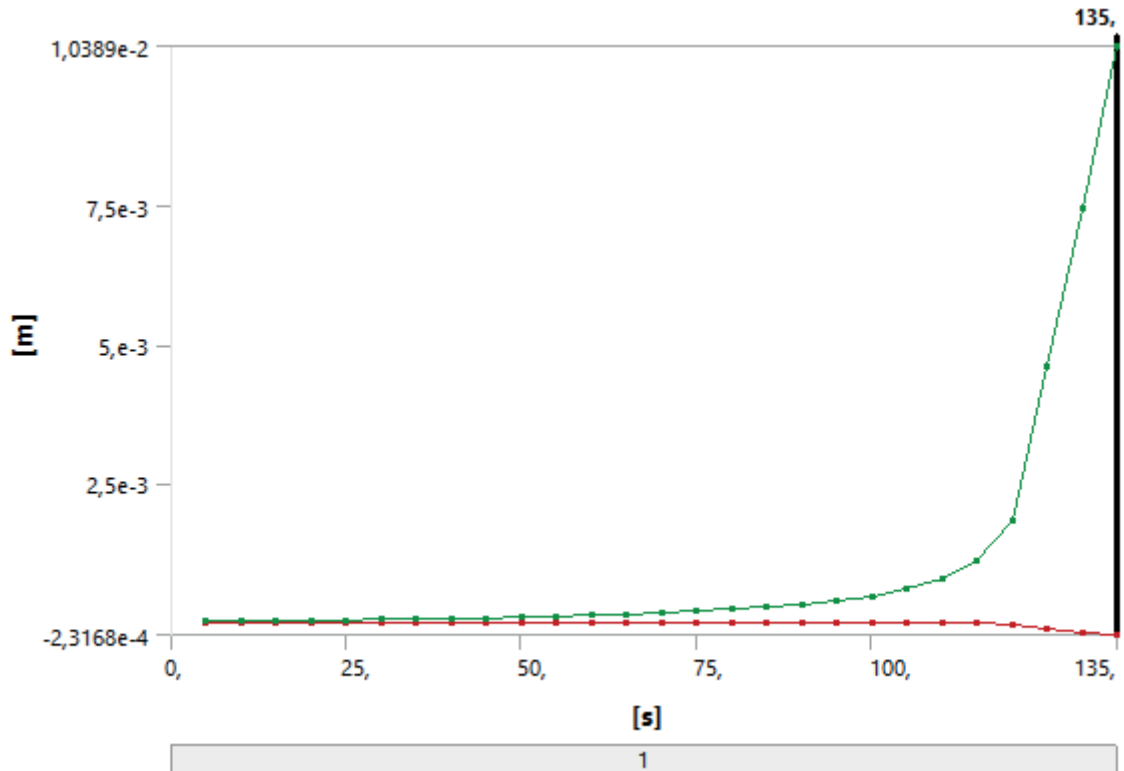


**TABLE 28**  
**Model (B4, C4, D4) > Static Structural 2 (D5) > Solution (D6) > Directional Deformation**

Time [s]	Minimum [m]	Maximum [m]
5,	-3,3389e-007	5,8879e-006
10,	-6,7893e-007	1,2203e-005
15,	-1,0366e-006	1,9005e-005
20,	-1,4085e-006	2,6359e-005
25,	-1,7964e-006	3,4347e-005
30,	-2,2025e-006	4,3064e-005
35,	-2,6297e-006	5,2629e-005
40,	-3,0814e-006	6,3187e-005
45,	-3,5618e-006	7,4915e-005
50,	-4,0763e-006	8,8039e-005
55,	-4,6316e-006	1,0284e-004
60,	-5,2367e-006	1,197e-004
65,	-5,9032e-006	1,391e-004
70,	-6,6467e-006	1,6168e-004
75,	-7,4887e-006	1,8836e-004
80,	-8,4596e-006	2,2039e-004
85,	-9,6038e-006	2,5962e-004
90,	-1,0988e-005	3,0885e-004
95,	-1,2749e-005	3,7312e-004
100,	-1,5038e-005	4,5948e-004
105,	-1,8224e-005	5,8264e-004
110,	-2,3063e-005	7,7299e-004
115,	-3,1433e-005	1,1059e-003
120,	-4,9315e-005	1,8203e-003
125,	-1,2273e-004	4,6058e-003
130,	-1,8465e-004	7,4539e-003
135,	-2,3168e-004	1,0389e-002

### 3. IPE200, 2.50 m

## Eigenvalue Buckling (C5)

### Solution (C6)

**FIGURE 8**  
Model (B4, C4, D4) > Eigenvalue Buckling (C5) > Solution (C6)

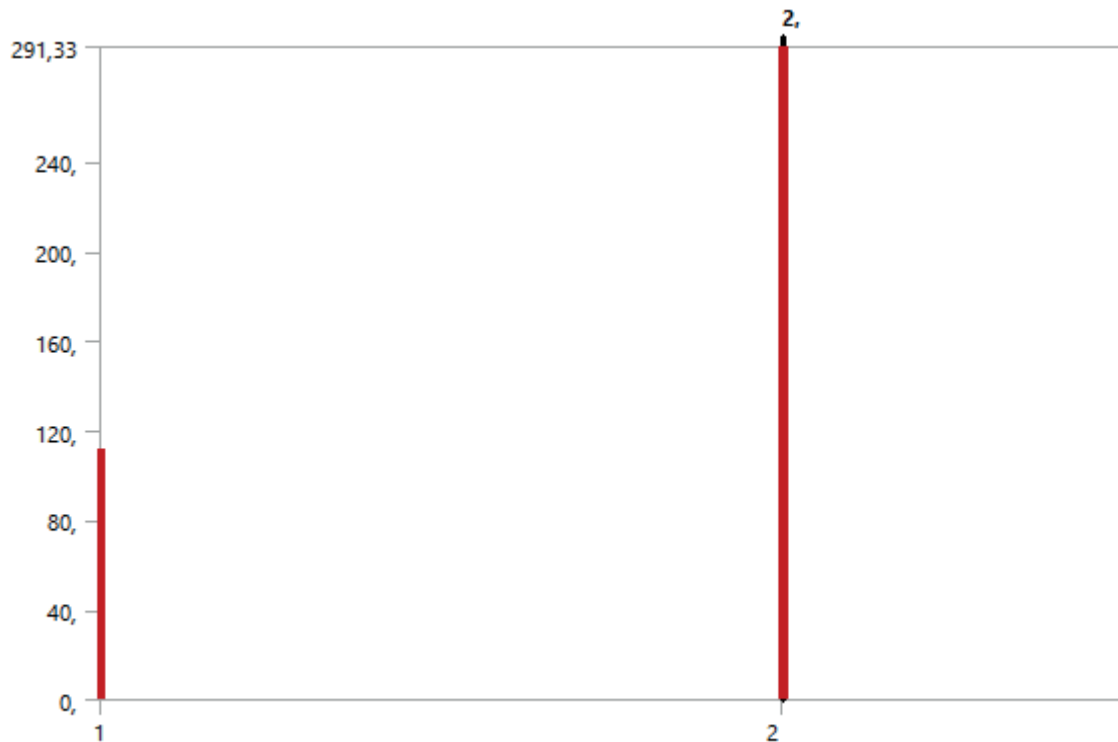


**TABLE 18**  
Model (B4, C4, D4) > Eigenvalue Buckling (C5) > Solution (C6)

Mode	Load Multiplier
1,	111,56
2,	291,33

# Static Structural 2 (D5)

## Solution (D6)

FIGURE 16  
Model (B4, C4, D4) > Static Structural 2 (D5) > Solution (D6) > Solution Information

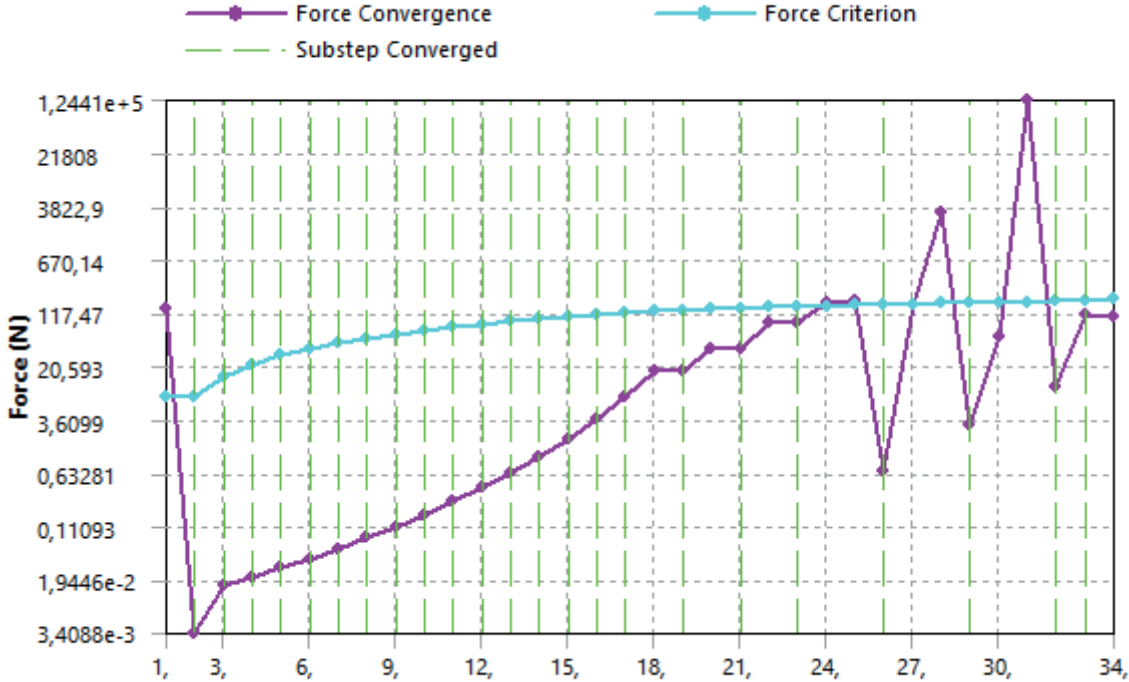


**FIGURE 17**  
**Model (B4, C4, D4) > Static Structural 2 (D5) > Solution (D6) > Solution Information**

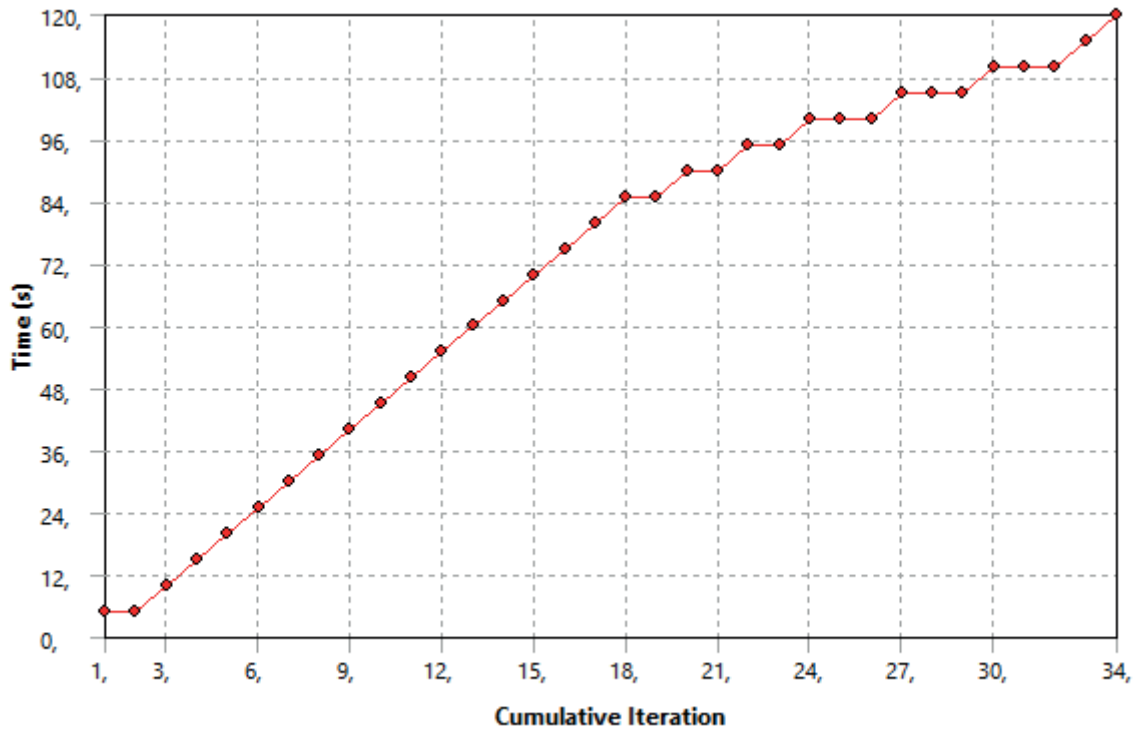


**FIGURE 18**  
**Model (B4, C4, D4) > Static Structural 2 (D5) > Solution (D6) > Directional Deformation**

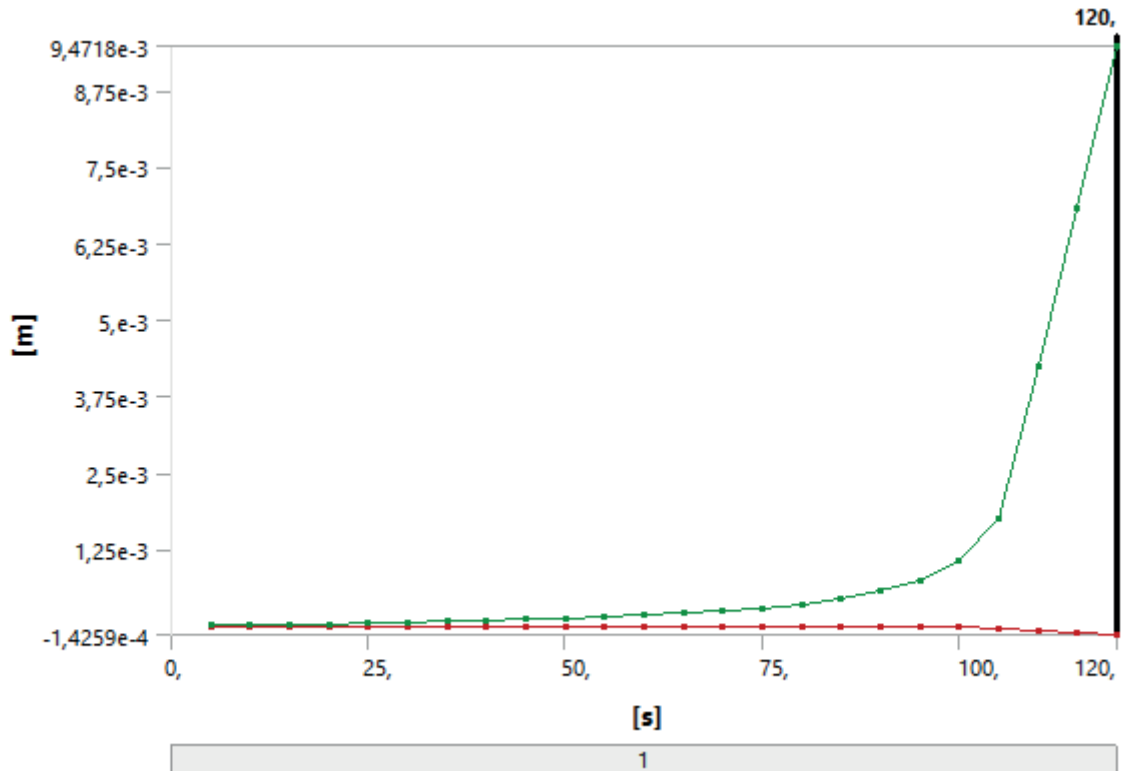


**TABLE 28**  
**Model (B4, C4, D4) > Static Structural 2 (D5) > Solution (D6) > Directional Deformation**

Time [s]	Minimum [m]	Maximum [m]
5,	-2,8109e-007	7,6106e-006
10,	-5,6194e-007	1,5854e-005
15,	-8,4251e-007	2,4832e-005
20,	-1,1228e-006	3,4661e-005
25,	-1,4027e-006	4,5484e-005
30,	-1,6821e-006	5,748e-005
35,	-1,9611e-006	7,0875e-005
40,	-2,2395e-006	8,5952e-005
45,	-2,5173e-006	1,0308e-004
50,	-2,7941e-006	1,2275e-004
55,	-3,0699e-006	1,456e-004
60,	-3,4854e-006	1,7253e-004
65,	-4,0915e-006	2,0478e-004
70,	-4,8229e-006	2,4419e-004
75,	-5,7267e-006	2,935e-004
80,	-6,8795e-006	3,5703e-004
85,	-8,4607e-006	4,4366e-004
90,	-1,0657e-005	5,6558e-004
95,	-1,4007e-005	7,5225e-004
100,	-1,9848e-005	1,0764e-003
105,	-3,2168e-005	1,7586e-003
110,	-7,9347e-005	4,2546e-003
115,	-1,1656e-004	6,8135e-003
120,	-1,4259e-004	9,4718e-003

## 4. IPE240, 2.00 m

### Eigenvalue Buckling (C5)

#### Solution (C6)

**FIGURE 8**  
Model (B4, C4, D4) > Eigenvalue Buckling (C5) > Solution (C6)

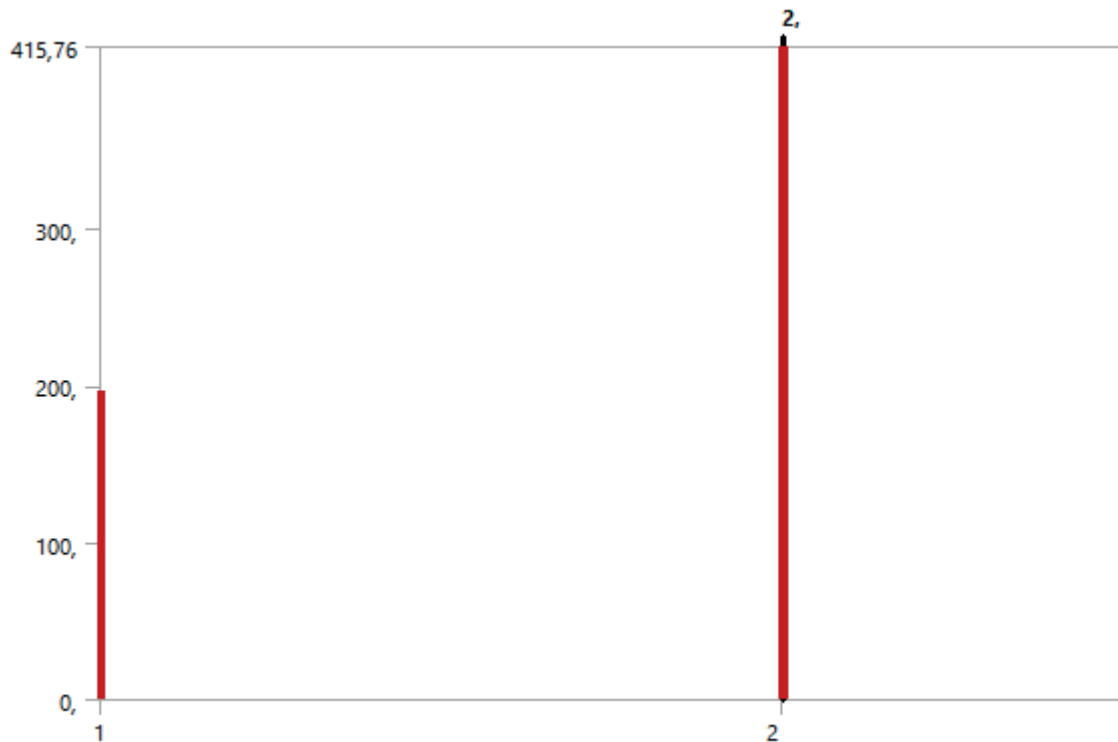


**TABLE 18**  
Model (B4, C4, D4) > Eigenvalue Buckling (C5) > Solution (C6)

Mode	Load Multiplier
1,	196,48
2,	415,76



# Static Structural 2 (D5)

## Solution (D6)

FIGURE 16  
Model (B4, C4, D4) > Static Structural 2 (D5) > Solution (D6) > Solution Information

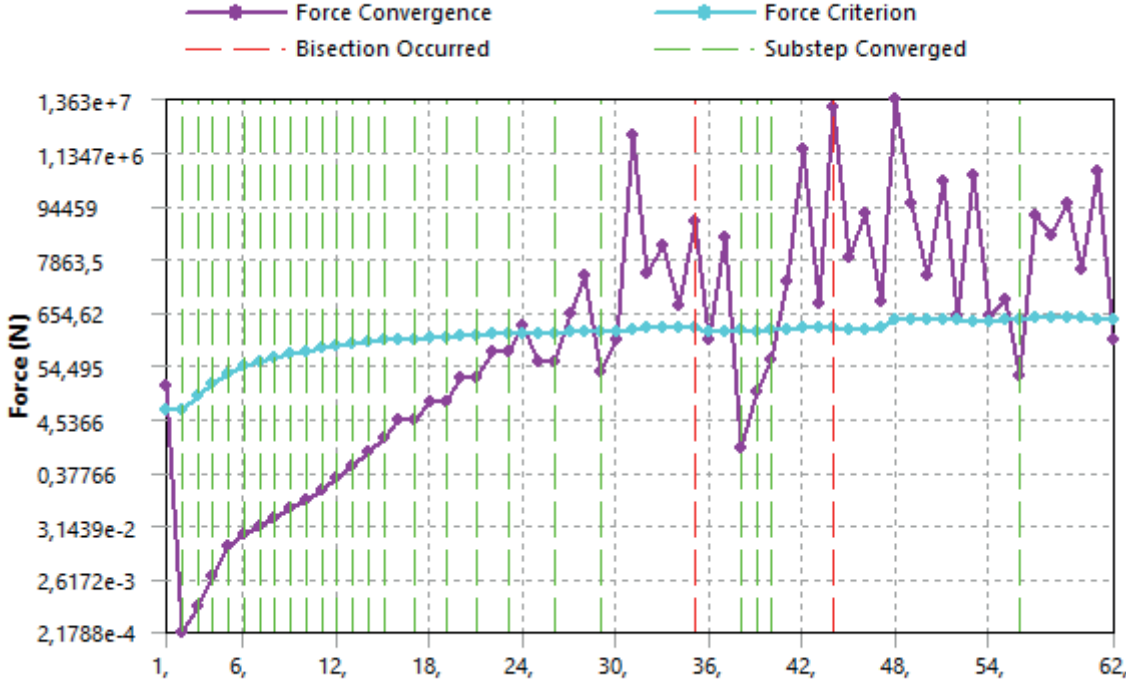


**FIGURE 17**  
**Model (B4, C4, D4) > Static Structural 2 (D5) > Solution (D6) > Solution Information**

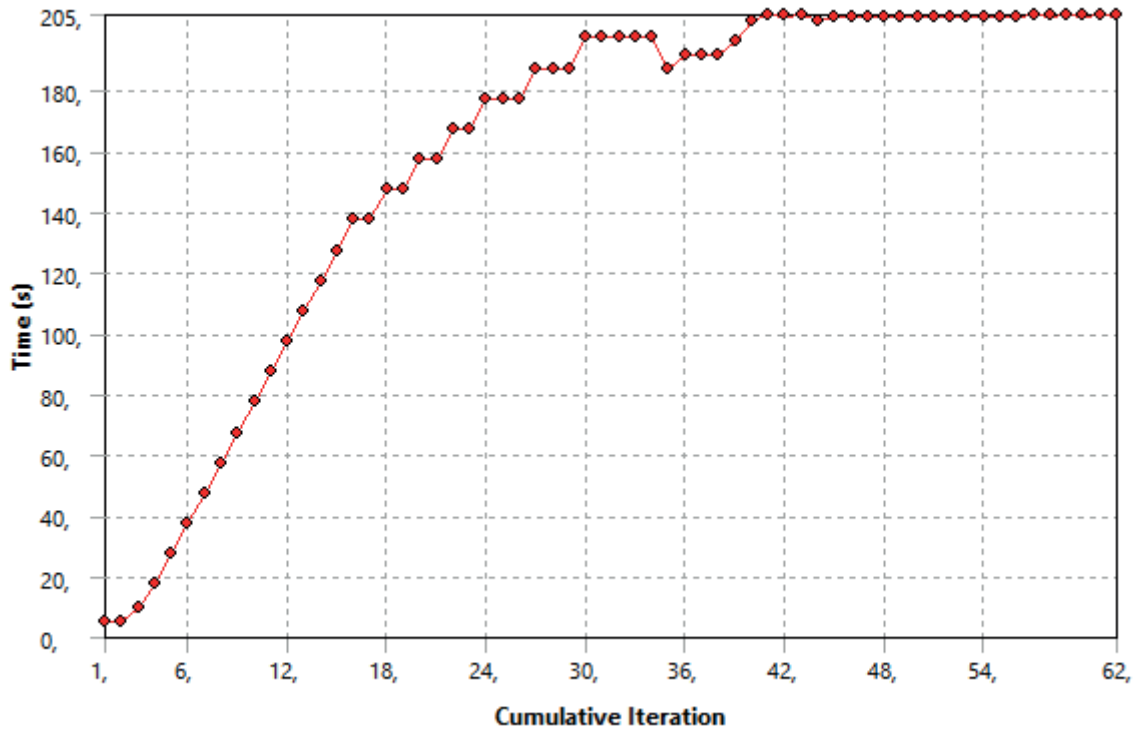


**FIGURE 18**  
**Model (B4, C4, D4) > Static Structural 2 (D5) > Solution (D6) > Directional Deformation**

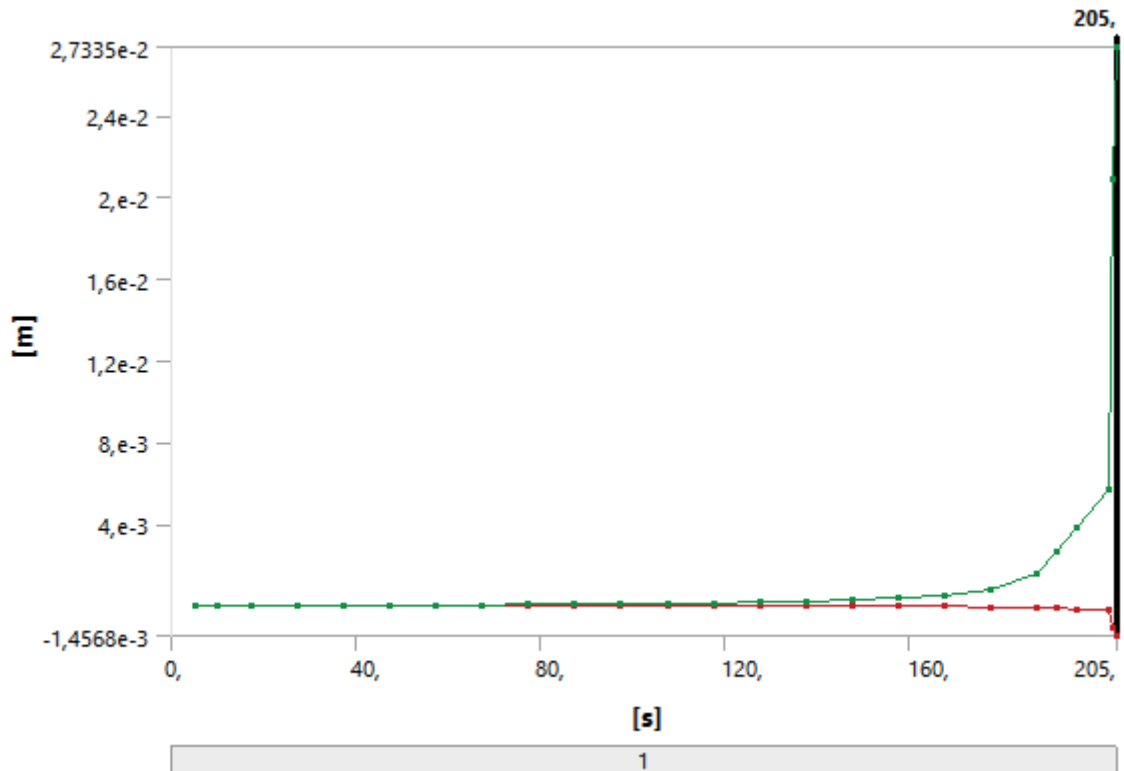


**TABLE 28**  
**Model (B4, C4, D4) > Static Structural 2 (D5) > Solution (D6) > Directional Deformation**

Time [s]	Minimum [m]	Maximum [m]
5,	-4,0281e-007	2,9408e-006
10,	-8,1047e-007	6,0081e-006
17,5	-1,432e-006	1,0869e-005
27,5	-2,2818e-006	1,7898e-005
37,5	-3,1602e-006	2,5663e-005
47,5	-4,0729e-006	3,431e-005
57,5	-5,0274e-006	4,4025e-005
67,5	-6,0332e-006	5,5054e-005
77,5	-7,1035e-006	6,7723e-005
87,5	-8,2557e-006	8,2477e-005
97,5	-9,5146e-006	9,9935e-005
107,5	-1,0915e-005	1,2099e-004
117,5	-1,2511e-005	1,4698e-004
127,5	-1,4385e-005	1,7998e-004
137,5	-1,6684e-005	2,236e-004
147,5	-1,9644e-005	2,8386e-004
157,5	-2,3765e-005	3,7317e-004
167,5	-3,0181e-005	5,1973e-004
177,5	-4,2268e-005	8,0671e-004
187,5	-7,3155e-005	1,5608e-003
192,	-1,2082e-004	2,7007e-003
196,5	-1,6573e-004	3,8642e-003
203,25	-2,2826e-004	5,6642e-003
204,25	-1,0226e-003	2,0874e-002
205,	-1,4568e-003	2,7335e-002

## 5. IPE240, 2.25 m

### Eigenvalue Buckling (C5)

#### Solution (C6)

**FIGURE 8**  
Model (B4, C4, D4) > Eigenvalue Buckling (C5) > Solution (C6)



**TABLE 18**  
Model (B4, C4, D4) > Eigenvalue Buckling (C5) > Solution (C6)

Mode	Load Multiplier
1,	183,82
2,	399,56

# Static Structural 2 (D5)

## Solution (D6)

FIGURE 16  
Model (B4, C4, D4) > Static Structural 2 (D5) > Solution (D6) > Solution Information

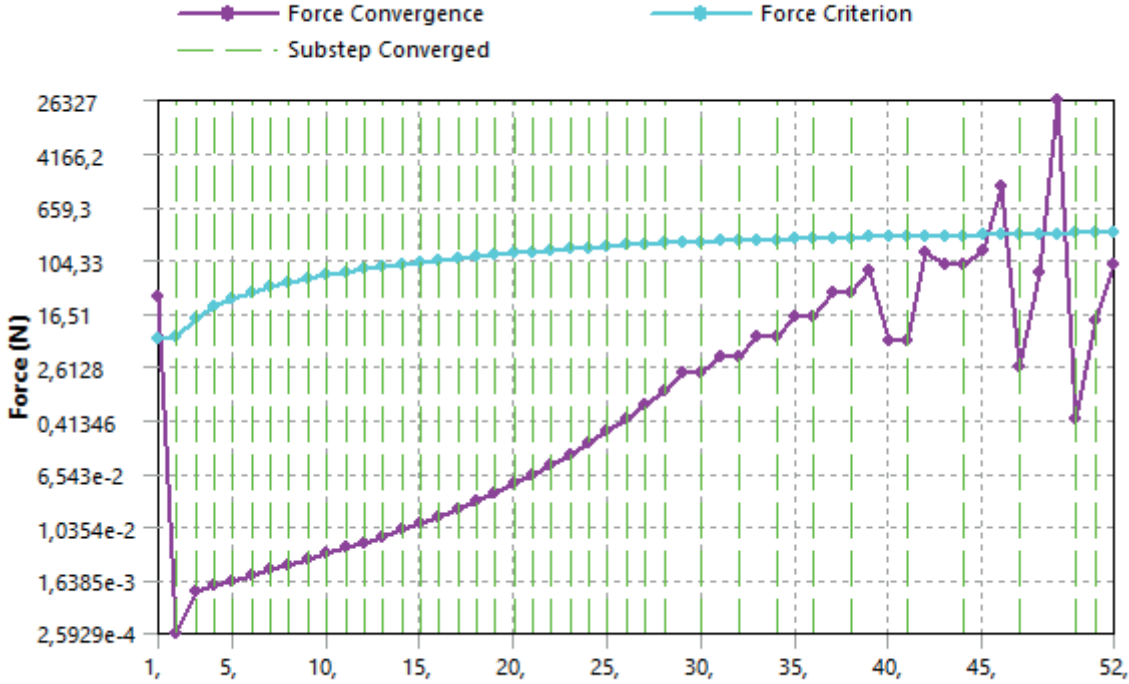


**FIGURE 17**  
**Model (B4, C4, D4) > Static Structural 2 (D5) > Solution (D6) > Solution Information**

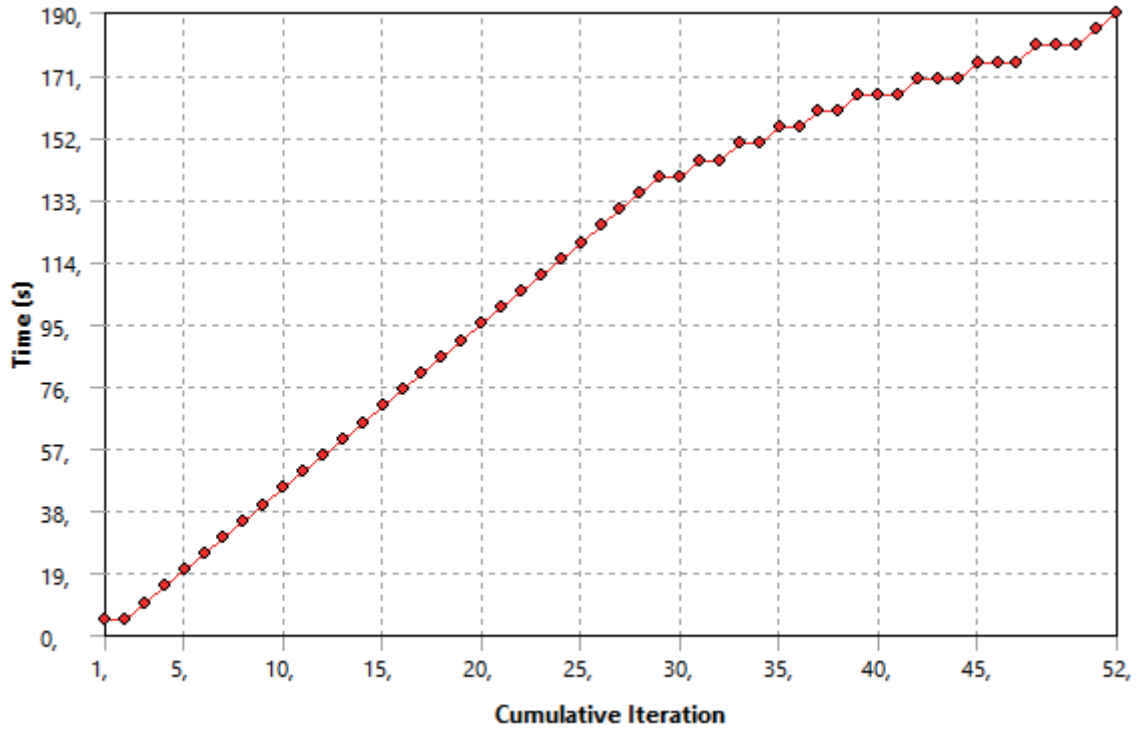


**FIGURE 18**  
**Model (B4, C4, D4) > Static Structural 2 (D5) > Solution (D6) > Directional Deformation**

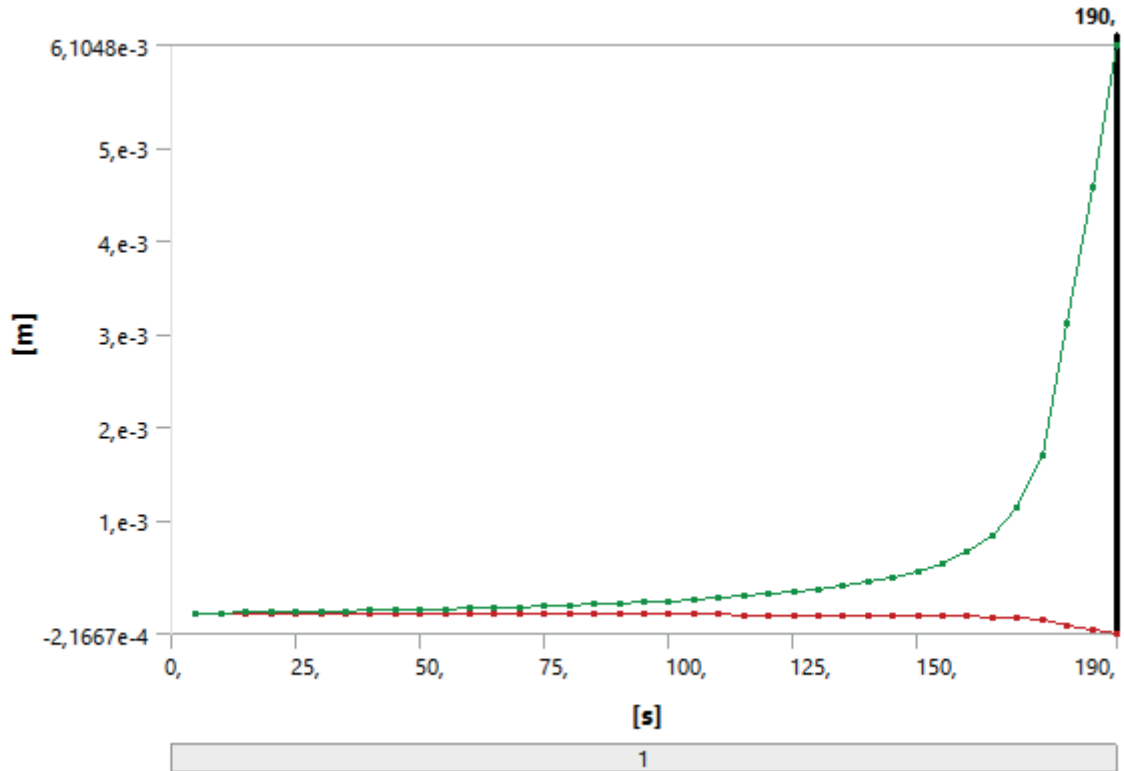


**TABLE 28**  
**Model (B4, C4, D4) > Static Structural 2 (D5) > Solution (D6) > Directional Deformation**

Time [s]	Minimum [m]	Maximum [m]
5,	-4,1456e-007	3,4769e-006
10,	-8,3478e-007	7,1173e-006
15,	-1,2612e-006	1,0936e-005
20,	-1,6943e-006	1,4948e-005
25,	-2,1348e-006	1,9173e-005
30,	-2,5834e-006	2,363e-005
35,	-3,0409e-006	2,8344e-005
40,	-3,5082e-006	3,3339e-005
45,	-3,9865e-006	3,8646e-005
50,	-4,4769e-006	4,43e-005
55,	-4,9808e-006	5,034e-005
60,	-5,4999e-006	5,6812e-005
65,	-6,0361e-006	6,377e-005
70,	-6,5916e-006	7,1277e-005
75,	-7,1691e-006	7,9408e-005
80,	-7,7717e-006	8,825e-005
85,	-8,4031e-006	9,7909e-005
90,	-9,068e-006	1,0851e-004
95,	-9,7719e-006	1,2022e-004
100,	-1,0522e-005	1,3322e-004
105,	-1,1326e-005	1,4775e-004
110,	-1,2195e-005	1,6412e-004
115,	-1,3144e-005	1,8272e-004
120,	-1,419e-005	2,0405e-004
125,	-1,5357e-005	2,2878e-004
130,	-1,6679e-005	2,5783e-004
135,	-1,82e-005	2,9247e-004
140,	-1,9993e-005	3,3462e-004
145,	-2,2146e-005	3,8687e-004

150,	-2,4819e-005	4,5353e-004
155,	-2,8264e-005	5,4159e-004
160,	-3,2935e-005	6,6346e-004
165,	-3,9725e-005	8,4348e-004
170,	-5,0658e-005	1,1362e-003
175,	-7,1278e-005	1,6901e-003
180,	-1,2562e-004	3,1245e-003
185,	-1,7382e-004	4,5835e-003
190,	-2,1667e-004	6,1048e-003



## 6. IPE240, 2.50 m

### Eigenvalue Buckling (C5)

#### Solution (C6)

**FIGURE 8**  
Model (B4, C4, D4) > Eigenvalue Buckling (C5) > Solution (C6)

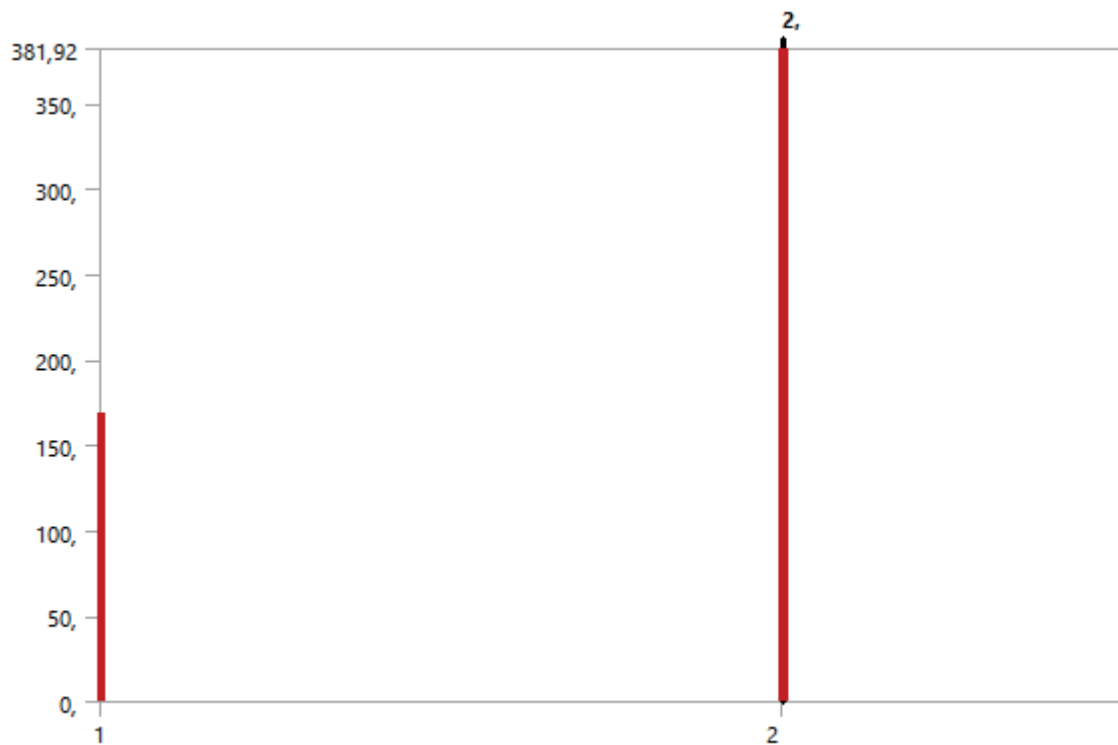


**TABLE 18**  
Model (B4, C4, D4) > Eigenvalue Buckling (C5) > Solution (C6)

Mode	Load Multiplier
1,	169,23
2,	381,92

# Static Structural 2 (D5)

## Solution (D6)

FIGURE 16  
Model (B4, C4, D4) > Static Structural 2 (D5) > Solution (D6) > Solution Information

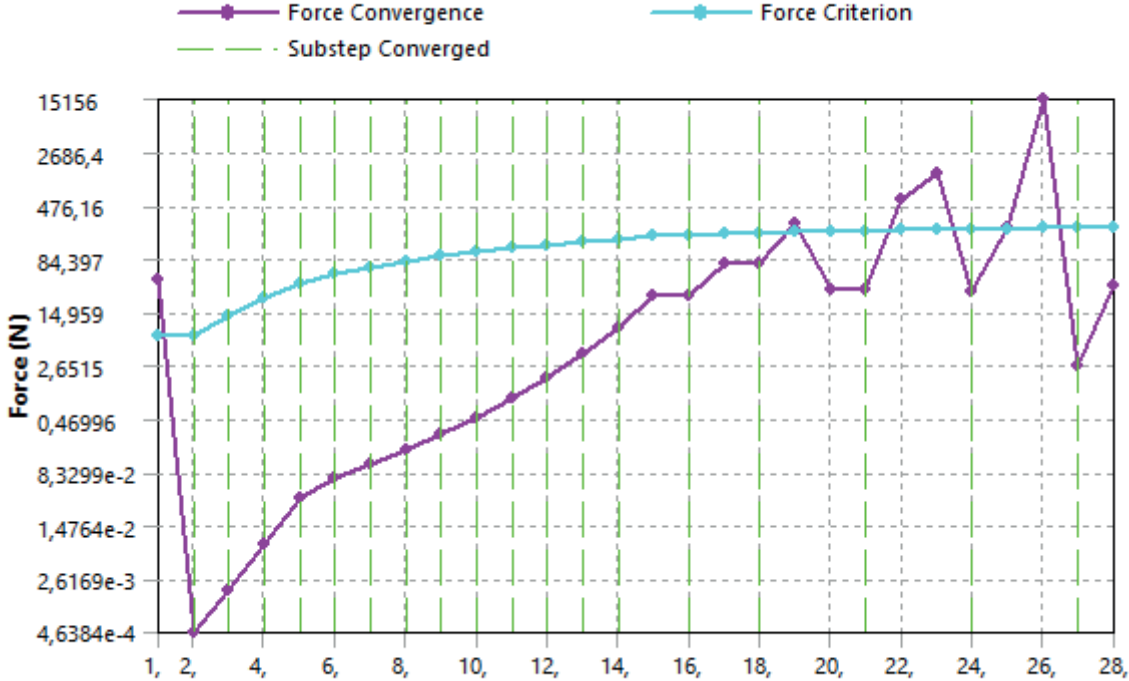


**FIGURE 17**  
**Model (B4, C4, D4) > Static Structural 2 (D5) > Solution (D6) > Solution Information**

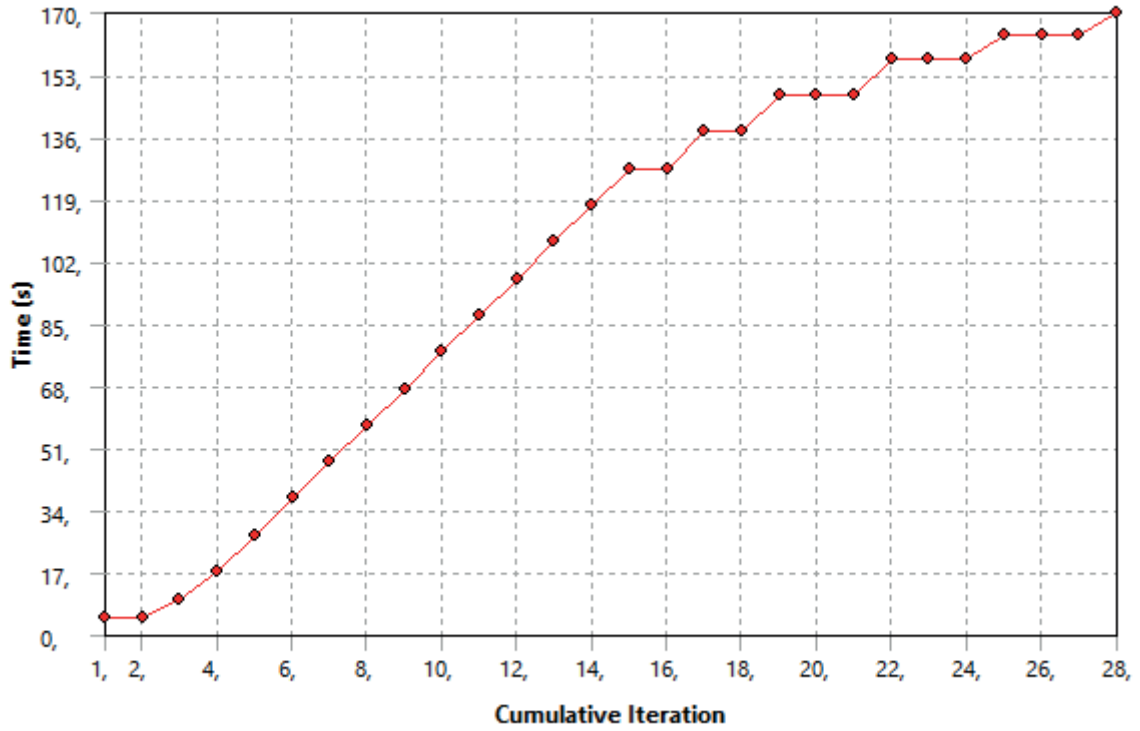


**FIGURE 18**  
**Model (B4, C4, D4) > Static Structural 2 (D5) > Solution (D6) > Directional Deformation**

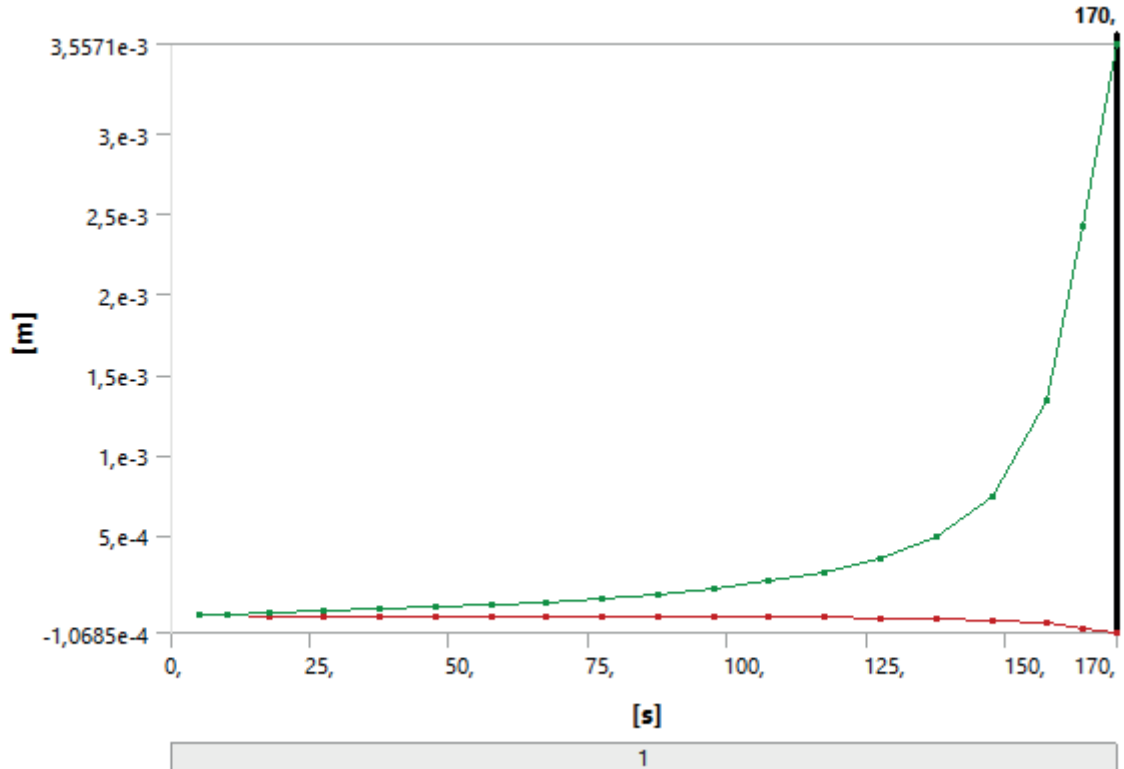


**TABLE 28**  
**Model (B4, C4, D4) > Static Structural 2 (D5) > Solution (D6) > Directional Deformation**

Time [s]	Minimum [m]	Maximum [m]
5,	-3,2554e-007	4,1968e-006
10,	-6,579e-007	8,6125e-006
17,5	-1,1705e-006	1,5692e-005
27,5	-1,884e-006	2,6116e-005
37,5	-2,6391e-006	3,7901e-005
47,5	-3,4453e-006	5,1376e-005
57,5	-4,3155e-006	6,6984e-005
67,5	-5,2677e-006	8,5342e-005
77,5	-6,3278e-006	1,0732e-004
87,5	-7,5338e-006	1,3423e-004
97,5	-8,9443e-006	1,6804e-004
107,5	-1,0654e-005	2,1197e-004
117,5	-1,2825e-005	2,7157e-004
127,5	-1,5846e-005	3,5868e-004
137,5	-2,0336e-005	4,9546e-004
147,5	-2,8253e-005	7,4556e-004
157,5	-4,6468e-005	1,337e-003
163,75	-8,0247e-005	2,4266e-003
170,	-1,0685e-004	3,5571e-003

## 7. IPE270, 2.00 m

### Eigenvalue Buckling (C5)

*Solution (C6)*

**FIGURE 8**  
Model (B4, C4, D4) > Eigenvalue Buckling (C5) > Solution (C6)



**TABLE 18**  
Model (B4, C4, D4) > Eigenvalue Buckling (C5) > Solution (C6)

Mode	Load Multiplier
1,	215,66
2,	442,47

# Static Structural 2 (D5)

## Solution (D6)

FIGURE 16  
Model (B4, C4, D4) > Static Structural 2 (D5) > Solution (D6) > Solution Information

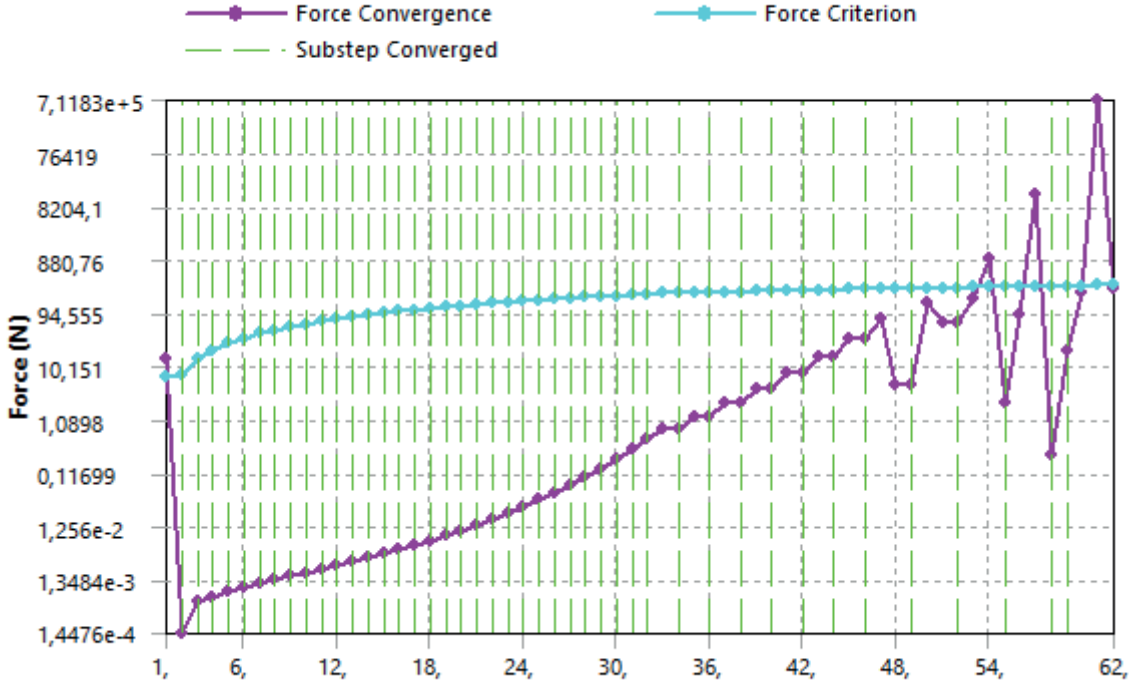


**FIGURE 17**  
**Model (B4, C4, D4) > Static Structural 2 (D5) > Solution (D6) > Solution Information**

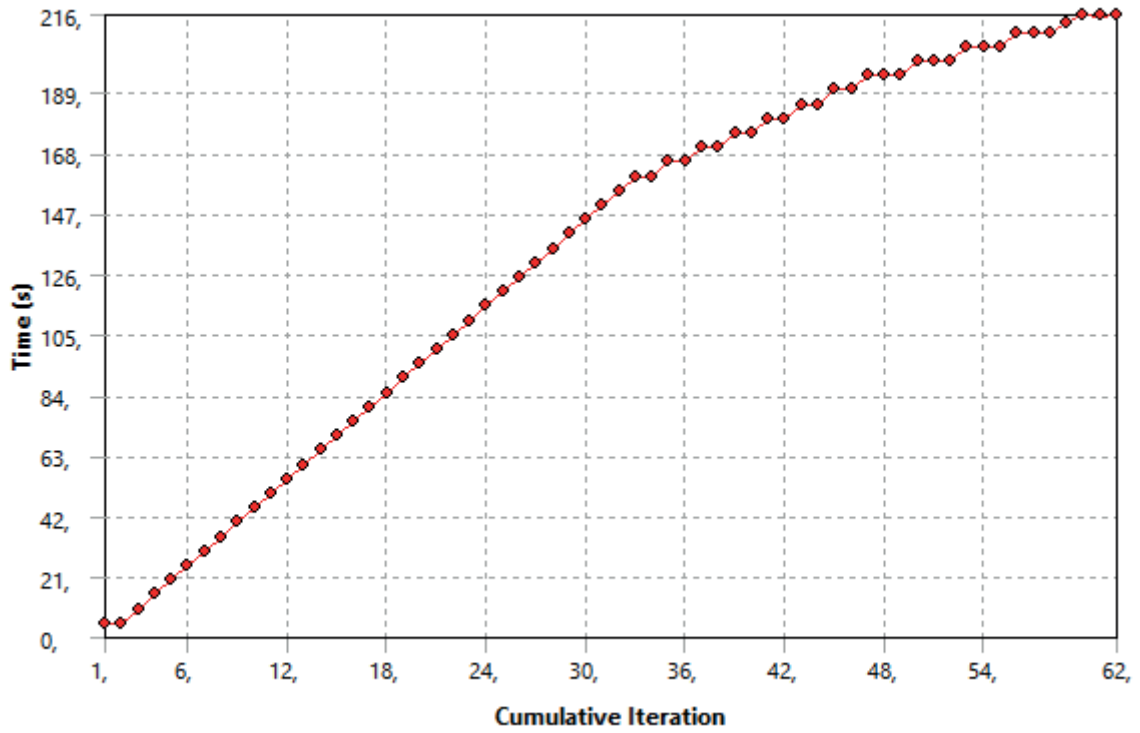


**FIGURE 18**  
**Model (B4, C4, D4) > Static Structural 2 (D5) > Solution (D6) > Directional Deformation**

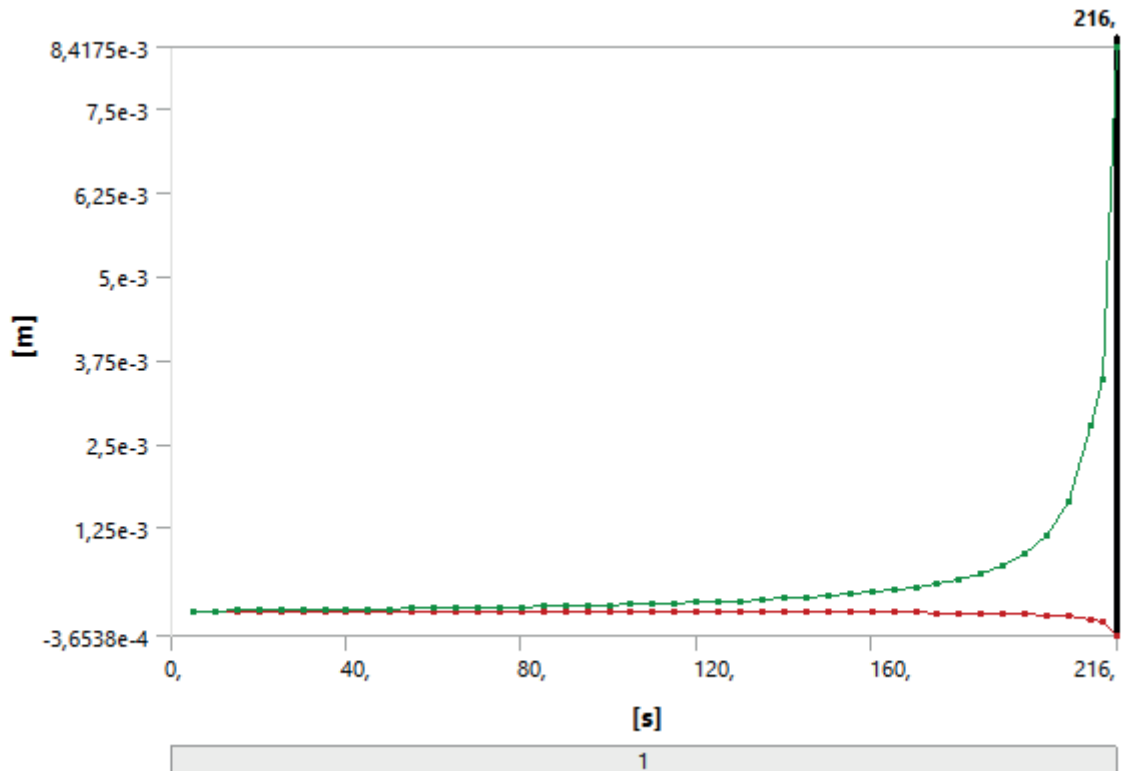


**TABLE 28**  
**Model (B4, C4, D4) > Static Structural 2 (D5) > Solution (D6) > Directional Deformation**

Time [s]	Minimum [m]	Maximum [m]
5,0233	-3,3719e-007	2,7913e-006
10,023	-6,7696e-007	5,6781e-006
15,023	-1,0212e-006	8,6811e-006
20,023	-1,3701e-006	1,1809e-005
25,023	-1,7243e-006	1,5072e-005
30,023	-2,084e-006	1,848e-005
35,023	-2,4498e-006	2,2046e-005
40,023	-2,8221e-006	2,5783e-005
45,023	-3,2016e-006	2,9705e-005
50,023	-3,5889e-006	3,3831e-005
55,023	-3,9847e-006	3,8177e-005
60,023	-4,3898e-006	4,2765e-005
65,023	-4,8053e-006	4,762e-005
70,023	-5,232e-006	5,2768e-005
75,023	-5,6714e-006	5,8241e-005
80,023	-6,1246e-006	6,4073e-005
85,023	-6,5934e-006	7,0307e-005
90,023	-7,0796e-006	7,6988e-005
95,023	-7,5853e-006	8,4172e-005
100,02	-8,113e-006	9,1924e-005
105,02	-8,6658e-006	1,0032e-004
110,02	-9,2471e-006	1,0945e-004
115,02	-9,8611e-006	1,1942e-004
120,02	-1,0513e-005	1,3036e-004
125,02	-1,1209e-005	1,4243e-004
130,02	-1,1957e-005	1,5583e-004
135,02	-1,2765e-005	1,708e-004
140,02	-1,3647e-005	1,8763e-004
145,02	-1,4618e-005	2,0673e-004



150,02	-1,5697e-005	2,286e-004
155,02	-1,691e-005	2,539e-004
160,02	-1,8294e-005	2,8356e-004
165,02	-1,9898e-005	3,188e-004
170,02	-2,1791e-005	3,6143e-004
175,02	-2,4079e-005	4,1406e-004
180,02	-2,692e-005	4,8075e-004
185,02	-3,0578e-005	5,6807e-004
190,02	-3,5505e-005	6,8745e-004
195,02	-4,2574e-005	8,6065e-004
200,02	-5,3672e-005	1,1345e-003
205,02	-7,3676e-005	1,629e-003
210,02	-1,1992e-004	2,761e-003
213,01	-1,4742e-004	3,4614e-003
216,	-3,6538e-004	8,4175e-003

## 8. IPE270, 2.25 m

### Eigenvalue Buckling (C5)

*Solution (C6)*

**FIGURE 8**  
Model (B4, C4, D4) > Eigenvalue Buckling (C5) > Solution (C6)

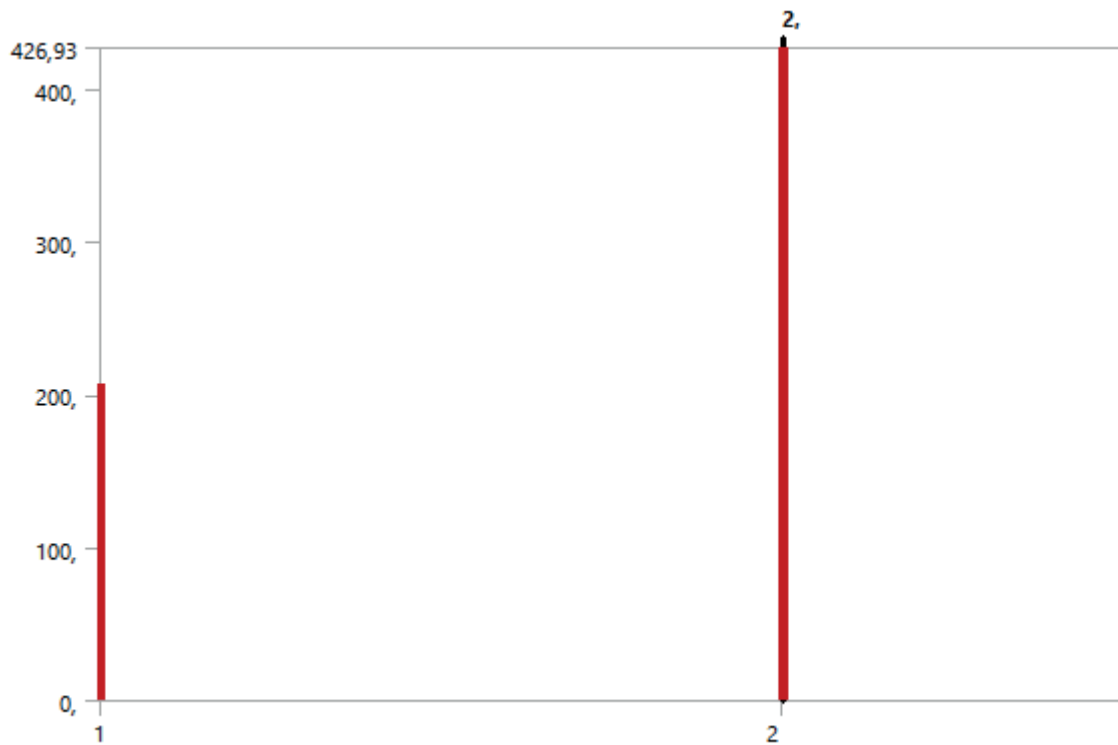


**TABLE 18**  
Model (B4, C4, D4) > Eigenvalue Buckling (C5) > Solution (C6)

Mode	Load Multiplier
1,	206,58
2,	426,93

# Static Structural 2 (D5)

## Solution (D6)

FIGURE 16  
Model (B4, C4, D4) > Static Structural 2 (D5) > Solution (D6) > Solution Information

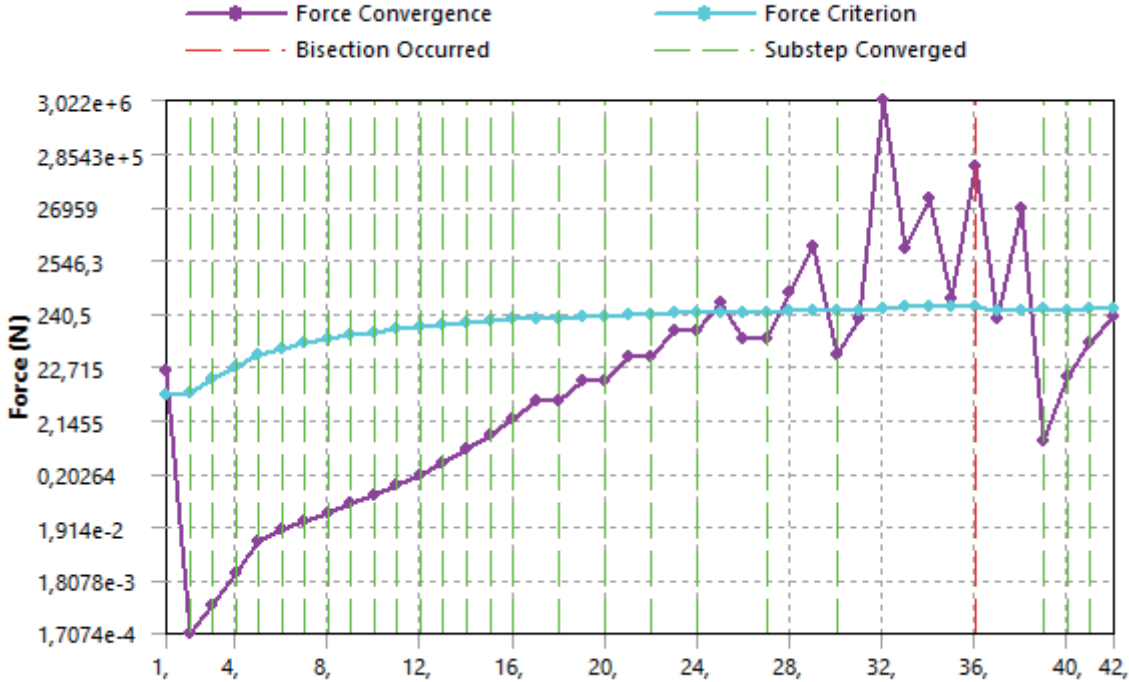


**FIGURE 17**  
**Model (B4, C4, D4) > Static Structural 2 (D5) > Solution (D6) > Solution Information**

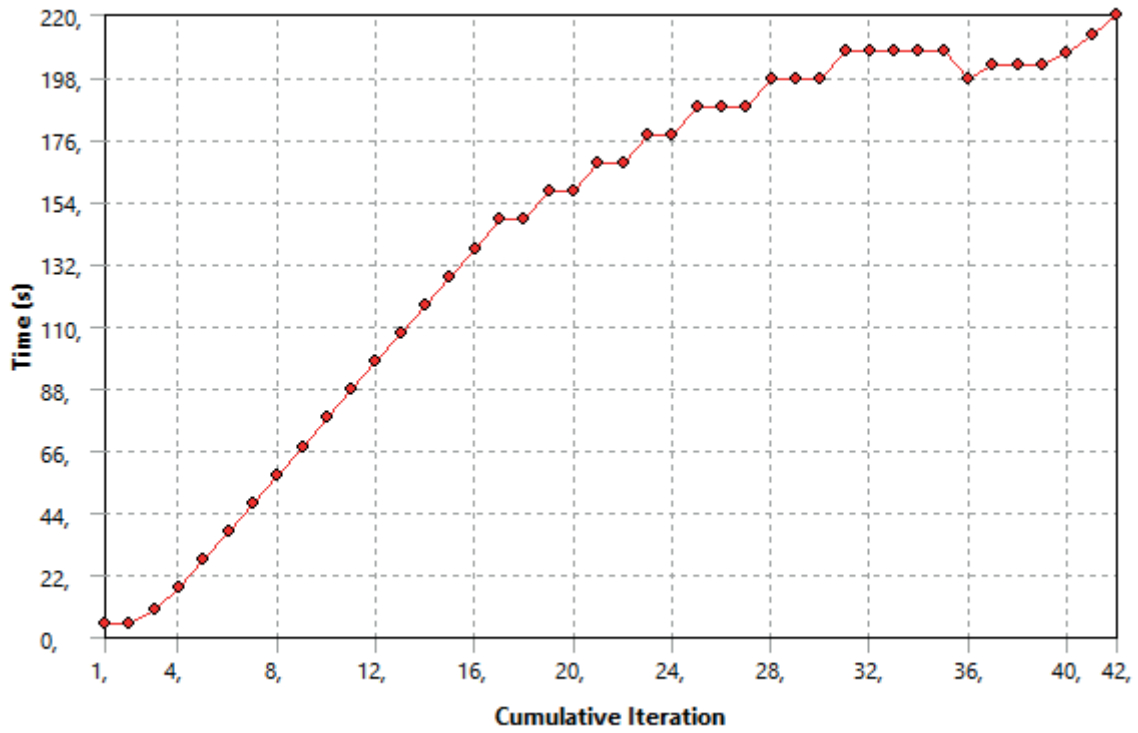


**FIGURE 18**  
**Model (B4, C4, D4) > Static Structural 2 (D5) > Solution (D6) > Directional Deformation**

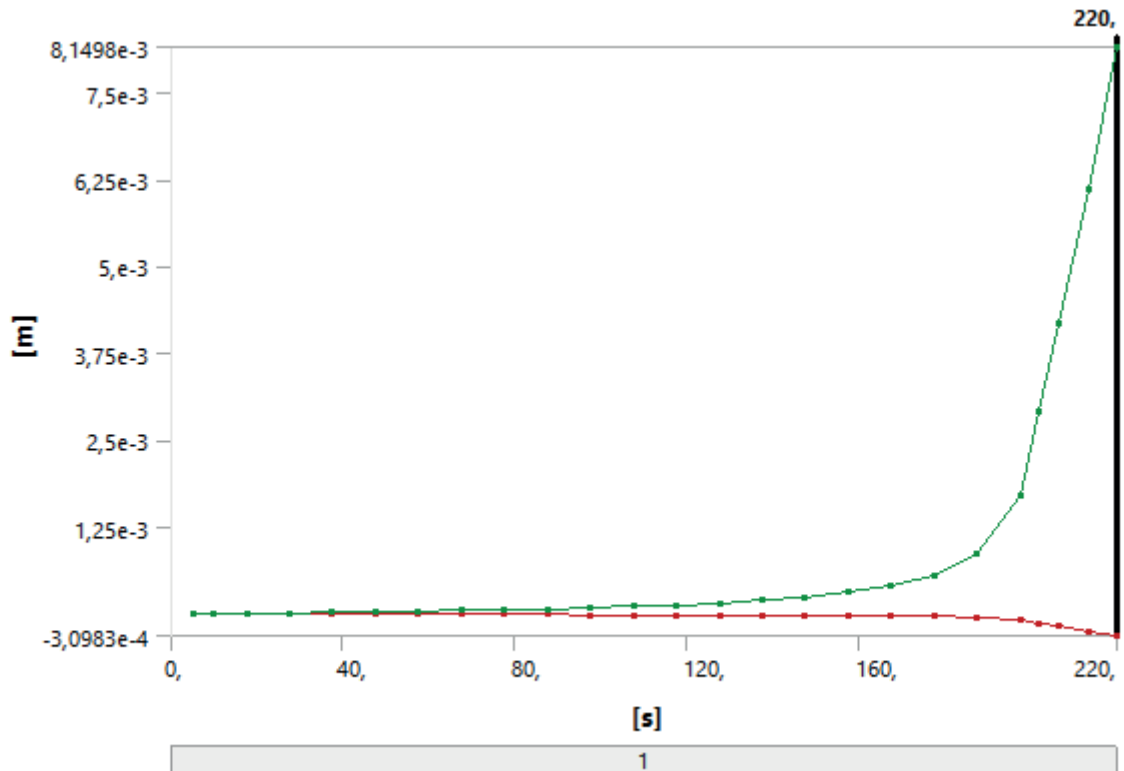


**TABLE 28**  
**Model (B4, C4, D4) > Static Structural 2 (D5) > Solution (D6) > Directional Deformation**

Time [s]	Minimum [m]	Maximum [m]
5,	-3,5164e-007	2,8934e-006
10,	-7,079e-007	5,9045e-006
17,5	-1,2518e-006	1,0662e-005
27,5	-1,9968e-006	1,751e-005
37,5	-2,7682e-006	2,503e-005
47,5	-3,5709e-006	3,3345e-005
57,5	-4,4111e-006	4,2614e-005
67,5	-5,2968e-006	5,3041e-005
77,5	-6,2385e-006	6,4891e-005
87,5	-7,25e-006	7,8516e-005
97,5	-8,3503e-006	9,4399e-005
107,5	-9,566e-006	1,1321e-004
117,5	-1,0935e-005	1,3592e-004
127,5	-1,2515e-005	1,6396e-004
137,5	-1,4394e-005	1,9961e-004
147,5	-1,673e-005	2,4674e-004
157,5	-1,9779e-005	3,1189e-004
167,5	-2,4076e-005	4,0848e-004
177,5	-3,0841e-005	5,6703e-004
187,5	-4,3701e-005	8,7748e-004
197,5	-7,6655e-005	1,6901e-003
202,	-1,2777e-004	2,9221e-003
206,5	-1,7642e-004	4,1768e-003
213,25	-2,451e-004	6,1119e-003
220,	-3,0983e-004	8,1498e-003

## 9. IPE270, 2.50 m

### Eigenvalue Buckling (C5)

#### Solution (C6)

**FIGURE 8**  
Model (B4, C4, D4) > Eigenvalue Buckling (C5) > Solution (C6)

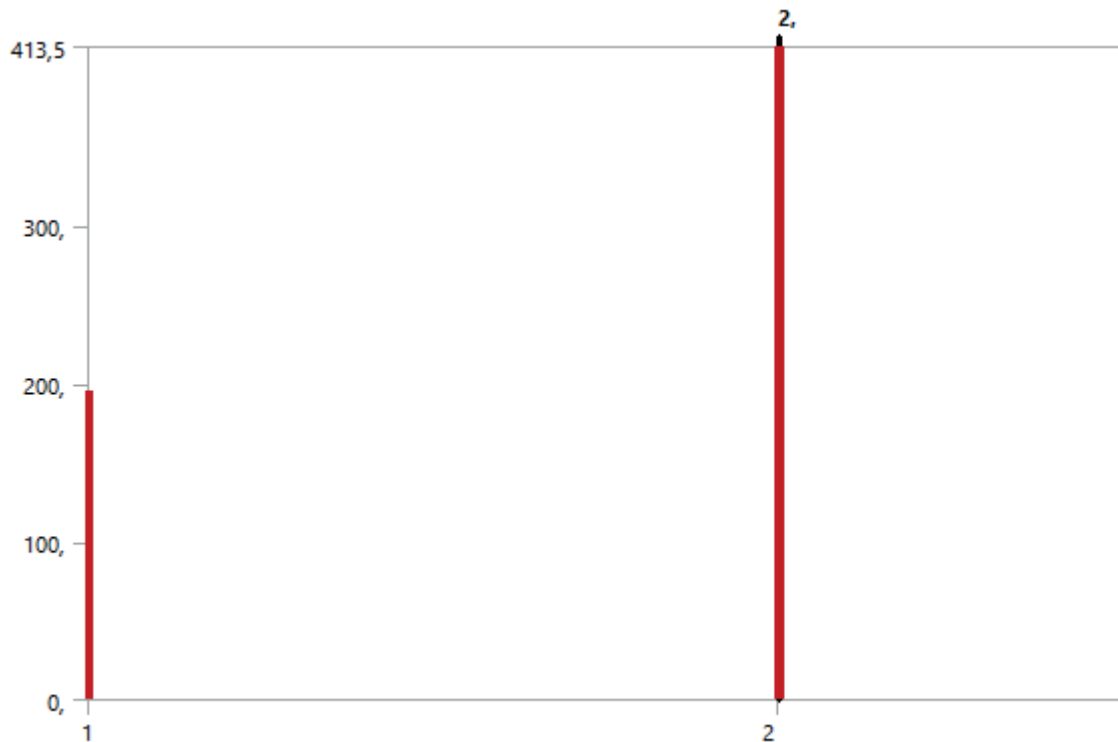


**TABLE 18**  
Model (B4, C4, D4) > Eigenvalue Buckling (C5) > Solution (C6)

Mode	Load Multiplier
1,	195,87
2,	413,5

# Static Structural 2 (D5)

## Solution (D6)

FIGURE 16  
Model (B4, C4, D4) > Static Structural 2 (D5) > Solution (D6) > Solution Information

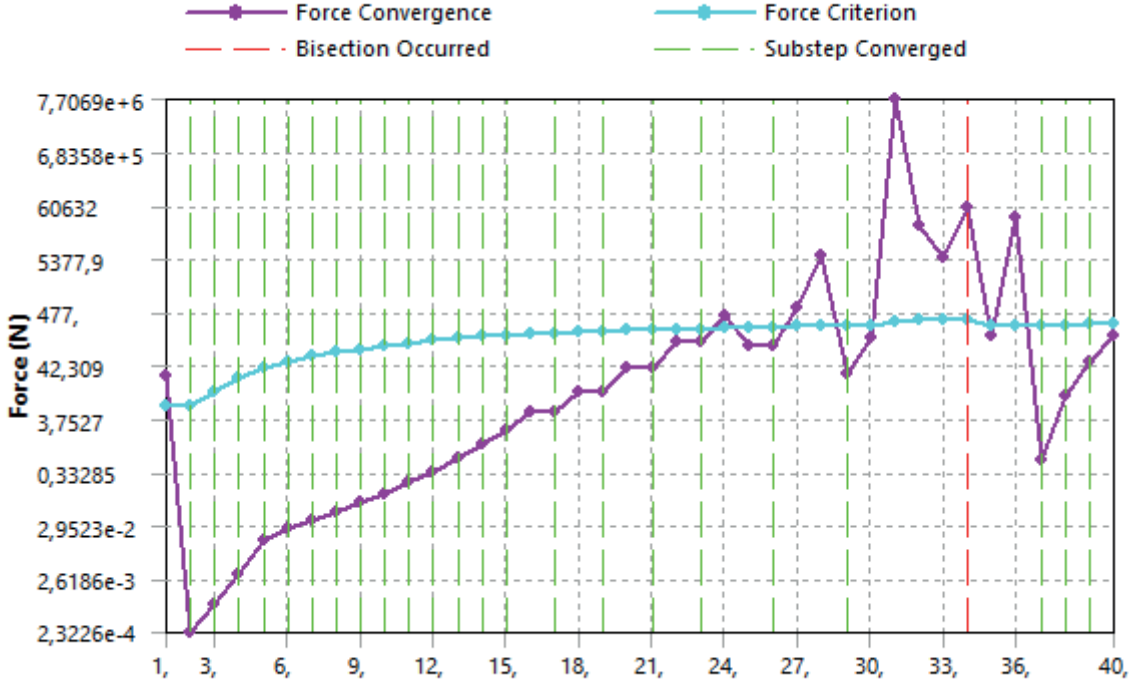


**FIGURE 17**  
**Model (B4, C4, D4) > Static Structural 2 (D5) > Solution (D6) > Solution Information**

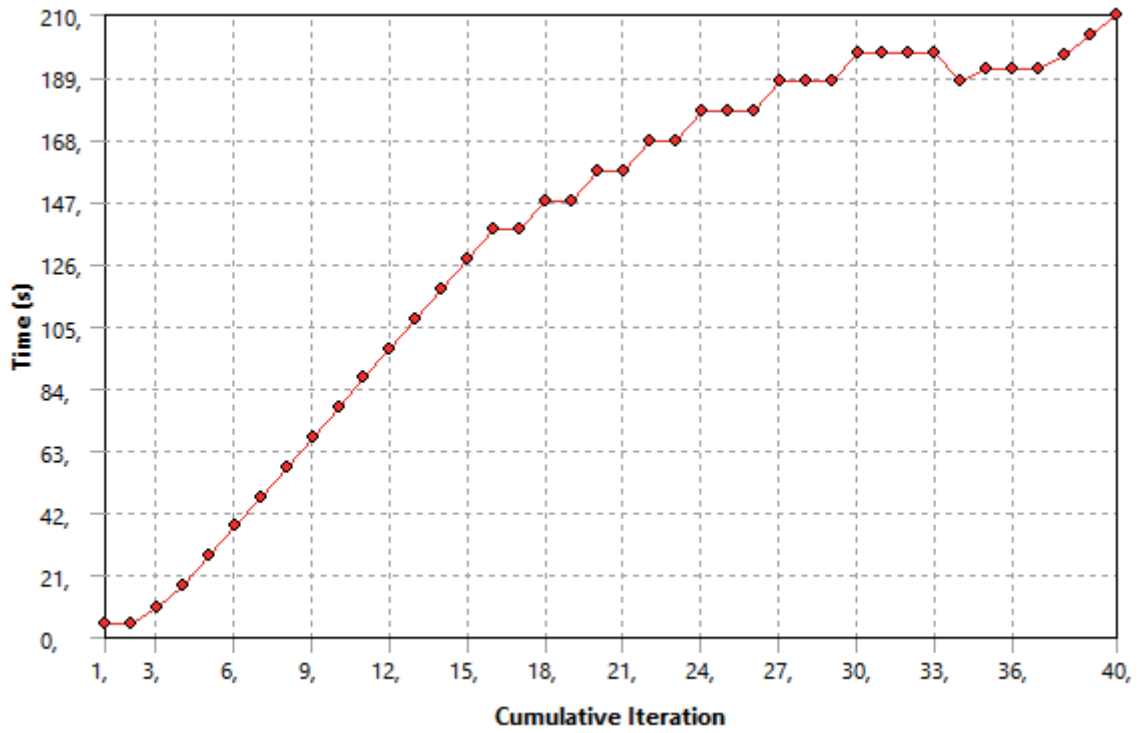


**FIGURE 18**  
**Model (B4, C4, D4) > Static Structural 2 (D5) > Solution (D6) > Directional Deformation**

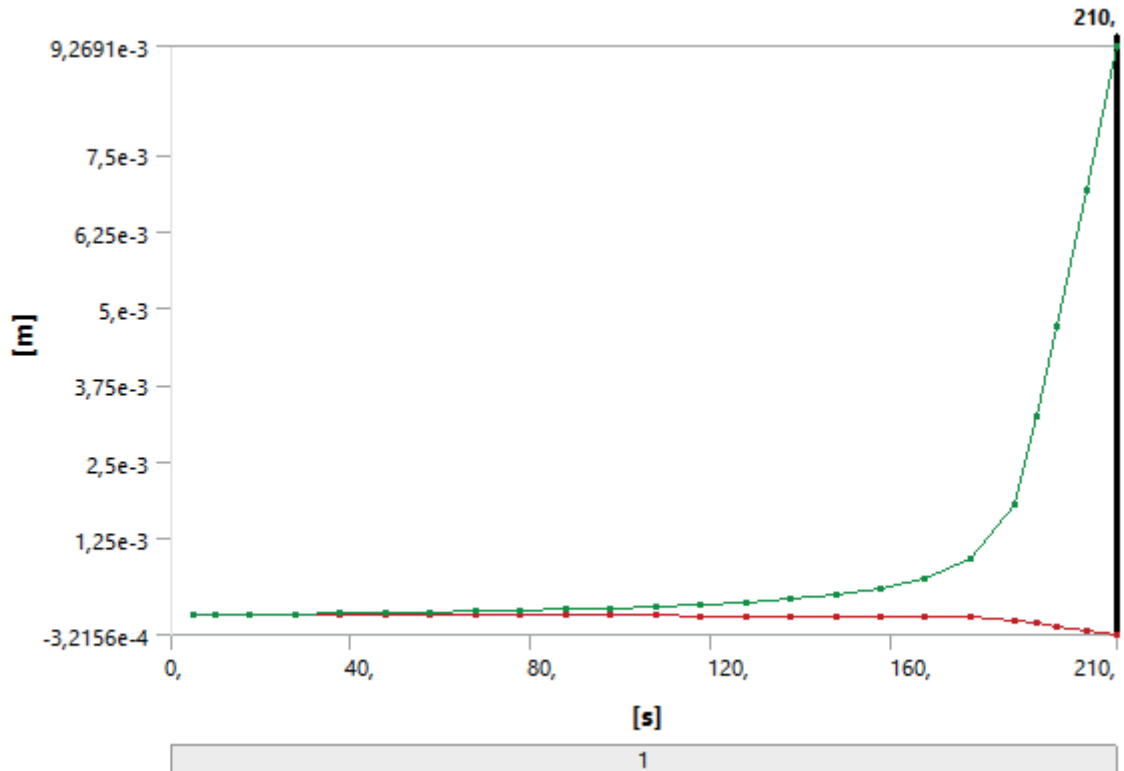




**TABLE 28**  
**Model (B4, C4, D4) > Static Structural 2 (D5) > Solution (D6) > Directional Deformation**

Time [s]	Minimum [m]	Maximum [m]
5,	-3,6355e-007	3,2505e-006
10,	-7,3247e-007	6,6427e-006
17,5	-1,2969e-006	1,2023e-005
27,5	-2,0726e-006	1,9811e-005
37,5	-2,8796e-006	2,8426e-005
47,5	-3,724e-006	3,8031e-005
57,5	-4,6137e-006	4,8838e-005
67,5	-5,5591e-006	6,1123e-005
77,5	-6,5741e-006	7,5255e-005
87,5	-7,6776e-006	9,1735e-005
97,5	-8,8961e-006	1,1127e-004
107,5	-1,0268e-005	1,3486e-004
117,5	-1,185e-005	1,6403e-004
127,5	-1,3731e-005	2,0115e-004
137,5	-1,6076e-005	2,5036e-004
147,5	-1,9136e-005	3,1853e-004
157,5	-2,3462e-005	4,1995e-004
167,5	-3,0306e-005	5,8738e-004
177,5	-4,3466e-005	9,1891e-004
187,5	-7,7654e-005	1,8019e-003
192,	-1,3503e-004	3,2349e-003
196,5	-1,8791e-004	4,6898e-003
203,25	-2,5908e-004	6,9255e-003
210,	-3,2156e-004	9,2691e-003